Chapter 4: Ethanol Steam Reforming

4.1: Introduction

Ethanol steam reforming holds promise because of the renewable source of feedstock (ethanol). This partially alleviates the issue of global warming and also helps to conserve fossil feedstock.

Both noble and non-noble metal catalysts have been studied for this reaction. Ogo et.al. [1] have reviewed the use of non-noble metal catalysts for steam reforming of ethanol over the years 2016-2019. Cobalt, Ni-Co bimetallic and Ni catalysts are covered. They infer that the particle size and oxidation state of the active metals and properties of the support such as redox and acid-base and choice of promoter are important for effective performance (lower coke and by-product formation).

Contreras et.al. [2] have reviewed published literature on catalysts used for the steam reforming of ethanol. They conclude that noble metals such as Rh, Ru, Pd and Ir and non-noble metals such as Ni, Co and Cu have selectivity 80% or better for H_2. Amongst the supports they list CeO_2, ZnO, MgO, Al_2O_3, zeolite HY, TiO_2, SiO_2, $La_2O_2CO_3$, ceria-zirconia and hydrotalcites give good performance due to a variety of properties such as microstructure, metal-support interaction, oxygen storage capacity, acidity-basicity which influence activity, selectivity, and stability of the catalyst. They also infer that impregnation produces catalysts with best performance.

Meng Ni et. al. [3] have reviewed the reforming of bioethanol for production of hydrogen. An advantage of using bioethanol instead of pure ethanol is the energy saving which is otherwise required for producing pure ethanol. Fortunately, the steam reforming uses water as co-feed. They infer that Rh (amongst noble metals and Ni (amongst non-noble metals) are the best reported with MgO, ZnO_2, CeO_2 and La_2O_3 as suitable supports. Interestingly they have not mentioned Al_2O_3 as a support. According to them bimetallic catalysts and tandem catalysis hold promise for increasing H_2 yield and catalyst stability.

Ashutosh Kumar et.al. [4] have reviewed published literature on the steam reforming of ethanol and catalysts used therein. Both noble and non-noble metal catalysts are covered. They conclude that extensive work is necessary with non-noble metal catalysts to improve performance and costs of ethanol steam reforming.

The general consensus is that noble metal catalysts show high activity and selectivity. Rh, Pt, Pd, Ru have been studied extensively. Different noble metals show differences in activity for water gas shift reaction. The high cost of noble metals is the key driver for developing non-noble metal catalysts. Catalysts which are inherently less prone to coking at a low S/C (steam: carbon) ratio are also desirable because of process energy savings.

Matoos et.al [5] have reviewed the reaction mechanism and mechanism of catalyst deactivation for this reaction. They highlight the importance of bifunctionality (interface between active metal and metal oxide of the support). Catalyst stability is reported as the biggest challenge for this reaction. Coking is reported as the major cause of catalyst deactivation in addition to sintering of active metal. It takes place due to C-C bond scission of ethanol and the nature of coke depends on the type of active metal used as well as reaction conditions. They observe that compounds such as acetates and carbonates form to a larger extent on metal oxides and supported metal catalysts than on surface. They postulate that ethanol adsorbs dissociatively to form ethoxy species.

ESR is a complex network of reactions described by Mattos et.al. [5], Zhurkha et. al [6] and Og et. al. [1]

$C_2H_5OH + 3H_2O \rightarrow 2CO_2 + 6H_2$ (Steam reforming) ΔHr^0_{298K} = 173.7 kJ/mol

$C_2H_5OH \rightarrow CH_4 + CO + H_2$ (Decomposition) ΔHr^0_{298K} = 49 kJ/mol

$C_2H_5OH + 2\ H_2 \rightarrow 2CH_4 + H_2O$ (Hydrogenolysis) ΔHr^0_{298K} = -157 kJ/mol

$C_2H_5OH \rightarrow C_2H_4 + H_2O$ (Dehydration) ΔHr^0_{298K} = 45.5 kJ/mol

$C_2H_5OH \rightarrow C_2H_4O + H_2$ (Dehydrogenation) ΔHr^0_{298K} = 68.9 kJ/mol

$C_2H_4O \rightarrow CH_4 + CO$ (Acetaldehyde decomposition) ΔHr^0_{298K} = -19.3 kJ/mol

$2\ C_2H_5OH + H_2O \rightarrow CH_3COCH_3 + CO_2 + 4\ H_2$
(Aldol condensation + Dehydrogenation)

$CO + H_2O \rightarrow CO_2 + H_2$ (WGS) ΔHr^0_{298K} = -41.4 kJ/mol

$CH_4 + H_2O \rightarrow CO + 3H_2$ (SMR)

$CH_4 + CO_2 \rightarrow 2CO + 2H_2$ (Dry reforming)

$CO + 3H_2 \rightarrow CH_4 + H_2O$ (Methanation) ΔHr^0_{298K} = -206.1 kJ/mol

$CO_2 + 4H_2 \rightarrow CH_4 + 2H_2O$ (Methanation) $\Delta Hr^0_{298k} = -164.8$ kJ/mol

$C_2H_4 \rightarrow$ Coke (Polymerization)

$2\ CH_3COCH_3 \rightarrow (CH_3)_2C(OH)CH_2COCH_3 \rightarrow (CH_3)_2C{=}CHCOCH_3 + H_2O$
(Acetone coupling)

$2CO \rightarrow CO_2 + C$ $\Delta Hr^0_{298K} = -172.6$ kJ/mol
(Boudouard reaction thermodynamically
favoured at low temperature)

$CO + H_2 \rightarrow C + H_2O$
(Reverse carbon gasification thermodynamically
favoured at low temperatures)

$CH_4 \rightarrow C + 2\ H_2$ $\Delta Hr^0_{298K} = 74.9$ kJ/mol
(Hydrocarbon decomposition thermodynamically
favoured at high temperature)

$C_2H_4 \rightarrow 2C + 2H_2$ $\Delta Hr^0_{298K} = -52.3$ kJ/mol

Zhurka et.al [6] have cited:

$CH_3CHO + H_2O \rightarrow CH_3COOH + H_2$

$CH_3COOH \rightarrow CH_4 + CO_2$

Ogo et.al. [1] have cited:

$2CH_3CHO \rightarrow CH_3COCH_3 + CO + H_2$ $\Delta Hr^0_{298K} = 4.1$ kJ/mol

$CH_3CHO + H_2O \rightarrow 2CO + 3H_2$ $\Delta Hr^0_{298K} = 186.8$ kJ/mol
(Acetaldehyde steam reforming)

While the yield of H_2 and the H_2/CO mole ratio are key performance metrics, the activity and stability of the catalyst are also important considerations. Thus, the catalysts for this application are expected to be multi-component compositions that promote the reactions which generate hydrogen while suppressing unwanted side reactions and catalyst deactivation.

4.2: Experimental

In the current study Ni is supported on a set of 13 metal oxide supports which are prepared by co-precipitation. These constitute lanthana and ceria in fixed concentration at nominal 5.5wt% each as minor components, and alumina, magnesia, and zirconia in variable concentrations as major components.

Binary supports consist of two components. Rare earths (lanthana and ceria) along with one of the three major components (alumina, magnesia, or zirconia), ternary (any two of the major components along with rare earths) and quaternary (all three of the major components along with rare earths, wherein the concentration of one of the major components is larger than the remaining two). Refer Table 2, chapter 3 for details.

Ternary supports are prepared both with balanced composition (equal quantities of major components by weight), and also with skewed composition wherein the concentration of zirconia or magnesia is higher than that of alumina. Ni content is varied over the range of 5-7.5-10 wt% in the case of the balanced ternary catalysts of Al-Mg and Al-Zr . Refer Table 2, chapter 3 for details.

The catalyst is sized to 0.5-1.0 mm size fraction. Reaction conditions are H_2O: EtOH 3 Molar, atmospheric pressure, LHSV $8h^{-1}$ (on liquid feed), Nitrogen: EtOH 1.0 molar. The reaction temperature is studied at five levels, 550°C, 600°C, 650°C, 700°C and 750°C. Time on stream is 8 hours. Select runs with ternary Al-Mg and all three quaternary catalysts are studied for a duration of 80 hours on stream at 650°C and 700°C at the above conditions.

4.3: Catalyst Activity and Correlation with catalyst characteristics

Catalyst activity: Catalyst activity is assessed based on ethanol conversion at the 2^{nd} hour on stream at a specified reaction temperature (other parameters being constant). As seen from Figure 53 below ethanol conversion is observed to increase with temperature for all the catalysts which is consistent with thermodynamics Matoos et.al [5].

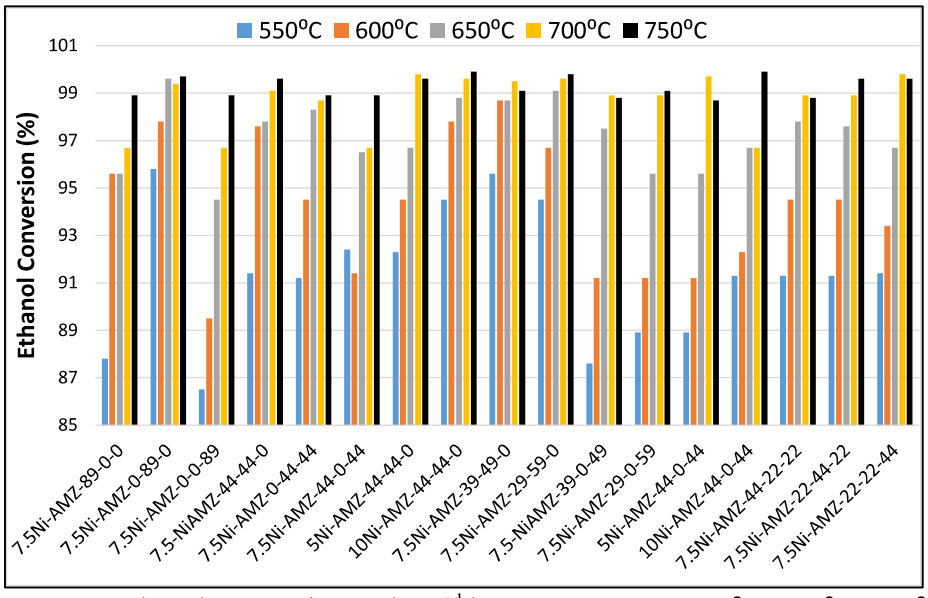

Figure 53: Ethanol conversion at the 2nd hour on stream at 550°C, 600°C, 650°C, 700°C and 750°C reaction temperature for various catalysts

Further, conversions at a given temperature depend on catalyst composition. Catalysts containing Mg show better conversion of ethanol at lower temperatures than the remaining catalysts. In the case of the ternary catalysts of Al-Mg, those with a composition skewed in favor of Mg show higher conversion at lower temperatures than catalysts with balance composition, whereas it is the reverse for ternary Al-Zr catalysts. The catalyst with a balanced composition of Al and Zr shows higher conversion at lower temperatures than the catalysts with a composition skewed in favor of Zr.

Bicomponent catalysts of Al and Mg are reported to inhibit the formation of $NiAl_2O_4$ which reduces high temperatures. This is thus reported to improve activity [7]. While activity is higher for catalysts containing Mg in the current study, it is observed to adversely affect reducibility of NiO as observed by H_2-TPR (refer Chapter 3). The higher activity is thus attributed to intrinsic higher chemical reactivity of Ni-Mg solid solution. Wurzler et.al [8] have studied Ni impregnated on precipitated MgO and identified the formation of NiO-MgO solid solution by TPR and XANES. This solid solution is reported to enhance activity and stability in dry reforming of methane [9]. Thus, incorporation of Mg is reported to improve activity. Results of the current study are consistent with those reported in literature.

To get a better understanding, the conversion at different reaction temperatures is segregated into three parts: a) conversion at 550°C, b) conversion at 600° and 650°C, c) conversion at 700° and 750°C in Figure 54 (a), 54 (b) and 54 (c) below.

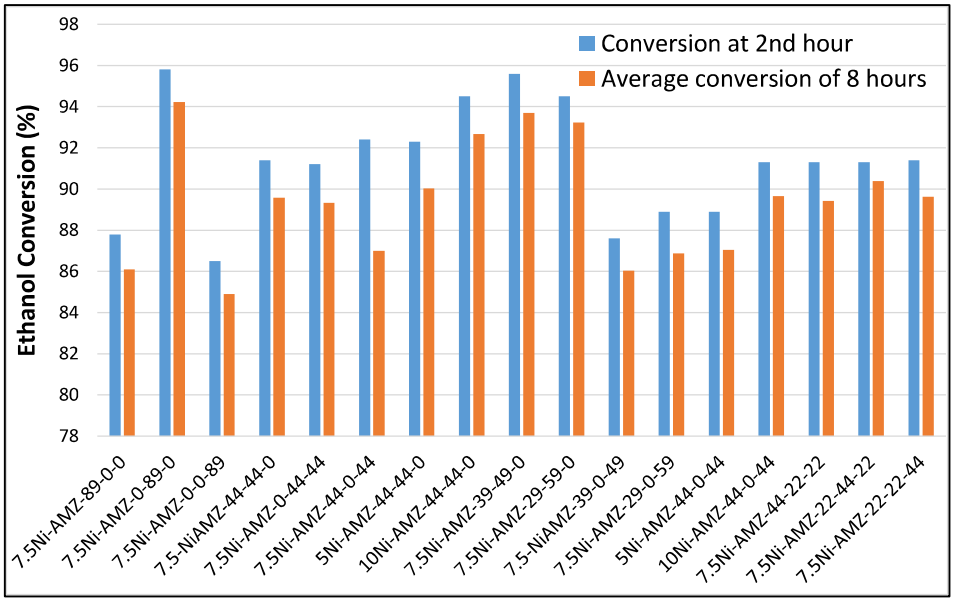

Figure 54(a): Ethanol conversion at the 2nd hour on stream and average conversion of 8hours at 550ºC reaction temperature for various catalysts.

The conversion at 2nd hour at 550°C is shown in Figure 54 (a) above. The average conversion over 8 hours is also shown for comparison. The latter reflect the trend of the former. As seen from this figure, the trends of conversion of ethanol for the catalysts are as follows. It is Mg>>Al>Zr for the binary catalysts, skewed Al-Mg>balanced Al-Mg = Mg-Zr >Al-Zr. Further, the ternary Al-Mg catalysts show the trend 10% Ni>5%Ni >7.5%Ni whereas it is 7.5%Ni >10%Ni>5%Ni for ternary Al-Zr catalysts. Thus, higher nickel content does not necessarily lead to higher conversion. The quaternary catalysts show the trend of Mg-rich=Al-rich=Zr-rich. Biswas et.al. [10] have also reported low activity for Ni supported on zirconia.

The conversion at 600°C and 650°C is shown in Figure 54 (b).

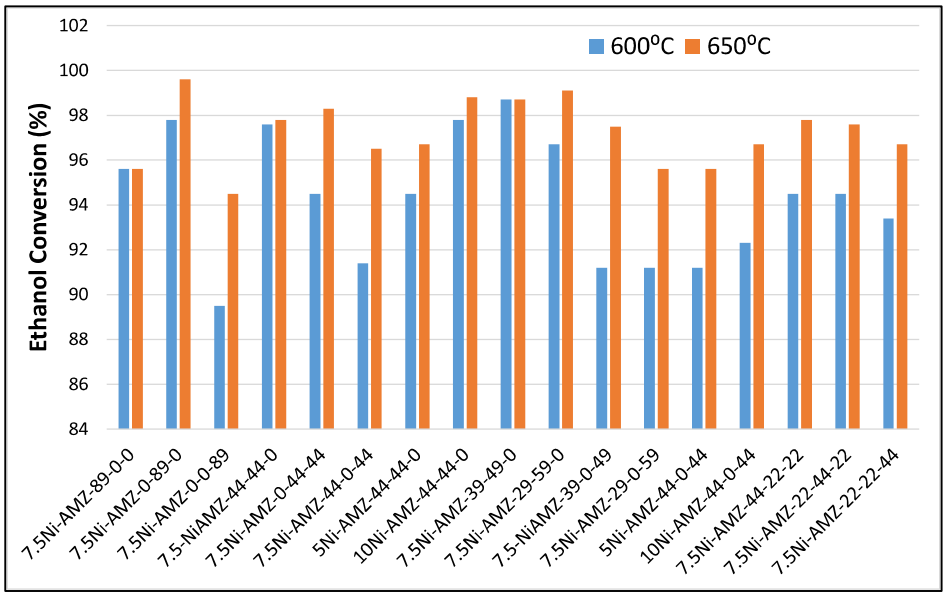

Figure 54(b): Ethanol conversion at the 2nd hour on stream at 600ºC and 650ºC reaction temperature for various catalysts

As seen from this Figure 54 (b), the trend of binary catalysts at 600°C and 650°C is Mg>Al>Zr which is the same as that at 550°C. The trend of ternary catalysts is skewed Al-Mg=balanced Al-Mg > Mg-Zr >Al-Zr. There is a slight change in the trend of Al-Mg catalysts. The quaternary catalysts show the trend Mg-rich=Al-rich>Zr-rich. The ethanol conversion observed in the current study at 650°C is similar to that obtained by Galetti et.al [11] in studies with Ni/$MgAl_2O_4$, at 650°C with S/C 4.9. They have reported conversion in the range 89.2%-97.1%.

These trends extend up to 750°C. The conversion of ethanol over the catalysts at 700°C and 750°C is shown in Figure 54(c) below.

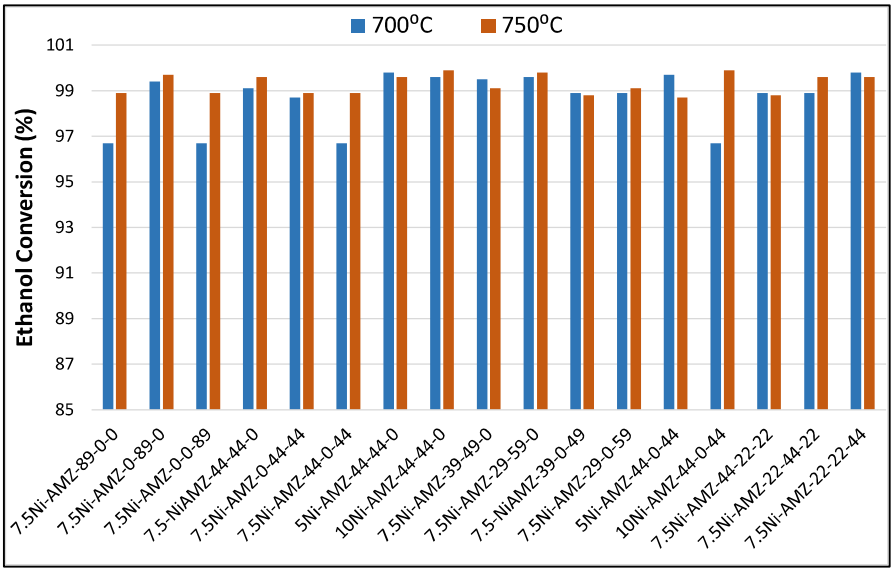

Figure 54(c): Ethanol conversion at the 2nd hour on stream at 700ºC and 750ºC reaction temperature for various catalysts

As seen from Figure 54(c), the gap in difference in activity of catalysts diminishes at the higher temperatures.

The trend of BET-specific surface area (BET SA) with ethanol conversion is shown in Figure 55 below.

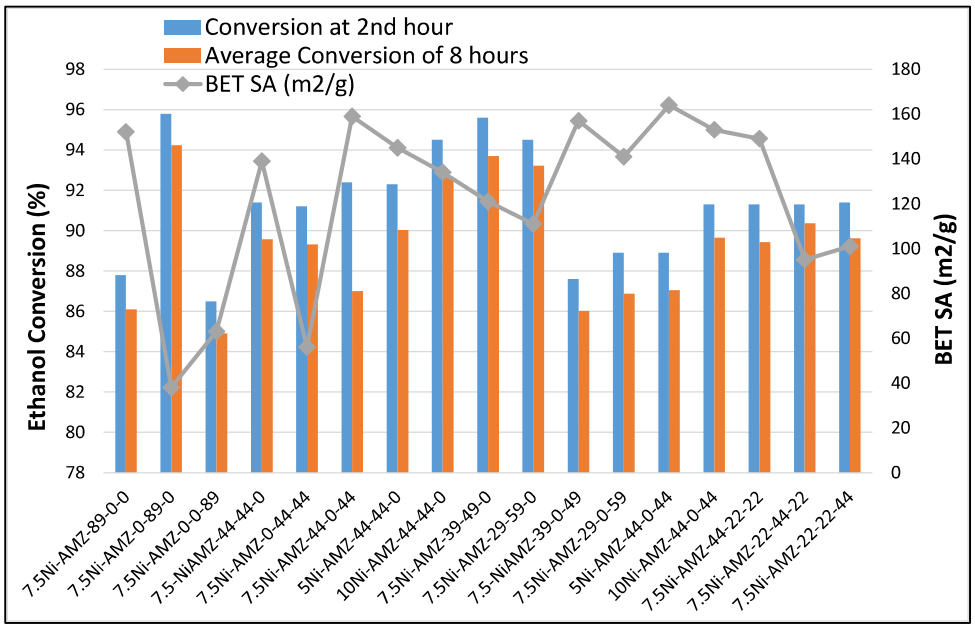

Figure 55: Correlation of BET-SA and Ethanol Conversion at 550ºC for various catalysts.

As seen from the above Figure there is no significant trend of ethanol conversion with BET specific surface area of the catalyst. The trend is random. 7.5%Ni-AMZ-0-89-0 which has a specific surface area of 38 m^2/g shows the highest activity. Similarly,

the ternary catalysts of Al-Zr with composition skewed in favor of Zr (7.5%Ni-AMZ-39-0-49 and 7.5%Ni-AMZ-29-0-59) show the highest specific surface area but amongst the lowest conversion of ethanol. Thus, conversion of ethanol is independent of BET-specific surface area. A general expectation is that active metal dispersion is dependent on the BET-specific surface area, which in turn influences conversion. In the current study it appears that other factors such as degree of reducibility (due to differences in metal support interaction) which affects active metal dispersion and intrinsic chemical reactivity play a major role. These aspects are examined in the subsequent sections of this chapter.

The trend of ethanol conversion at 550°C is plotted against the peak temperature of reduction of Ni of the catalysts observed in TPR studies in Figure 56 below. In catalysts which exhibit two reduction peaks, the terminology LT = low temperature and HT = high temperature peak is used.

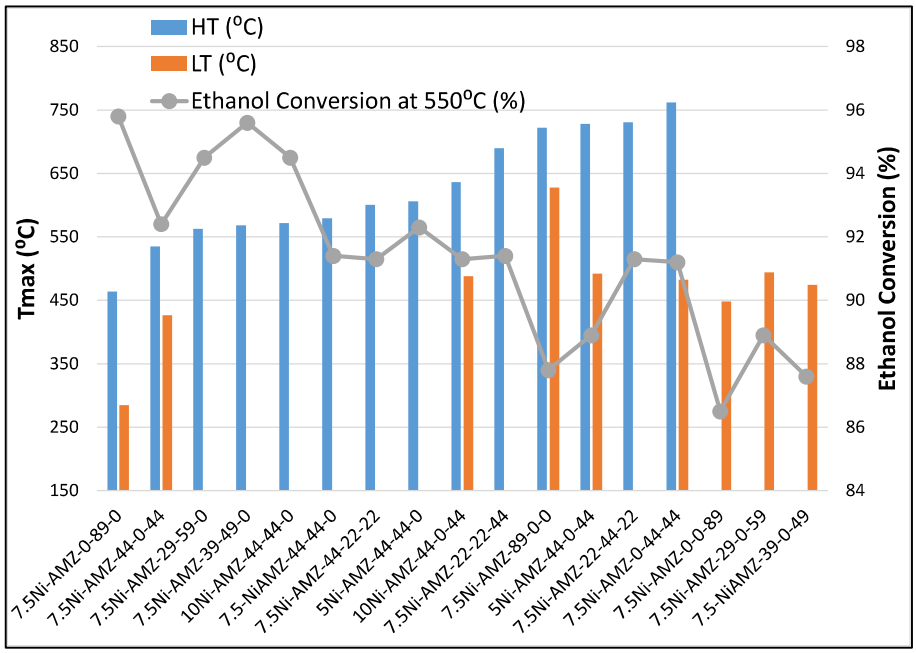

Figure 56: Trend of ethanol conversion at 550°C and peak temperature of reduction of Ni for various catalysts

As seen from the above Figure catalysts which present a high temperature reduction peak in the window 563°C -572°C show higher conversion of ethanol than the remaining catalysts in which NiO reduces at >579°C or <494°C. Incidentally, these former catalysts are ternary Al-Mg catalysts. The catalysts show the following trends of activity with a temperature of reduction of NiO:

- Binary catalyst 7.5%Ni-AMZ-0-89-0 (peak reduction temperature 464°C), shows the highest conversion (95.8%) amongst all the catalysts. NiO reduces at a low temperature (464°C) in this catalyst. TPR also indicates that a relatively small fraction of NiO (32%) reduces. Results of XRD indicate the formation of Ni-Mg solid solution, which may be the reason for the difference. It appears to have high intrinsic activity.
- Binary Al catalyst, 7.5%Ni-AMZ-89-0-0 shows significantly lower conversion (87.8%) of ethanol than binary Mg catalyst. NiO reduces at 722°C in this catalyst, which is much higher than binary Mg but not very different from that of quaternary Mg-rich catalyst, 7.5%Ni-AMZ-22-44-22 (731°C) which gives higher (91.3%) ethanol conversion. The probable cause for the lower activity of binary Al catalyst may be the formation of Nickel aluminate (as indicated by the high reduction temperature of Ni) or lower intrinsic activity.
- Ternary Al-Zr catalyst, 5%Ni-AMZ-44-0-44 Ni reduces at 728°C which is close to that of the two catalysts mentioned immediately above. It shows reducibility about 109 %. At firsthand the lower conversion of ethanol (88.9%) in this catalyst can be attributed to its lower Ni content. However, ternary Al-Mg catalyst, 5%Ni-AMZ-44-44-0, which also has 5wt% Ni shows reduction of Ni at 606°C, and reducibility of 72 % (which is lower than that of the Al-Zr catalyst) shows 92.3% conversion of ethanol (which is significantly higher than that of the corresponding ternary Al-Zr catalyst with the same Ni content). Thus, intrinsic chemical activity due to composition appears to play a role.
- Binary Zr catalyst 7.5%Ni-AMZ-0-0-89, ternary Al-Zr catalysts 7.5%Ni-AMZ-29-0-59 and 7.5%Ni-AMZ-39-0-49 show reduction temperature of NiO in the range 448-494°C which is not very different from that of binary Mg catalyst 7.5%Ni-AMZ-0-89-0 (464°C), however the former present significantly lower activity (86.5%-88.9% ethanol conversion) than the latter catalyst.
- These trends indicate that the interaction of Ni with the oxide composition of the support influences catalytic activity in ESR.

The trend of activity at 550°C, 600° and 650°C is compared with the surface area of Ni determined by O_2 chemisorption in Figure 57 (a) and 57 (b) below.

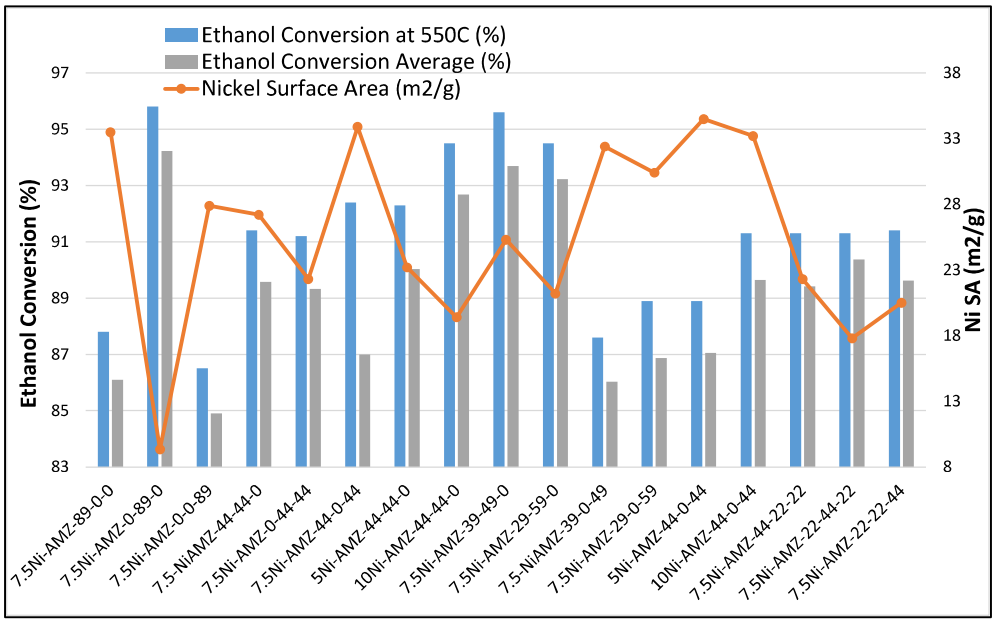

Figure 57(a): Trend of activity at 550°C is compared with a surface area of Ni determined by O_2 chemisorption.

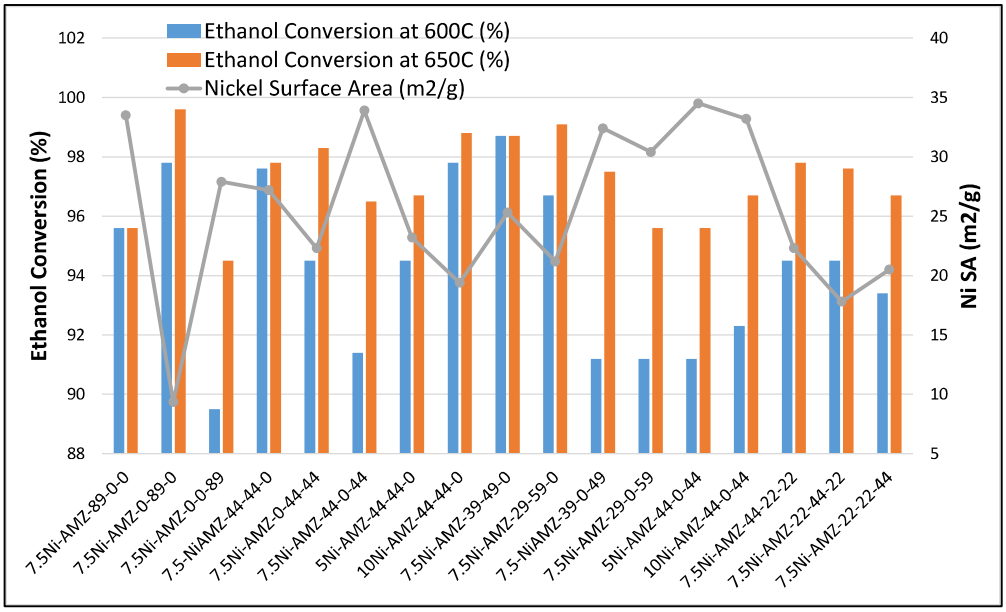

Figure 57(b): Trend of activity at 600° and 650°C is compared with a surface area of Ni determined by O_2 chemisorption.

As seen from these Figures, the trend between ethanol conversion and Ni metal surface area determined by O_2 chemisorption is random (similar to the trend with BET-specific surface area). Binary 7.5% AMZ-0-89-0 which has the lowest metal surface area shows the highest activity, whereas ternary Al-Zr catalysts 7.5%Ni-AMZ-44-0-44, 7.5%Ni-AMZ-39-0-49 and 7.5%Ni-AMZ-29-0-59, which have amongst the highest Ni metal surface area show the lowest conversion of ethanol. Ternary Al-Mg catalysts with

medium Ni metal surface area show high activity. It is to be noted that a comparison is attempted between catalysts with different compositions of support. Hence, inherent chemical reactivity, which depends on the composition of catalyst (interaction of active metal with support) has a larger influence than metal dispersion. Hyun-Seog Rho et.al. [12] too report that the composition of the support influences H_2 yield to larger extent than metal dispersion for Rh supported on γ-Al_2O_3, $MgAl_2O_4$ and ceria-zirconia.

Since some of the catalysts do not show stoichiometric / complete reduction of NiO, the particle size of Ni(0) of reduced catalysts was determined by HRTEM. A plot of the percentage conversion of ethanol in ESR studies at 550°C versus the median particle size of Ni(0) of reduced and stabilized catalysts determined by HRTEM is plotted in Figure 58 below.

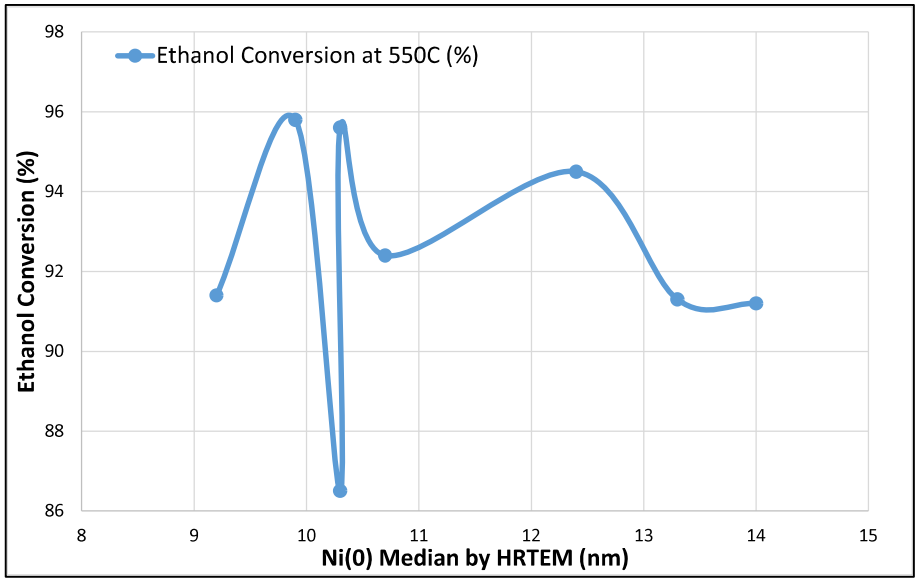

Figure 58: Plot of conversion of ethanol at 550°C versus median Ni(0) size of R&S catalysts determined by HRTEM.

The particle size of Ni(0) was determined by HRTEM in reduced and stabilized catalysts (Reduction done using 10% H_2 balance Nitrogen gas at 550°C with hold up time of 60 minutes. After Reduction catalysts were cooled down to ambient temperature under Nitrogen and stabilized by air at ambient temperature). As seen from this plot there is no clear trend of ethanol conversion with the median particle size of Ni(0). TEM micrographs are presented in Appendix 10. It is to be noted that a comparison is made between catalysts with different compositions of support.

Since the interaction of Ni(0) with supports of different compositions can complicate matters by influencing energetics of reaction differently, the effect of particle size on ethanol conversion was tested for a smaller group of catalysts with similar composition viz. Ni supported on binary Mg and ternary Al-Mg supports rich in Mg, wherein the interaction between Ni(0) and the support is expected to be similar. The plot is shown in Figure 59 below.

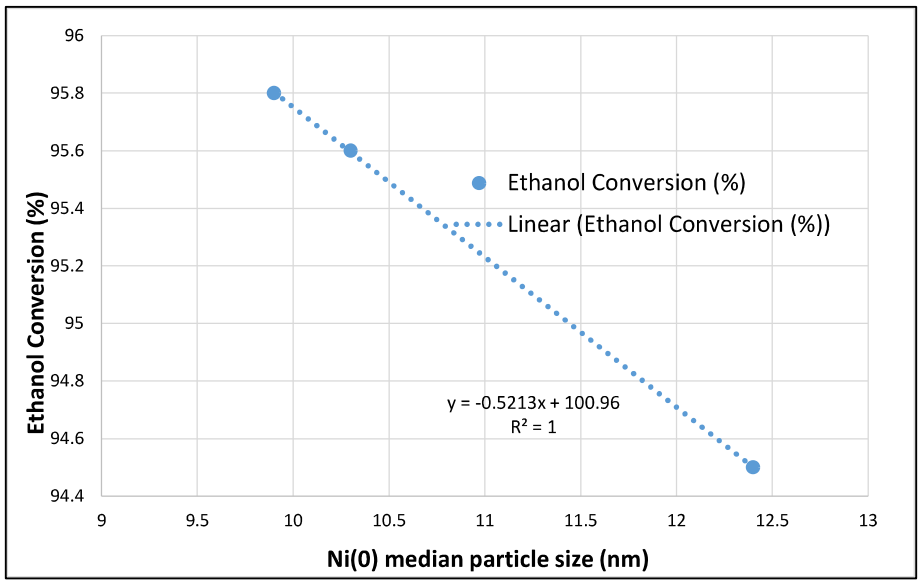

Figure 59: Plot of ethanol conversion in ESR at 550°C versus median Ni(0) particle size determined by HRTEM.

As seen from the Figure above there is a completely linear fit between the median particle size of Ni(0) and conversion of ethanol. Conversion of ethanol increases linearly with decreasing particle size of Ni(0). A change in particle size changes the distribution of facets such as terraces, steps and corners in metal particles. Ogo et.al. [1] have reviewed literature and quote references of Song et.al. [13] and Parlett et.al. [14] who have studied Ni supported on mesoporous silicas such as SBA-15 and KIT-6. They have reported that activity is dependent on particle size of nickel. Thus, it indicates that the ESR reaction may be a structure-sensitive reaction. These results are in line with those of Song et.al. who have studied steam reforming of ethanol on mesoporous Ni-alumina-zirconia and Parlett et.al. who have observed structure sensitivity when they carried out ESR with Ni supported on mesoporous silica. Both report Ni metal particle size dependent TOF for ethanol conversion.

Thus, while catalytic activity for ESR is dependent on the particle size of Ni(0) for supports with similar composition, catalytic activity is more dependent on the

inherent chemical nature/reactivity of Ni(0) which is influenced by its interaction with the specific composition of the support. Such behavior is reported by Matoss et. al. in their review [5]. Dispersion or particle size of Ni(0) is of secondary or minor importance for catalytic activity for this reaction when the comparison is made across supports of different compositions. The specific interaction of Ni(0) with the specific composition of the support influences the energetics of conversion of ethanol on the active site on these individual catalysts.

An attempt is also made to correlate the activity of the catalysts for ESR with the crystallite size of NiO in calcined catalysts. The XRD crystallite size of NiO of the calcined catalysts is plotted against the conversion of ethanol at 550°C at 2nd hour.

The XRD crystallite size of NiO of calcined catalysts is plotted against ethanol conversion at 2nd hour at 550°C in Figure 60 below.

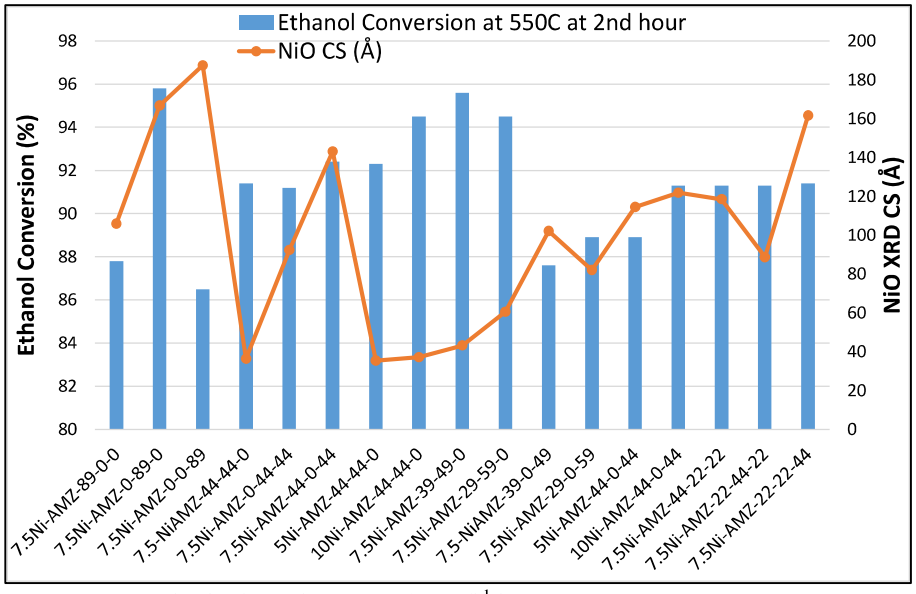

Figure 60: Trend of ethanol conversion 2nd hour on stream at 550°C versus XRD crystallite size of NiO of calcined catalysts

As seen from Figure 60 above most of the catalysts show an inverse relation between XRD crystallite size and conversion of ethanol indicating that smaller particles of NiO give higher activity. It is expected that the particle size of Ni metal in reduced catalysts will also follow the same trend as that of NiO in calcined catalysts. However, redispersion of Ni is possible during reduction which can lead to anomalies. Such redispersion is reported by Phichitkul et.al [15] and Nakayama et.al [16]. This aspect is discussed in detail in Chapter 3. Similar results of correlation between activity and XRD

crystallite size of ZrO_2 are reported for non-oxidative dehydrogenation of propane (PDH) over bare m-ZrO2 and t-ZrO_2 with crystallite size varying from 3.7 nm to 43.4 nm [6]. Yaoyuan Zhang et.al. [17] and R.Z.C. van Meerten et.al. [18] have also reported similar results for the methanation of CO with H_2. Their studies show that crystallite size ~4nm gives the highest specific activity. Thus, the conversion of ethanol appears to be a structure-sensitive reaction. Vogt et.al [19] have studied SMR (steam reforming of methane) and DRM (dry reforming of methane) on Ni/SiO_2 catalysts in operando FTIR at 500°C and 600°C, CH_4:H_2O and CH_4:CO_2 at two ratios 4:1 and 3:2. Their results (HAADF-STEM) indicate that Ni particle size of ~3 nm is optimal for both these reactions. They report that carbon nanofibers form for particles of ~4.5 nm in SMR and Ni particles ≥4.5 nm in the case of DMR. In the current study Ni(0) particle size of ~10 nm (estimated by HRTEM) shows the highest activity amongst all the catalysts. However, it should be noted that, unlike the study by R.Z.C. van Meerten et.al. [18], where all the catalysts are Ni supported on SiO_2, the catalysts of the current study vary in the composition of the support.

The yield of hydrogen in ESR at 550°C also shows a similar trend with the XRD crystallite size of NiO. This is shown in Figure 61 below.

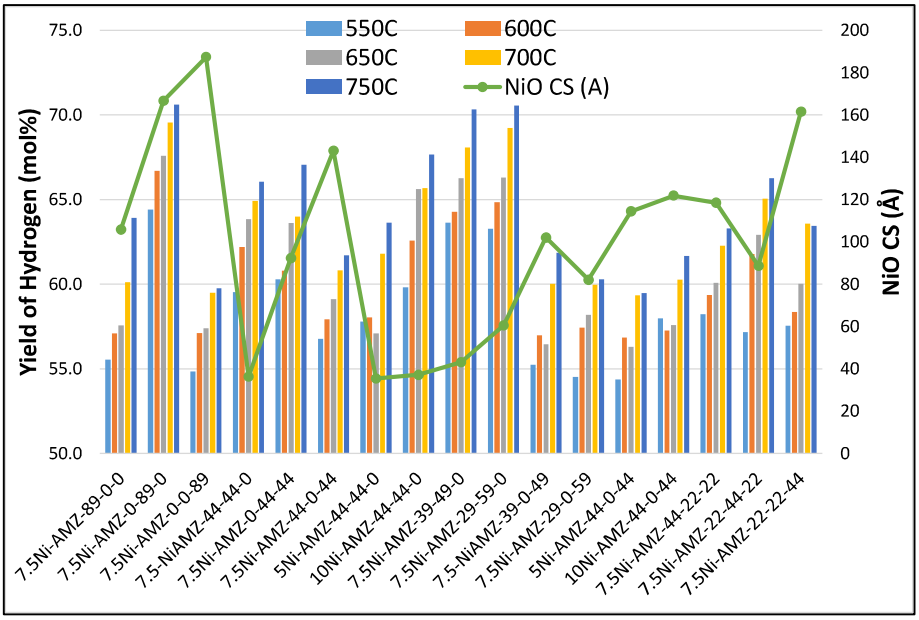

Figure 61: Plot of the yield of Hydrogen at 550°C versus XRD crystallite size of NiO in calcined catalysts.

As seen from the above figure catalysts with smaller XRD crystallite size of NiO give a higher yield of H_2. Hence, it is clear that H_2 yield is also influenced by metal dispersion.

4.4: Product Yields

The trend of H_2 yield with reaction temperature is shown in Figure 62 below.

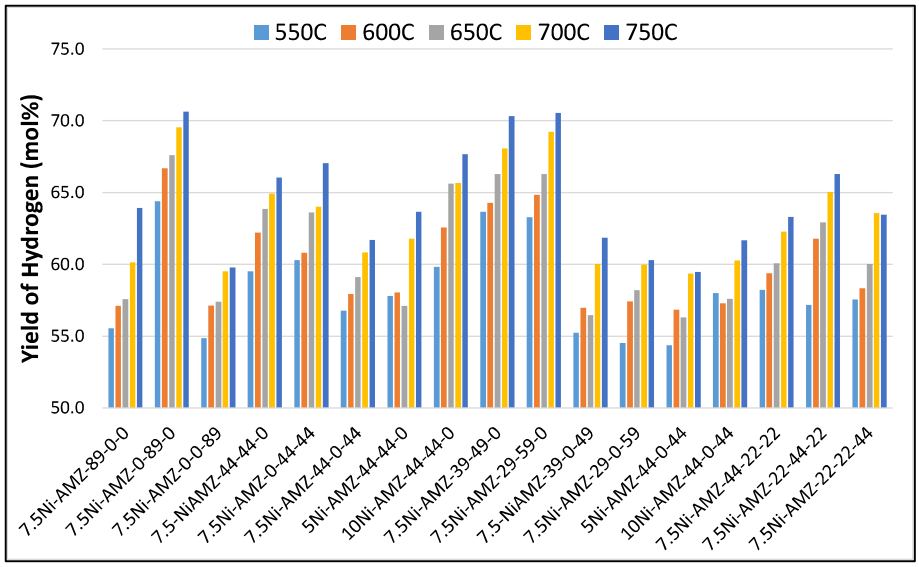

Figure 62: Trend of Yield of H_2 at various Temperatures for various catalysts

As seen from this Figure the yield of H_2 increases with increasing temperature for all the catalysts. This is consistent with the literature on thermodynamic calculations which is reviewed by Mattos et.al. [5]. The trend for binary catalysts is Mg>Al≥Zr. The trend of ternary catalysts is Skewed Al-Mg>Bal Al-Mg=Bal Mg-Zr>Bal Al-Zr>Skewed Al-Zr. This is largely similar to that of the trend of ethanol conversion. The binary Mg and ternary Al-Mg catalysts clearly show significantly larger yields than the remaining catalysts. Quaternary catalysts show the trend Mg-rich>Al-rich=Zr-rich. The Al-Mg catalysts of the current study show H_2 yields (68%-69.6%) that are comparable with that of Galetti et.al. [11] for Ni supported on magnesium aluminate promoted with rare earth Ce or Pr (H_2 yield 71%) and those of Romero et.al. [20] (H_2 yield 59%) on double layered hydroxides of Ni-Mg-Al. Wurzler et.al. [8] have studied 5wt% Ni supported on MgO supports prepared by precipitation to a final pH 10 with ageing (12 hours) and without ageing and also MgO prepared by thermal decomposition of the nitrate at 773°K 2 hours. The Ni is impregnated on the support and the catalyst calcined at 673°K (3 hours). They report H_2 selectivity around 65% which is similar to that obtained in the current study. Zhurka et.al [6] have reported thermodynamic equilibrium

yield of H_2 ~75% at 600°C, S/C: 3 at 0.7 bar. H_2 yield achieved on binary Mg and ternary Al-Mg catalysts in the current study is 64.3%-67.6% which is 86-90% of the thermodynamic equilibrium value.

Between the series binary Mg shows yields equal to skewed Al-Mg followed by balanced Al-Mg followed by ternary Mg-Zr which equals quaternary Mg-rich catalyst. The binary Zr and ternary Al-Zr catalysts show the lowest yield of H_2. The H_2 yield increases with Ni content for the ternary balanced Al-Mg series (AMZ-44-44-0). In the case of ternary Al-Zr catalysts, the catalyst with 5wt% Ni shows a lower yield than catalysts containing 7.5 and 10 wt% Ni. However, it is difficult to distinguish between the latter two.

The trend of the yield of CO with reaction temperature is shown in Figure 63 below.

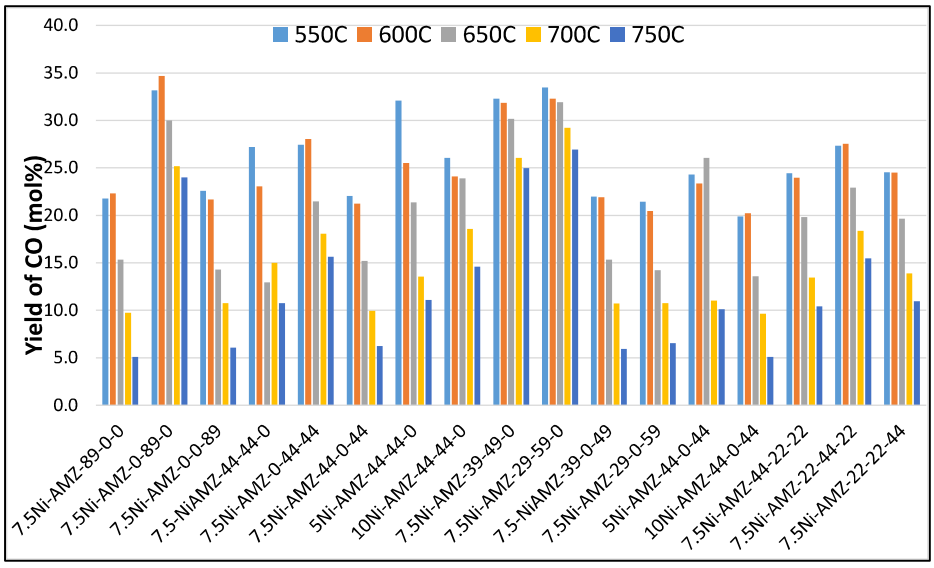

Figure 63: Trend of Yield of CO at various Temperatures for various catalysts

As seen from this Figure the yield of CO decreases with increasing reaction temperature for all the catalysts. As per thermodynamics literature which is reviewed by Mattos et.al. [1] The yield of CO is reported to increase with temperature since it is a co-product of the main steam reforming reaction. However, the WGS (water gas shift) ability of catalysts converts CO to CO_2 and H_2. A similar trend is reported by Zuogang Guo et al. [21] in the temperature range 625°C-825°C, S/C 9.2 GHSV on ethanol $345h^{-1}$. The yield of CO_2 increases while that of CO decreases with increasing temperature. Prakash Biswas et.al. [22] also report a similar trend for Ni-CeO_2-ZrO_2 catalysts doped with Cu, Co and Ca in the temperature range 400°C - 650°C. However, the results of

the latter show that while the yield of CO_2 increases with reaction temperature, that of CO does not decrease appreciably. Two other reactions which convert CO are methanation and disproportionation which produce methane and CO_2+C respectively. The trend of the yield of CO concerning catalyst composition for a given reaction temperature is similar to that of H_2. The trend of binary catalysts is Mg>Al≥Zr. In the case of ternary catalysts, it is skewed Al-Mg>Mg-Zr>Bal Al-Mg>Al-Zr. There is no differentiation between balanced and skewed Al-Zr catalysts. The quaternary catalysts show the trend of Mg-rich>Al-rich=Zr-rich. The trend in terms of values is largely similar to that of the yield of H_2. Catalysts containing Mg present higher yields of CO than those containing Zr. Ternary Al-Mg and Al-Zr catalysts with 5 wt% Ni show a higher yield of CO than the catalysts containing 7.5 or 10 wt% Ni. The binary MgO and ternary skewed Al-Mg catalysts show a smaller change in CO yield with temperature than the remaining catalysts.

Between the series binary Mg shows CO yield comparable to the skewed Al-Mg followed by Mg-Zr = quaternary Mg-rich followed by balanced Al-Mg and quaternary Al-rich or Zr-rich followed by balanced Al-Zr followed by skewed Al-Zr. The binary Zr and ternary Al-Zr catalysts show the lowest yield of CO.

The trend of the yield of CO_2 with reaction temperature is shown in Figure 64 below.

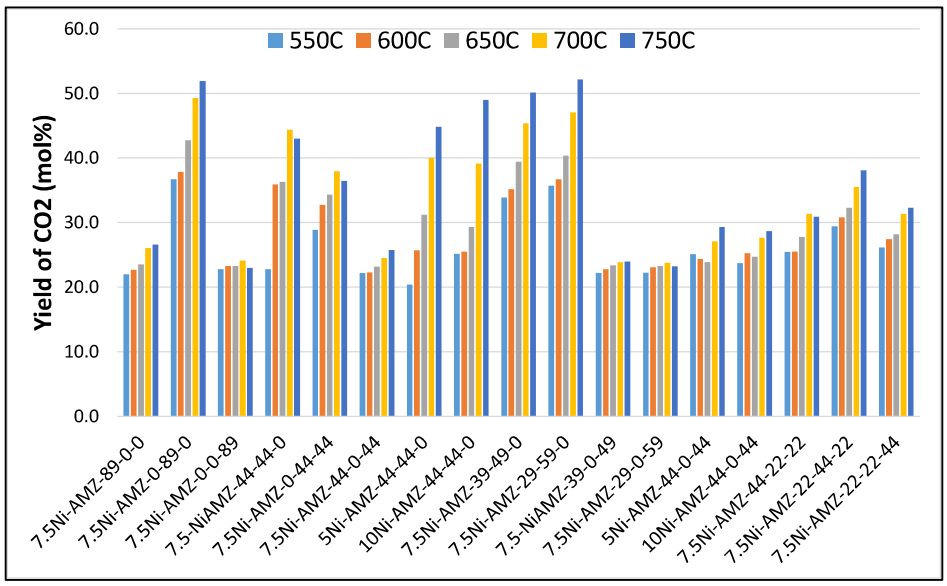

Figure 64: Trend of Yield of CO_2 at various Temperatures for various catalysts

As observed from this Figure, catalysts containing Mg show a significant increase in yield with reaction temperature, whereas those that do not contain Mg show a slight increase or a plateau. The trend of CO_2 yield for binary catalysts is Mg>>Al>Zr. For ternary catalysts, it is skewed Al-Mg> Balanced Al-Mg > Mg-Zr >balanced Al-Zr> skewed Al-Zr. The quaternary catalysts show the trend of Mg-rich>Al-rich=Zr-rich. Between the series binary Mg shows yields equal to skewed Al-Mg followed by balanced Al-Mg followed by ternary Mg-Zr which equals quaternary Mg-rich catalyst. The quaternary Al and Zr-rich catalysts show higher yields than the ternary Al-Zr catalysts. Between the series trend is binary Mg ≥skewed Al-Mg > Mg-Zr = Quat Mg-rich ≥bal Al-Mg >Quat Al-rich = Quat Zr-rich> skewed Al-Zr. There is no trend with Ni content for both the AMZ-44-44-0 and AMZ-44-0-44 series.

4.5: Reaction Mechanism

As seen from Figure 64 the trend of CO_2 yield with temperature is different from that of CO. It increases with increasing reaction temperature for all catalysts containing Mg. Within the ternary catalysts, the catalysts containing Al or Al-Mg show a clear increase in yield of CO_2 with increasing temperature over the entire temperature range studied, whereas, binary and ternary Zr-containing catalysts show a very slight increase or relative independence of yield of CO_2 with reaction temperature. Further, the binary and ternary catalysts which contain Mg show a higher yield of CO_2 compared to the remaining catalysts.

Comparing the trend of yields of CO and CO_2 from Figures 63 and Figure 64 it is observed that the decrease in yield of CO with temperature is disproportionately larger than the associated trend of change in the yield of CO_2 for these catalysts.

CO is consumed by the following reactions:

1. WGS (Water Gas Shift): $CO + H_2O = CO_2 + H_2$
2. CO Methanation: $CO + 3H_2 = CH_4 + H_2O$
3. Boudouard reaction: (CO Disproportionation) $2CO = CO_2 + C$

These reactions affect the ratios of H_2/CO, H_2/CO_2 and H_2/CH_4. These ratios are also affected by the route of reforming ethanol.

$C_2H_5OH + H_2O = 4H_2 + 2CO$ $\quad H_2/CO = 2$

$C_2H_5OH + 3H_2O = 6H_2 + 2CO_2$ $H_2/CO_2 = 3$

and the hydrogenation of ethanol [$C_2H_5OH + 2H_2 = 2CH_4 + H_2O$]

Thus, a comparison of the molar ratio of H_2/CO, H_2/CO_2 and H_2/CH_4 could provide better clarity about the actual reactions which are occurring on these catalysts.

The effect of relevant reactions (which are reported to occur in ESR) on the above three ratios is compiled in Table 4 below:

Table 4: Effect of reactions on molar ratios of H_2/CO, H_2/CO_2 and H_2/CH_4

Type	**Reaction**	**H_2**	**CO**	**CO_2**	**CH_4**	**C_2H_4**	**H_2/CO**	**H_2/CO_2**	**H_2/CH_4**	**C**
Reforming (ESR)	$C_2H_5OH + H_2O$	4	2				2			
Reforming (ESR)	$C_2H_5OH + 3H_2O$	6		2				3		
Decomposition	C_2H_5OH	1	1		1		1		1	
Hydrogenation	$C_2H_5OH + 2H_2$	-2			2		DEC	DEC	DEC	
Decomposition	CH_3CHO		1		1		DEC		DEC	
Reforming (SMR)	$CH_4 + H_2O$	3	1				3		INC	
Reforming (SMR)	$CH_4 + 2H_2O$	4		1			INC	4	INC	
Dehydration	C_2H_5OH					1				
WGS	$CO+H_2O$	1	-1	1			INC	NC		
Methanation	$CO+3H_2$	-3	-1		1		DEC	DEC	DEC	
Methanation	CO_2+4H_2	-4		-1	1		DEC	DEC	DEC	
Boudouard	2CO		-2	1			INC	DEC		1
Decomposition	CH_4	2					INC	INC	INC	1
Decomposition	C_2H_4	2								2

INC: Increases, DEC: Decreases. **Note: Water formation is not shown in Table

The trend of H_2/CO with reaction temperature is shown in Figure 65 below.

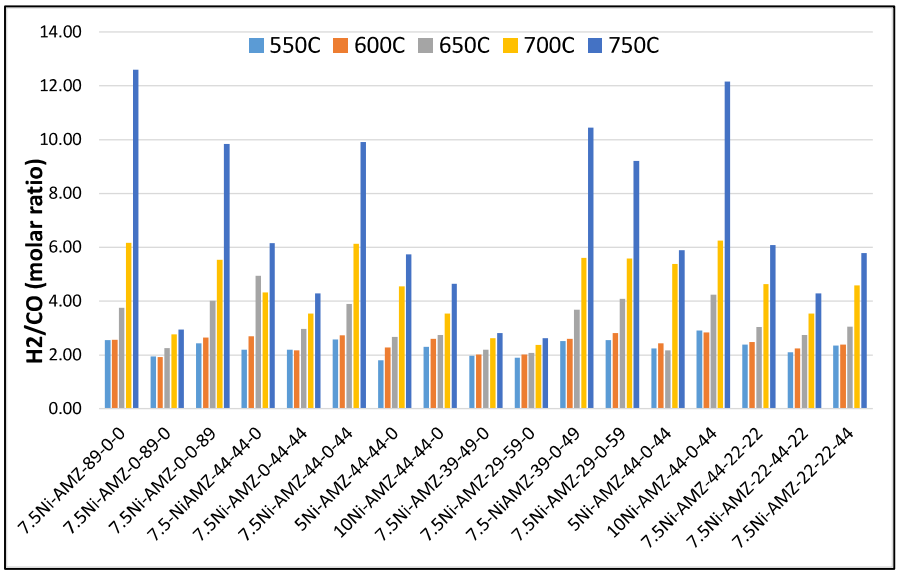

Figure 65: Trend of H_2/CO molar ratio at various reaction temperature

As seen from this Figure the trend increases exponentially with reaction temperature. The increase is significantly larger for catalysts that do not contain Mg than for catalysts that contain Mg. The ratio is about 2-2.5 at 550°C and 600°C and increases to about 3-4 at 650°C and further to about 6 and 10-12 at 700°C and 750°C. Catalysts that contain Mg show a significantly smaller increase with increasing reaction temperature. A sharp increase is observed from 700°C onwards for catalysts that do not contain Mg. This trend of increase in H_2/CO at ≥700°C is larger in the quaternary catalysts than in binary and ternary catalysts which contain Mg. This behavior is attributed to the presence of Zr in the former catalysts.

The trend of H_2/CO_2 with reaction temperature is shown in Figure 66 below.

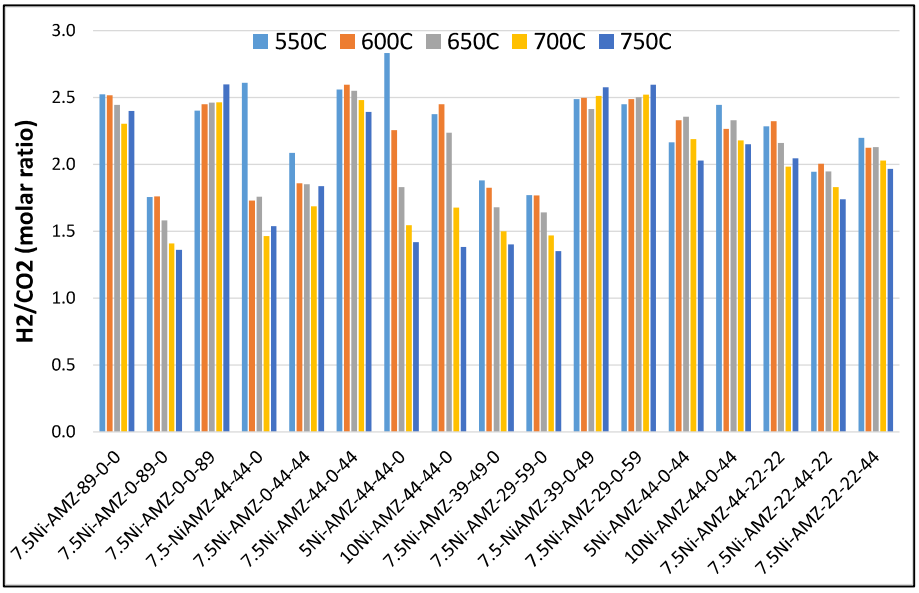

Figure 66: Trend of H_2/CO_2 molar ratio at various reaction temperature

As seen from this figure a clear decrease in ratio is observed for all catalysts which contain Mg. The catalysts which do not contain Mg show an almost independent trend (plateau) with increasing reaction temperature. Further, the ratio is higher for catalysts not containing Mg.

The trend of the ratio of H_2/CH_4 with reaction temperature is shown in Figure 67 below.

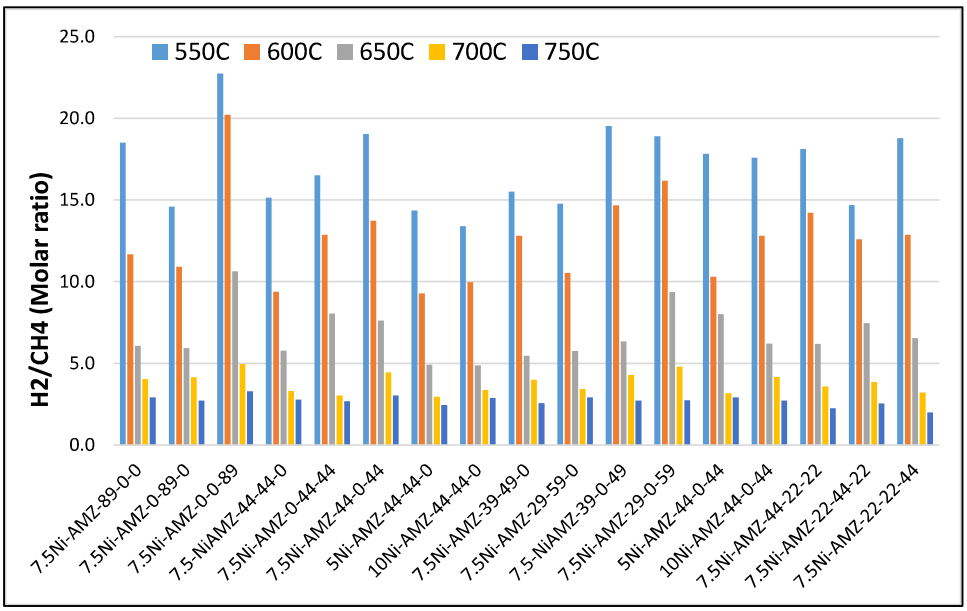

Figure 67: Trend of H_2/CH_4 molar ratio at various reaction temperature

As seen from this Figure the ratio decreases exponentially with increasing temperature for all catalysts. The decrease is significant in the temperature range 650°C to 750°C. Amongst the binary catalysts, the trend is Zr > Al ≥ Mg. In the case of ternary catalysts, the trend is Al-Zr > Al-Mg. There is no significant difference between catalysts with balanced and skewed compositions. There is also no significant difference in trend with composition amongst the quaternary catalysts.

Thus, to summarize trends of the ratios of H_2 with CO, CO_2 and CH_4 with increasing reaction temperature:

- H_2/CO ratio (Figure 65) increases with increasing reaction temperature. Value is close to 2 in the temperature range 550°C-600°C and increases sharply with further increase in temperature for catalysts containing Zr and slightly for catalysts containing Mg. The yield of H_2 increases (Figure 62 above) whereas the yield of CO decreases (Figure 63 above) indicating that the increase in the ratio is clearly due to the consumption of CO with associated formation of H_2. There is a sharp (exponential) increase in the ratio between 650°C and 750°C for catalysts containing Zr, whereas the change is slight for catalysts containing Mg.
- H_2/CO_2 ratio (Figure 66) decreases mostly linearly for catalysts containing Mg, whereas it is largely independent of temperature for those catalysts which do not contain Mg. The yield of H_2 (Figure 62) increases for all catalysts, whereas the yield of CO_2 (Figure 64) increases sharply (exponentially) for catalysts containing Mg and slightly for catalysts that do not contain Mg. Thus, the overall decrease in the ratio H_2/CO_2 is attributed to the generation of relatively more CO_2 than H_2 or partial consumption of the H_2 produced in some other reaction that does not involve CO_2.
- H_2/CH_4 ratio (Figure 67) decreases exponentially with increasing temperature for all catalysts. Yields of both H_2 (Figure 62) and CH_4 (Figure71) increase with temperature, whereas their ratio decreases. The change in the ratio (decrease) is significant (exponential) from 650° to 750°C.

These trends indicate the following:

1. A value close to 2 for H_2/CO ratio indicates that the reaction $C_2H_5OH + H_2O = 2CO + 4H_2$ (water lean reforming) predominates at lower temperatures for all

the catalysts. Although the S/C ratio of reactants is 3, competition from WGS appears to limit the availability of H_2O for the reforming of ethanol by the reaction $C_2H_5OH + 3H_2O = 2CO_2 + 6H_2$.

2. In the case of binary catalysts of Al or Zr, ternary catalysts of Al-Mg with balanced composition and ternary catalysts of Al-Zr and all quaternary catalysts the H_2/CO increases (Figure 65) whereas H_2/CO_2 remains largely unchanged with an increase in reaction temperature (Figure 66) for binary Zr and ternary Al-Zr catalysts which are rich in Zr (skewed composition). The ratio of H_2/CO_2 is 2.5 for catalysts containing Zr. Yields of H_2 and CO_2 (Figures 62 and 64) increase with temperature whereas that of CO decreases (Figure 63). As seen from Table 4 such a trend is consistent with WGS (Water Gas Shift) reaction where CO reacts with water to form CO_2 and H_2. $CO + H_2O = CO_2 + H_2$. Equimolar quantities of H_2 and CO_2 are formed because of which the ratio of H_2/CO_2 remains unchanged while the ratio of H_2/CO increases.
3. In the case of binary and ternary catalysts containing Mg with skewed composition, H_2/CO ratio (Figure 65) is close to 2 at 550°C - 600°C and increases to 2.6-2.9 with an increase in temperature above 600°C. These catalysts are Mg-rich. Whereas the H_2/CO_2 ratio (Figure 66) which has a value of about 1.75-1.85 decreases to about 1.4 with increasing reaction temperature. Since yields of both H_2 and CO_2 (Figures 62 and 64) increase with temperature, whereas that of CO decreases (Figure 63), this trend requires the formation of CO_2 without change in H_2 (such as Boudouard reaction $2CO = CO_2 + C$). Or at least part of the ethanol which is reacting switches to a water-rich reactant case viz. $C_2H_5OH + 3H_2O = 6H_2 + 2CO_2$. Between the two reactions the occurrence of the latter reaction increases the H_2/CO_2 ratio, hence it is inferred that the Boudouard reaction (disproportionation of CO) takes place in these Mg-rich catalysts. It consumes two moles of CO and produces 1 mole of CO_2 without producing or consuming any H_2. This explains the trend of a slight increase in H_2/CO with an attendant decrease in H_2/CO_2.
4. The ratio of H_2/CH_4 (Figure 67) decreases sharply with temperature from 650°C-750°C, whereas the H_2/CO ratio (Figure 65) increases sharply in the same temperature range. The hydrogenation of ethanol: $C_2H_5OH + 2H_2 = 2CH_4 + H_2O$ consumes 2 moles H_2 per mole ethanol to produce 2 moles CH_4, which

results in a decrease in the H_2/CH_4 molar ratio. The methanation of CO [$CO + 3H_2 = CH_4 + H_2O$] results in a larger decrease in H_2/CH_4 because it consumes 3 moles of H_2 to produce 1 mole of CH_4. This latter reaction would, however, decrease the H_2/CO ratio unless additional H_2 is formed by some other reaction such as the decomposition of ethanol ($C_2H_5OH = CO + 3H_2 + C$) or steam reforming of ethanol in the steam-rich environment ($C_2H_5OH + 3\ H_2O = 6H_2 + 2\ CO_2$). Water is also available from the dehydration of ethanol ($C_2H_5OH = C_2H_4 + H_2O$). It is observed that yield of ethylene increases with increasing reaction temperature (Figure 68 below). Amongst these reactions $C_2H_5OH + 3\ H_2O = 6H_2 + 2\ CO_2$ produces (the highest) 6 mole H_2/mole Ethanol and also coproduces CO_2. Hence the probability of this reaction occurring along with the methanation of CO is high at higher temperatures. The exact reactions taking place could not be identified. Methanation of CO_2 is ruled out because the H_2/CO_2 ratio decreases with increasing reaction temperature. However, the methanation of coke at the higher temperatures is still possible. It is consistent with the markedly slower deactivation at higher temperature (see sections on catalyst stability below).

The trend of the yield of ethylene with catalyst composition is shown in Figure 68 below.

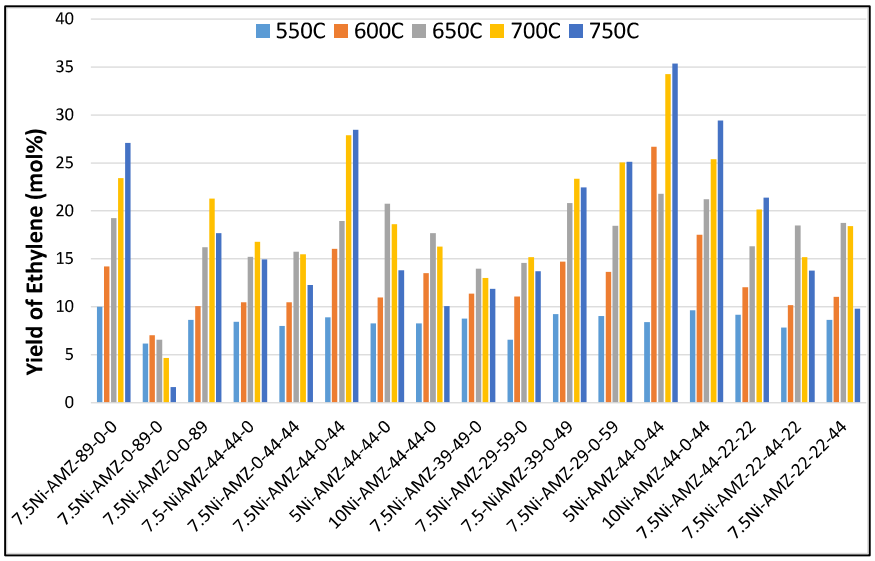

Figure 68: Trend of Yield of Ethylene at various Temperatures for various catalysts

As seen from this Figure the trend with composition for binary catalysts is Al>Zr>Mg. Vizcaino et.al. [23]. has studied the effect of Mg on Ni/Al_2O_3 catalysts.

They have prepared Mg(II)Ni(II)Al(III) layered double hydroxides (LDH) by homogeneous alkalization method with (Ni+Mg)/Al 3 (atomic) and Mg/Ni atomic 0-4. They have tested the catalysts for ESR at 650°C, S/C 5.5 atmospheric pressure, 14h on stream. They report higher yields of H_2 and significantly lower coke formation on the LDH catalysts when Mg/Ni ≥0.5 (atomic). However, the quantity of coke deposited on their catalysts ranges from 15-22 wt% as against 50-52 wt% when Mg/Ni ≤ 0.1. The higher yield of H_2 is attributed by them to availability of more ethanol for steam reforming due to decreased selectivity of ethanol dehydration, and the concurrent reforming of methane (byproduct). The lower selectivity to ethylene by dehydration of ethanol is attributed to low acidity of the catalysts. However, they have not characterized the catalysts for acidity. The results of the current study do show a relation between acidity and ethylene yield; however, yield of methane increases with reaction temperature. The difference could be due to the significantly lower S/C which is 3 in the current study compared to that of Vizcaino et.al.

In the current work, the 7.5%Ni-AMZ-0-89-0 catalyst of the current study also shows a lower yield of ethylene as well as lower acidity by ammonia TPD. Trend is Mg < Zr < Al.

The ternary catalysts of Al-Mg also show significantly lower yield of ethylene. For ternary catalysts, the trend is balanced Al-Zr > Skewed Al-Zr >balanced Al-Mg>skewed Al-Mg. Catalysts with 5wt% Ni show a higher yield of ethylene than those containing higher Ni content (7.5 or 10 wt%) indicating lower surface coverage of the support at 5 wt% Ni content. Quaternary catalysts show the trend Al-rich>Zr-rich=Mg-rich. Between the series, the trend is balanced Al-Zr ternary=binary Al>skewed Al-Zr>binary Zr≥ quaternary Al-rich> quaternary Zr-rich>balanced Al-Mg=Mg-Zr>skewed Al-Mg. Also seen from this Figure, the yield of ethylene increases with increasing reaction temperature for catalysts having either Al or Zr or their combination. Whereas, it shows a maxima with temperature at about 650°C in the case of catalysts containing Mg.

The trend of strong acidity determined by NH_3-TPD is overlaid with the yield of ethylene at 550°C and 750°C in Figure 69 below.

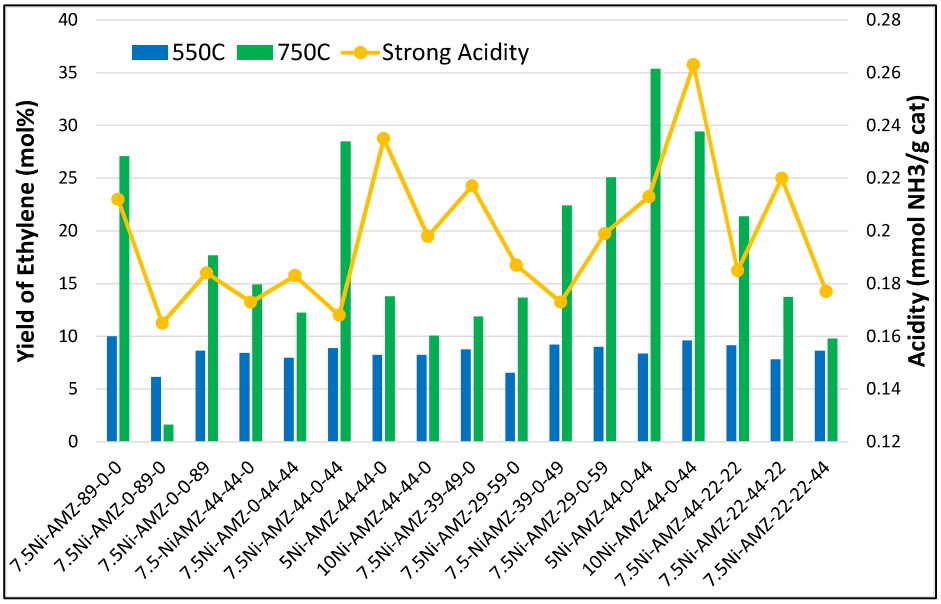

Figure 69: Trend of Strong acidity of catalysts and corresponding Yield of Ethylene at 550°C and 750°C.

As seen from this Figure the catalysts containing Al or Zr or their combination show a significantly higher yield of ethylene at 750°C. This also correlates qualitatively with the trend of strong acidity of these catalysts. However, the acidity trend of ternary Al-Mg catalysts does not correlate well with yield of ethylene. The yield is significantly low in spite of higher acidity. Ethylene is reported to form by dehydration on acidic supports such as Al_2O_3 and as well as on basic catalysts such as $MgAl_2O_4$ by Rho et.al.[12]. These authors have studied Rh supported on γ-Al_2O_3, $MgAl_2O_4$ and ceria-zirconia and observe that the basic $MgAl_2O_4$ also forms ethylene with lower yield than on γ-alumina. Alessandro Di Michele et.al [24] have studied ESR on Ni supported on $MgAl_2O_4$. The support is prepared by precipitation and Ni content varied from 1.5 to 10wt%. They report an increase in acidity with increasing Ni content with attendant formation of ethylene byproduct (41%-77% selectivity at 400°C-625°C, S/C: 3). However, neither Rho et. al. nor Alessandro Di Michele et. al. have compared the acidity with that of Ni supported on γ-Al_2O_3.

Navarro et.al [25] have studied M_xO_y-Al_2O_3 catalysts, where M= Zr, Ce, La or Mg, M/Al 0.035 (atomic) at S/C of 3, atmospheric pressure and 500°C for 24 hours. They report 18%-20% selectivity of ethylene for the Ni on Al-Mg catalysts, which is not very different from that of the remaining catalysts. The acidity reported by them is also within a narrow range 3.61-4.31 mmol NH_3/g cat, but an order of magnitude higher

than that reported in other studies, including the current study. The reason for the narrow range in acidity and ethylene yield appears to be the low concentrations of the promoters (7.0 wt% ZrO_2, 8.4 wt% CeO_2, 5.0 wt% La_2O_3 and 2.5 wt% MgO balance Al_2O_3) when compared to the concentrations used in the current study which range from 39-59 wt%. Significant differences in acidity and selectivity to ethylene with catalyst composition is observed in the current study.

The trend of the yield of methane with catalyst composition is shown in Figure 70 below.

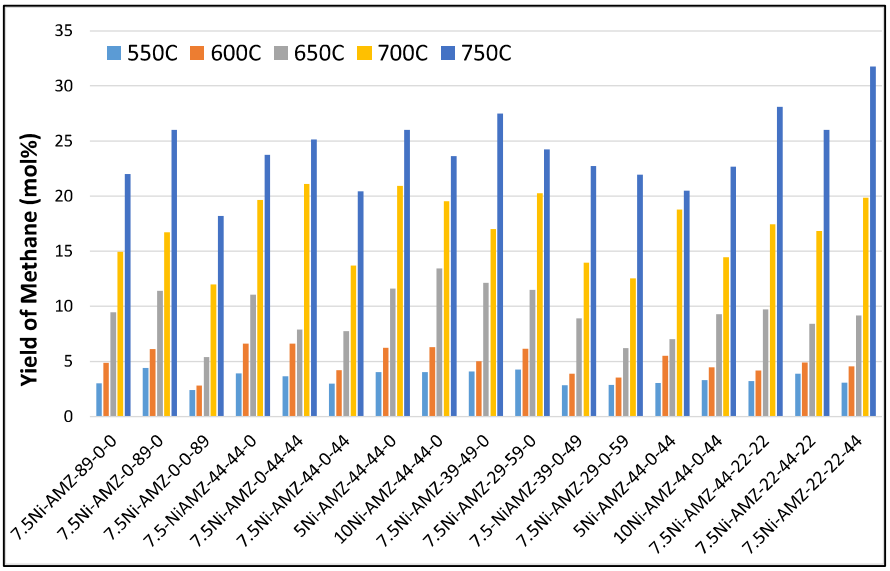

Figure 70: Trend of the yield of CH_4 with reaction temperature.

As seen from this Figure, the trend of the yield of CH_4 for the binary catalysts is Mg>Al>Zr. For ternary catalysts, it is skewed Al-Mg≥Mg-Zr≥Balanced Al-Mg>skewed Al-Zr>Balanced Al-Zr. For quaternary catalysts, the trend is Zr-rich>Al-rich≥Mg-rich. Between the series, quaternary catalysts show yield ≥ skewed Al-Mg and Binary Mg. The remaining catalysts show lower yields comparable to each other.

Methane can form from the following reactions:

Decomposition of ethanol: $C_2H_5OH = CH_4 + CO + H_2$ (Produces CO, H_2 and CH_4)

Hydrogenation of ethanol: $C_2H_5OH + 2H_2 = 2CH_4 + 2H_2O$

Methanation of CO: $CO + 3H_2 = CH_4 + H_2O$ (Consumes H_2 and CO to produce CH_4)

Methanation of CO_2: $CO_2 + 4H_2 = CH_4 + 2H_2O$ (Consumes H_2 and CO_2 to produce CH_4)

Hydrogenation of coke: $C + 2H_2 = CH_4$

As seen from Figure 70 the yield of methane increases exponentially with increasing reaction temperature for all the catalysts. Binary and ternary catalysts containing Mg show a relatively higher yield of CH_4 at higher temperatures. All three quaternary catalysts also show relatively higher yields. Literature on thermodynamic calculations which is reviewed by Mattos et.al. [5] shows that yield of CH_4 passes through a maxima between 200°C-300°C and then decreases due to its steam reforming. The trend of the current study is contrary to this. As explained in detail in the section above, the increase in the yield of methane with reaction temperature can be attributed to the methanation of CO occurring concurrently with the steam reforming of ethanol under water-rich conditions. An alternate possibility is the methanation of coke at the higher reaction temperatures. This is consistent with the markedly slower deactivation observed at higher reaction temperature (see sections below).

4.6: Catalyst Stability: Screening runs

The decay constants (which are the slopes of ethanol conversion versus time on stream) for different catalysts at 550°C and 750°C are shown in Figure 71 below. The catalysts were operated at LHSV $8h^{-1}$, atmospheric pressure, S/C: 3, with Nitrogen diluent (Nitrogen /EtOH 1.0 molar) for a duration of 8 hours.

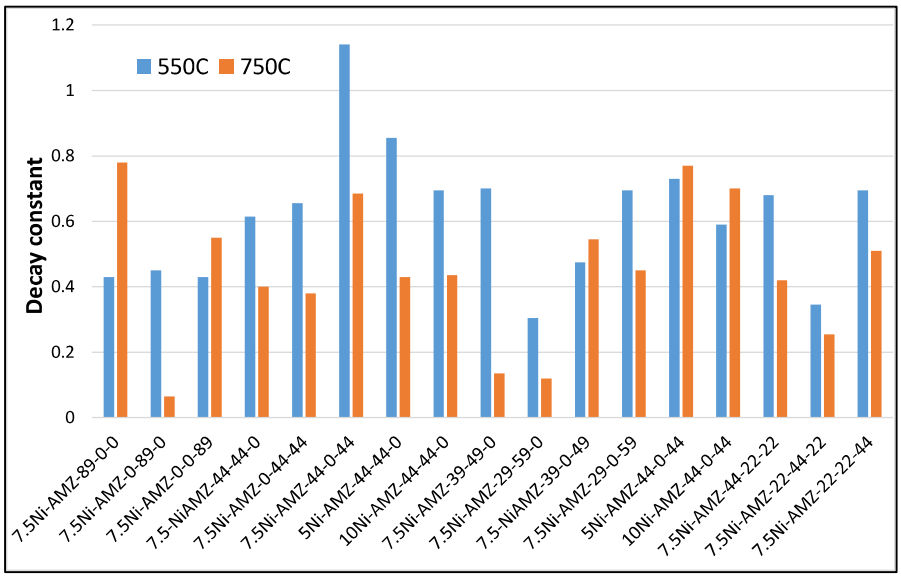

Figure 71: Decay constants of different catalysts at 550°C and 750°C

As seen from the Figure, decay constants are significantly smaller for most of the catalysts at 750°C than at 550°C. Binary alumina, binary zirconia and ternary Al-Zr catalysts with balanced composition are outliers to this trend. Thus, deactivation is considerably slower at 750°C. Similar results are reported by Wang et.al. [26] for steam reforming with Co/CeO_2 catalysts. They report severe deactivation when the reaction is carried out at 350°C-450°C with metal particles covered by encapsulating coke. Increasing reaction temperature to 500°C-550°C improves catalyst stability and the type of carbon changes to filamentous. This indicates that the latter type of coke does not affect activity as much as encapsulating type of coke. Llorca et.al [27] also report similar change in coke morphology with reaction temperature for Co supported on ZnO. The trend of value of decay constant at 750°C is Mg<Zr<Al for binary catalysts. It is Skewed Al-Mg< Balanced Al-Mg = Balanced Mg-Zr<skewed Al-Zr<Balanced Al-Zr for the ternary catalysts. The trend with Ni content is 10wt% Ni < 7.5wt% Ni < 5wt%Ni for the ternary balanced Al-Zr catalysts. The ternary Al-Mg catalysts do not show any specific trend with Ni content. The quaternary catalysts show the same trend as the binary catalysts Mg<Al<Zr. Between the series, the trend is Binary Mg <skewed Al-Mg<quaternary Mg-rich<balanced Al-Mg=Mg-Zr=Quaternary Al-rich<skewed Al-Zr<quaternary Zr-rich=Binary Zr<balanced-Al-Zr<binary Al.

Notably, the ternary Al_2O_3-ZrO_2 and binary ZrO_2 supports show the highest OSC (oxygen storage capacity), which is reported to oxidize coke, yet they show faster deactivation than the ternary Al_2O_3-MgO and binary magnesia catalysts. However, for equitable Ni content, within the ternary Al-Zr series decay constants decrease with increasing zirconia content of support. Thus, OSC appears to influence deactivation in ESR. Similar results are reported by Paula Osorio Vargas et.al. [28] who have studied Ni/Al_2O_3 promoted with La_2O_3 and CeO_2 for ESR. The lanthana content is fixed at 15wt% while the ceria content is varied from 5-15 wt% in their studies. The promoters and Ni are impregnated on the Al_2O_3. ESR is carried out at S/C of 3, 400°C-650°C atmospheric pressure for 24 hours. The authors report slower decay in conversion of ethanol with time on stream and also less coke deposition with increasing ceria content. They attribute this to oxygen mobility of ceria which brings about coke gasification.

Galetti et.al. [11] have reported decay in conversion ranging from 2.2-6.6% (for Ce promoted catalyst) and 14.7-31.1% (for Pr promoted catalyst) in 350 minutes on

stream for Ni supported on magnesium aluminate (1:1 MgO: Al_2O_3) promoted with rare earth Ce or Pr. Excepting for the Ce-promoted catalyst prepared with Ni acetate as a precursor, the decay is significantly higher than that observed in the current study despite a higher S/C ratio (4.9:1) in their studies. The reason for this appears to be the oxygen storage capacity of Ceria which is reported to scavenge coke.

According to Mattos et.al [5] who have reviewed literature on ESR, studies in literature attribute deactivation in steam reforming catalysts to coke laydown and/or sintering of Ni. The former is reported to be much faster than the latter. Based on a compilation of literature data, coke formation is reported to take place due to the following reactions:

C_2H_4 = Coke (Ethylene polymerization). Does not influence H_2/CO or H_2/CO_2 or H_2/CH_4 ratios directly.

$C_2H_4 = 2C + 2H_2$. Increases H_2 thus influencing (increasing) H_2/CO or H_2/CO_2 or H_2/CH_4 ratios.

$2CH_3COCH_3 = (CH_3)_2C(OH)CH_2COCH_3 > (CH_3)_2C{=}CHCOCH_3 + H_2O$ (Acetone coupling) Does not influence H_2/CO or H_2/CO_2 or H_2/CH_4 ratios.

$2CO = CO_2 + C$ (Boudouard reaction thermodynamically favored at low temperature). Increases H_2/CO and decreases H_2/CO_2.

$CO + H_2 = C + H_2O$ (Reverse carbon gasification thermodynamically favored at low temperatures). Does not influence H_2/CO but decreases H_2/CO_2 and H_2/CH_4.

$CH_4 = C + H_2$ (Hydrocarbon decomposition thermodynamically favored at high temperature). Increases H_2/CO, H_2/CO_2 and H_2/CH_4

In light of the ratios of H_2 with CO, CO_2 or CH_4 with increasing reaction temperature observed in the current study, it appears that the Boudouard reaction which increases H_2/CO and decreases H_2/CO_2 is the most likely reaction responsible for coke deposition. However, the Boudouard and reverse carbon gasification reactions are reported to be favored at lower temperature whereas hydrocarbon decomposition of methane and/or ethylene are favored at higher temperature. In the current study both methane and ethylene are observed to increase with increasing reaction temperature, hence coke laydown by these reactions cannot be ruled out.

Thermodynamic calculations by Rabenstein and Hacker [29] show a maximum in coke formation with increasing reaction temperature at a given S/C. The coke content decreases and shifts to a lower temperature progressively with increasing S/C. Coke content is predicted to be negligible above 277°C (550°K) for S/C of 3. Higher temperatures 800°C at S/C (3.0) is reported to decrease carbon laydown compared to 500°C on Pt supported on ceria-zirconia by Sania de Lima et.al. [30]. Similar results are observed in the current study. Deactivation of catalysts operated at 750°C is significantly slower in comparison to 550°C in the current work. Experimental data showing faster deactivation at lower temperatures and higher space velocity is also reported by Hyun-Seog Roh et.al. [12] for $Rh/Ce_xZr_{1-x}O_2$ and by Sania de Lima et.al. [30] for 1.5wt% $Pt/CeZrO_2$ [30]. Oxygen mobility [31] and acidity [32, 33] are reported to influence coke formation. The data of the current work is consistent with these studies which are reported in the literature.

Coke laydown can be partially reversed by the following reactions:

Steam gasification or hydrogasification. These processes are used for producing SNG (synthetic natural gas) from coal or biomass. The non-catalytic reaction requires severe reaction conditions viz. 850-1200°C, 7 MPa, H_2 pressure. The subject has been reviewed by Saraceno et.al. [34]. The reaction produces a mixture of H_2, CH_4, CO and CO_2. The CO and CO_2 are further hydrogenated to SNG in presence of H_2. Catalysts such as Rh, Pt, Pd, Ru or Fe, Co, Ni are used for decreasing reaction temperature down to 600°C.

These reactions and their influence on ratios H_2/CO, $H_2/CO2$ and H_2/CH_4 are provided below.

Steam gasification of coke/carbonaceous compounds:

$C + H_2O = CO + H_2$. Reaction Number: 1 (Both CO and H_2 are produced in equimolar hence, H_2/CO is not affected, whereas H_2/CO_2 and H_2/CH_4 are expected to increase.

$C + 2\ H_2O = CO_2 + 2H_2$. Reaction Number: 2 ($H_2/CO$ and H_2/CO_2 increase)

$2C + 2H_2O = CH_4 + CO_2$ Reaction Number: 3 (H_2/CO_2 and H_2/CH_4 decrease)

Hydrogasification viz. Hydrogenation of Coke/carbonaceous compounds:

$C + 2H_2 = CH_4$ Reaction Number: 4 (which consumes H_2 and produces CH_4) This reaction decreases H_2/CO, H_2/CO_2 and H_2/CH_4)

Dry reforming of C by CO_2 (reverse Boudouard reaction):

$C + CO_2 = 2CO$ Reaction Number: 5 (2 moles CO is produced per mole C and CO_2 is consumed) This reaction increases H_2/CO_2 and decreases H_2/CO)

The trends of the ratios of H_2 (H_2/CO, H_2/CO_2 and H_2/CH_4) with increasing reaction temperature observed in the current study are as follows: H_2/CO increases, H_2/CO_2 decreases and H_2/CH_4 decreases significantly. The steam gasification reaction (No #3) which produces CH_4 and CO_2 is consistent with this observation.

The trend of coke content with the composition of the catalysts is shown in Figure 72 below. These catalysts were operated at 750°C for 8 hours, S/C molar ratio of 3, WHSV on ethanol feed $8h^{-1}$, N_2/Ethanol 1.0 molar. The values are plotted in ascending order of Coke content.

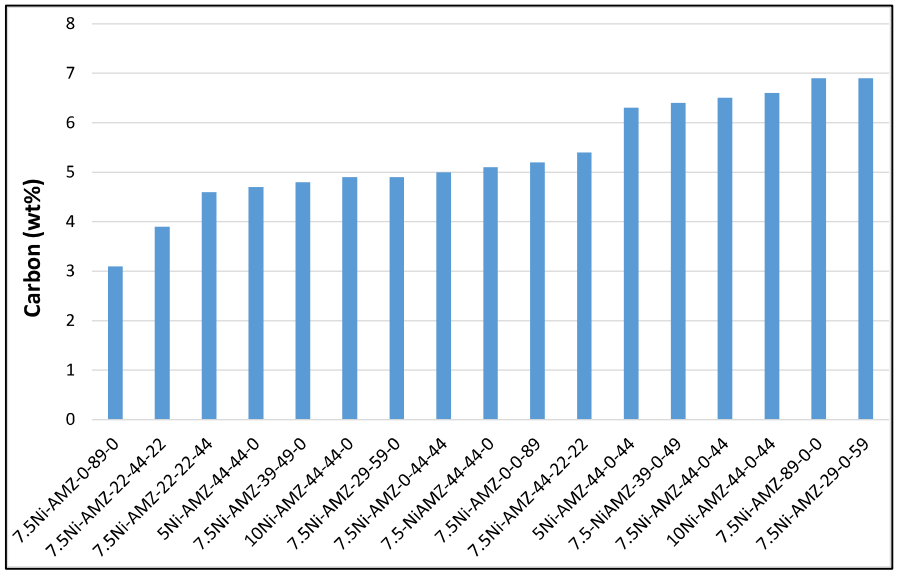

Figure 72: Trend of Coke content of catalyst after operation at 750°C for 8 hours

As seen from the above figure there is a clear trend with catalyst composition. All the catalysts containing Mg show less coke whereas those containing Al, Zr or their combination show higher coke. Binary Mg shows significantly less coke than the remaining catalysts whereas the binary Al, ternary balanced and skewed Al-Zr catalysts show significantly more coke than the remaining catalysts. There is no clear trend of coke content with Ni content of the catalysts for the AMZ-44-44-0 series whereas coke

content increases with Ni content for the AMZ-44-0-44 series. Fusteri et.al [35] have studied 21 wt% Ni impregnated of MgO and 30 wt% Ni supported on CeO_2. The spent catalysts after testing for steam reforming of ethanol at 650°C, GHSV 40000h^{-1}, S/C of 4.2, 25 hours on stream show about 5 wt% C on the MgO-based catalyst and 22wt% C on the ceria-supported catalyst. Thus, the low acidity of MgO appears to be more effective at restricting coke formation than the lattice oxygen of ceria. Similar behavior is also observed in the current study. The binary zirconia catalyst 7.5%Ni-AMZ-0-0-89, which has high OSC shows higher coke content than the binary Mg catalyst 7.5%Ni-AMZ-0-89-0). Wurzler et.al. [8] have studied 5wt% Ni supported on MgO supports prepared by strike precipitation to a final pH 10 with ageing (12 hours) and without ageing and also MgO prepared by thermal decomposition of the nitrate at 773°K 2 hours. The Ni is impregnated on the support and the catalyst calcined at 673°K (3 hours). They report 6.2% coke on catalysts after reaction at 773°K at S/C 3. The coking rate reported is 0.163-0.230 mg C/gcat/h/mole EtOH reacted. They contend that deactivation takes place predominantly due to carbon deposition rather than the sintering of Ni because there is an insignificant change in Ni crystallite size. However, it is not clear how crystallite size can be related to the particle size of the Ni cluster. Seung Han et.al. [7] have studied 10%Ni-Al_2O_3-ZrO_2 xerogel catalysts with different Zr/Al mole ratio (0-0.4), which are prepared by single step epoxide driven sol-gel method. They report that coke content decreases with increasing zirconia content which is contrary to the observation of the current study.

The trend of coke content with strong acidity of catalyst is shown in Figure 73 below.

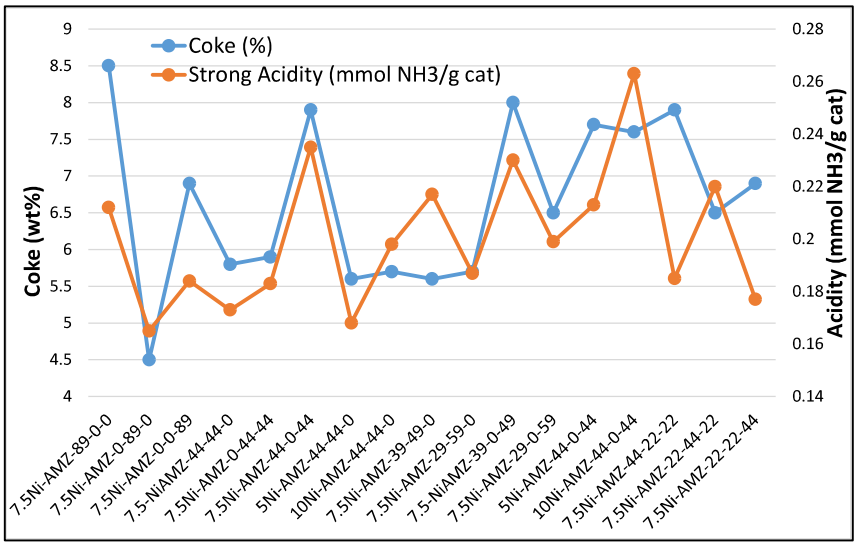

Figure 73: Trend of coke content and Strong Acidity of various catalysts

As seen from this Figure a trend of low acidity = low coke is observed for some catalysts whereas it is not observed for others. The trend is especially poor for ternary Al-Mg catalysts. The reason for this is attributed to the coke laydown due to the Boudouard reaction on these catalysts (as shown in the earlier section correlating trends of H_2/CO and H_2/CO_2 with reaction temperature). This reaction is not influenced by acidity. The possibility of catalytic methane decomposition [$CH_4 = C + 2H_2$] is unlikely because the H_2/CH_4 ratio is observed to decrease with reaction temperature which is contrary from the outcome of this reaction. The ratio is at its lowest at 750°C.

Further, the trend of coke content of the catalysts operated at 750°C for 8 hours is correlated with decay constants for conversion of ethanol with time on stream. Trends of coke formed on the catalyst are plotted with the value of decay constant at 750°C in Figure 74.

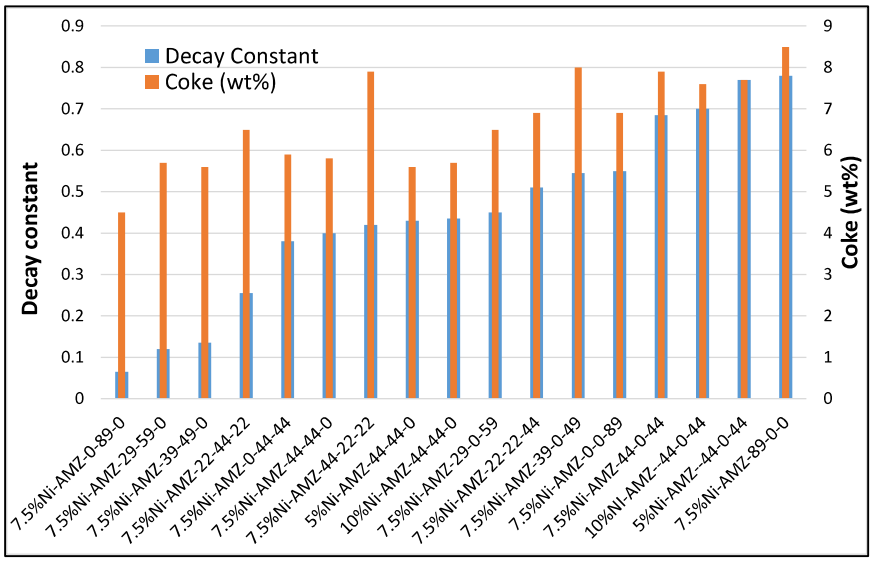

Figure 74: Trend of coke content of the catalysts operated at 750°C for 8 hours and decay constants for conversion of ethanol with time on stream.

As seen from this Figure there is a reasonable qualitative trend between coke content and decay constant. Coke content increases with an increase in decay constant indicating that coke formation is responsible for deactivation. Binary Al and Zr and ternary Al-Zr catalysts show higher coke content with attendant faster deactivation. However, the coke content on catalysts containing Mg is disproportionately higher in relation to the decay constant, when compared to catalysts comprising Al, Zr or their combination. This appears due to the filamentous nature of coke on these catalysts as confirmed by HRTEM. (Refer HRTEM figures in Appendix 10). Filamentous coke makes the Ni particle accessible to the reactant. Trimm [36] has discussed this aspect in detail. According to him the carbon dissolves in the Ni crystallites and then nucleates and grows into filaments which are also described as whiskers. The active metal particle is located at the tip of the carbon filament and is hence accessible to the reactants. As cited in earlier section Wang et.al. [26] have correlated coke morphology with catalyst stability for steam reforming with Co/CeO2 catalysts. Their results show that filamentous carbon causes significantly less deactivation than encapsulating carbon.

To correlate decay in ethanol conversion with physical properties the trend of decay constant was compared with trends of BET surface area, Ni dispersion, acidity, and reducibility of Ni. There were no significant trends with any of the parameters other than acidity. Hence only the trend of decay constant with acidity is shown below. The decay constant largely increased with the acidity of the catalyst, which is an expected trend (see Figure 75 below).

The trend of strong acidity by NH_3-TPD and decay constant at 750°C is shown in Figure 75 below.

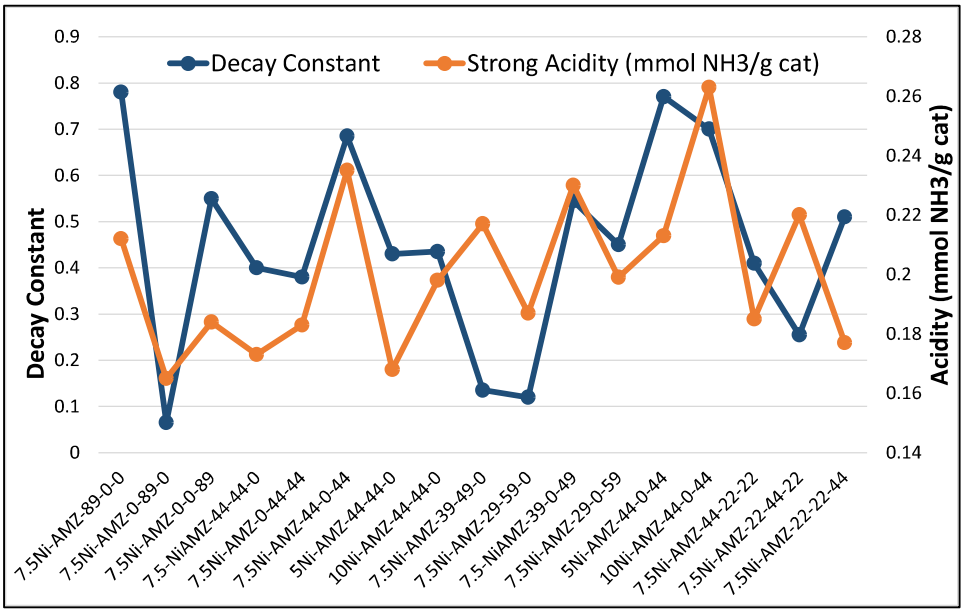

Figure 75: Trend of strong acidity by NH_3-TPD and decay constant at 750°C

As seen from the Figure there is a reasonable qualitative trend between decay constant and strong acidity. Decay constants are invariably higher for catalysts that show strong acidity. Catalysts containing Zr show higher coke content than those containing Mg. Ethylene yield also shows similar correlation with catalyst composition. Thus, ethylene polymerization may also be the source of carbon in catalysts with higher acidity. Mattos et.al. [5] have reviewed the work of Guisnet and Magnoux [37] who have studied deactivation of zeolites in the conversion of heptane. These authors conclude that coke is formed by polymerization of olefinic cracked products such as ethylene.

The trend of acetaldehyde yield is shown in Figure 76 below.

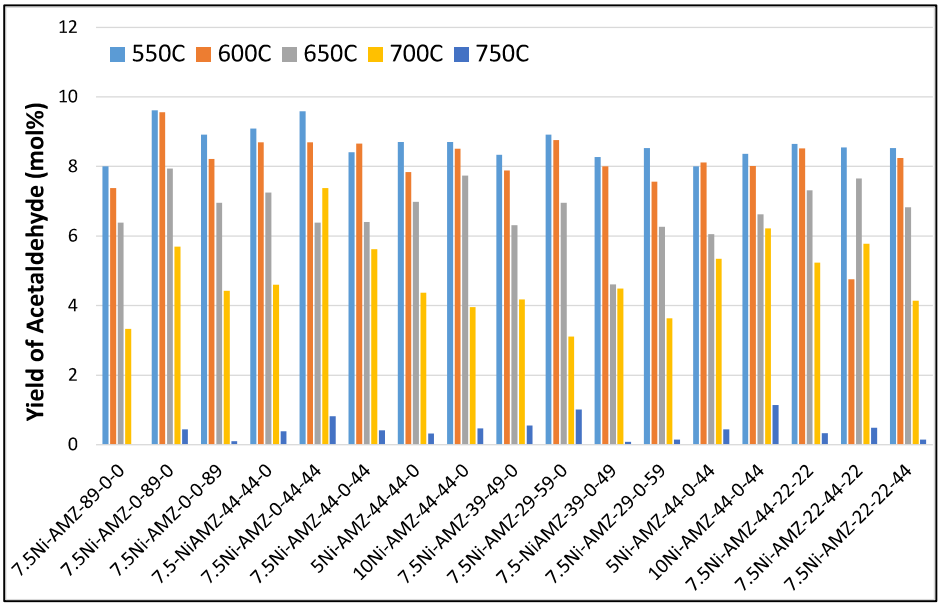

Figure 76: Trend of Acetaldehyde Yield at various temperatures for various catalysts

As seen from the Figure the trend for binary catalysts is Mg>Zr>Al. Amongst the ternary catalysts the Mg-Zr catalyst shows relatively higher yield. The remaining catalysts largely show similar yields. The yield of acetaldehyde decreases with increasing reaction temperature. This is expected because acetaldehyde is an intermediate and transitions to other products such as syngas, methane and acetone by the following reactions.

$CH_3CHO + H_2O = 2CO + 3H_2$ (Steam reforming)

$CH_3CHO = CH_4 + CO$ (Decomposition)

$2CH_3CHO = CH_3COCH_3 + CO + H_2$ (Aldol Condensation)

Notably, there is a very sharp decrease in yield of acetaldehyde when temperature is increased beyond 650°C for most of the catalysts. Mattos et.al [5] state that acetaldehyde, acetone, and ethylene are not predicted at equilibrium because of their thermodynamic instability. Thus, the results are consistent with this statement.

The yield of acetone is shown in Figure 77 below.

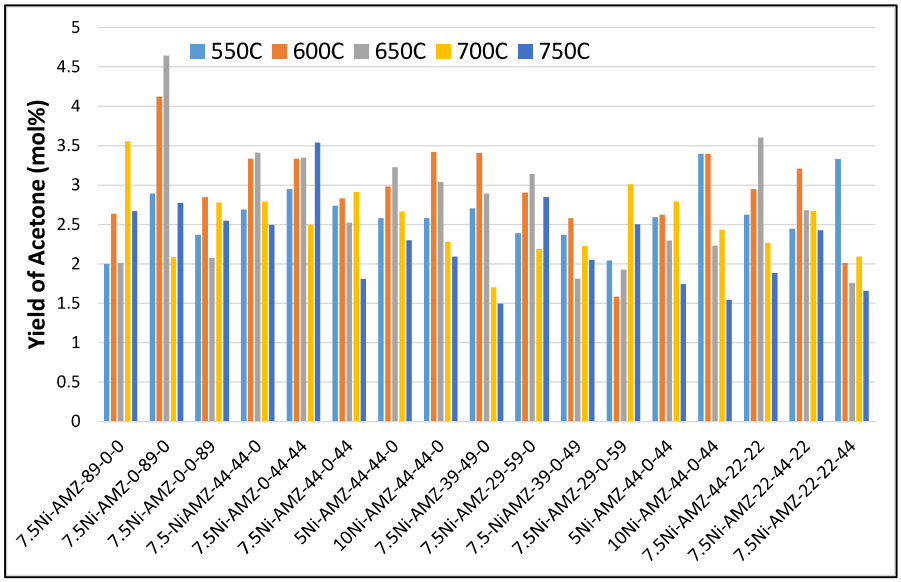

Figure 77: Trend of Acetone Yield at various temperatures for various catalysts

As seen from the above Figure the binary Mg catalyst shows the higher yield of acetone. The remaining catalysts largely show similar yields. The ternary Al-Zr catalysts show slightly lower yields than Al-Mg catalysts. The trend of yield varies in different ways with temperature for different catalysts. There is no specific trend in temperature.

4.7: Catalyst Stability: Long-duration runs

Select catalysts which presented good performance in the short duration 8 hours runs were further operated for 80 hours on stream each at 650°C and 700°C respectively. The catalyst was sized to 0.5-1.0 mm size fraction. Reaction conditions were H_2O: EtOH 3 Molar, atmospheric pressure, LHSV $8h^{-1}$ (on liquid feed), Nitrogen/EtOH 1.0 molar. The reaction temperature was studied at two levels, 650°C and 700°C. Time on stream 80 hours at each temperature. Catalysts 7.5wt% Ni/AMZ-0-89-0 (binary magnesia), 7.5wt% Ni/AMZ 44-44-0 (balanced Al-Mg composition), 7.5wt% Ni/AMZ 39-49-0 and 7.5wt% Ni/AMZ 29-59-0 (Al-Mg catalysts with composition skewed in favor of Mg), 7.5wt% Ni-AMZ-44-0-44 (ternary Al-Zr with balanced composition) and all three quaternary catalysts were tested.

The trend of conversion of ethanol at 650°C is shown in Figure 78 below.

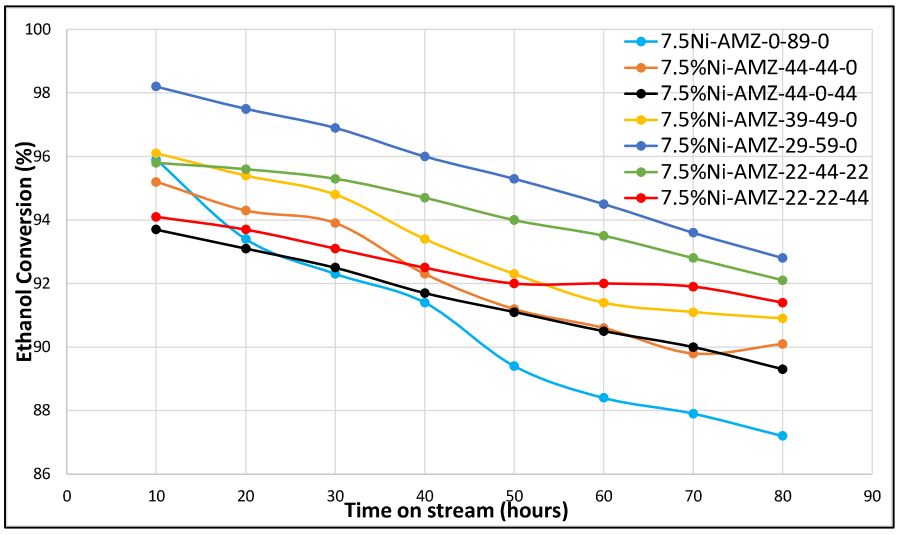

Figure 78: Trend of Ethanol Conversion at 650°C for various catalysts

As seen from this Figure the trend of initial conversion of ethanol of the ternary catalysts is 7.5%Ni-AMZ-29-59-0 > 7.5%Ni-AMZ-22-44-22 ≥ 7.5%Ni-AMZ-39-49-0 = 7.5%Ni-AMZ-0-89-0 > 7.5%Ni-AMZ-44-44-0> 7.5%Ni-AMZ-22-22-44 = 7.5%Ni-AMZ-44-22-22 > 7.5%Ni-AMZ-44-0-44. Ternary Al-Zr catalyst 7.5%Ni-AMZ-44-0-44 shows lower conversion than ternary Al-Mg catalysts. The trend at 700°C is similar to that of the trend at 650°C and is hence not shown here. Thus, increasing the Mg content of the catalyst increases activity for ethanol conversion for ternary Al-Mg catalysts. This is consistent with results of the short duration of 8 hour runs. Interestingly, the binary 7.5%Ni-AMZ-0-89-0 catalyst which stood out for its high activity at 2 hours and good stability in the short runs (8 hour's time on stream) shows lower activity at 10 hours on stream and fastest deactivation in the long duration 80 hours runs.

Amongst the quaternary catalysts, the trend is Mg-rich >>Al-rich=Zr-rich catalysts. The trend remains the same at 700°C. It is interesting to note that the 7.5%Ni-AMZ-22-44-22 quaternary catalyst shows better conversion than 7.5%Ni-AMZ-39-49-0, and only next to 7.5%Ni-AMZ-29-59-0. The Al and Zr-rich quaternary catalysts show activity comparable with the ternary Al-Zr catalyst with a balanced composition.

All the catalysts present deactivation with time on stream. The decay constant for ethanol conversion with time on stream at 650°C and 700°C for these catalysts is shown in Figure 79 below.

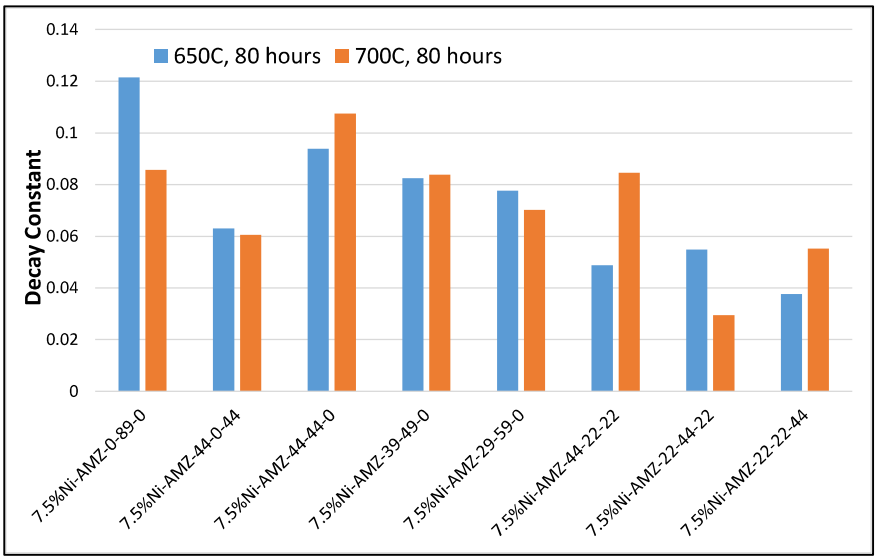

Figure 79: Decay Constants of Ethanol Conversion at 650°C and 700°C for various catalysts

As seen from this Figure the 7.5%Ni-AMZ-0-89-0 binary magnesia catalyst which showed the slowest deactivation in 8 hours runs, deactivates the fastest amongst all the catalysts at 650°C. Amongst the ternary Al-Mg catalysts deactivation decreases with increasing Mg content at both 650°C and 700°C. Hence, the catalysts with composition skewed in favor of Mg show slower deactivation. The ternary Al-Zr catalyst with balanced composition, 7.5%Ni-AMZ-44-0-44 shows a slower deactivation rate than the ternary Al-Mg catalysts but its initial conversion is significantly lower than the latter (Figure 78 above). All three quaternary catalysts show slower deactivation than the ternary catalysts at 650°C. The Mg-rich quaternary catalyst shows the slowest deactivation among all the catalysts followed by the Zr-rich quaternary catalyst. Both these quaternary catalysts show slower deactivation than the ternary Al-Mg catalysts. The Al-rich quaternary catalyst shows deactivation similar to the 7.5%Ni-AMZ-39-49-0 catalyst at 700°C. OSC appears to contribute to slowing down the decay of the quaternary catalysts (all of which contain Zr). Their decay constants are smaller than or equal to that of the ternary Al_2O_3-MgO catalysts. The 7.5%Ni-AMZ-44-0-44 ternary Al-Zr catalyst also shows slower deactivation than ternary Al-Mg catalysts. As seen from results in chapter 2, all these four catalysts show higher OSC than the ternary Al-Mg catalysts (Figure 15, chapter 2)

The trend of the decay constant of ethanol conversion for these catalysts is compared for operation 8 hours and 80 hours at 650°C in Figure 80 below.

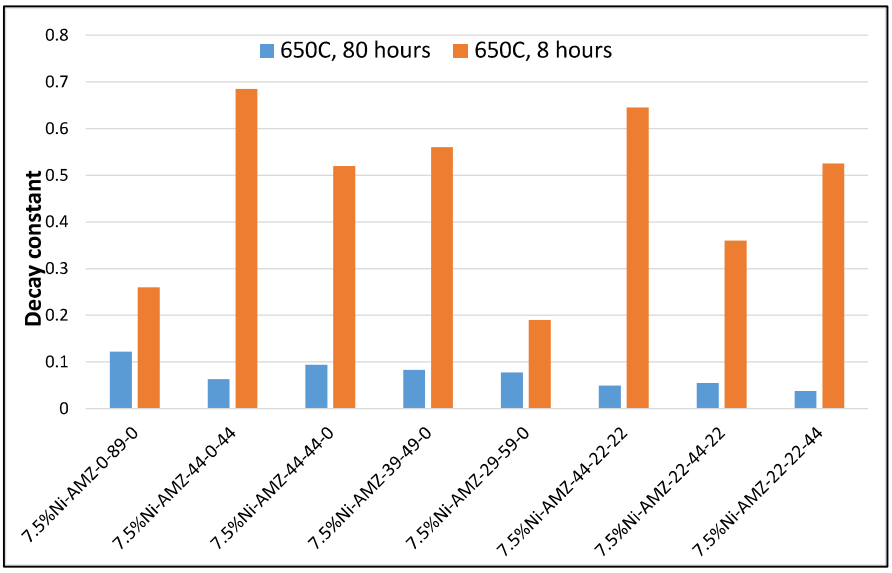

Figure 80: Decay Constants of Ethanol Conversion operated at 8 hours and 80 hours at 650°C.

As seen from this Figure, the decay constant of conversion is significantly smaller (by almost an order of magnitude) when the catalysts are operated for a longer duration (80 hours), indicating that deactivation is faster during the initial 8h on stream. Further, while the binary magnesia catalyst 7.5%Ni-AMZ-0-89-0 shows slower deactivation than the remaining catalysts in short duration (8 hours) runs, the remaining catalysts viz. ternary Al-Mg, ternary Al-Zr and all three quaternary catalysts show slower deactivation than the binary magnesia catalysts in long duration runs. Still further, the ternary Al-Zr and quaternary catalysts shows slower deactivation than the ternary Al-Mg catalysts in 80 hours runs. This is attributed to differences in their deactivation mechanism. Magnesia based catalysts deactivate by both coking and Ni metal sintering whereas the zirconia-based catalysts deactivate predominantly by coking alone. Metal sintering data is shown in Table 7. Between the two mechanisms of deactivation, metal sintering is a slower process and hence reflects in the long duration runs. The quaternary catalysts notably show significantly slower deactivation among all the catalysts tested. These contain both magnesia and zirconia in addition to alumina. It appears that they benefit from both lower acidity imparted by magnesia, better resistance to sintering of Ni (Table 7) and mobile lattice oxygen from the combination of ceria with zirconia.

A similar trend is observed at 700°C (Figure 81 below)

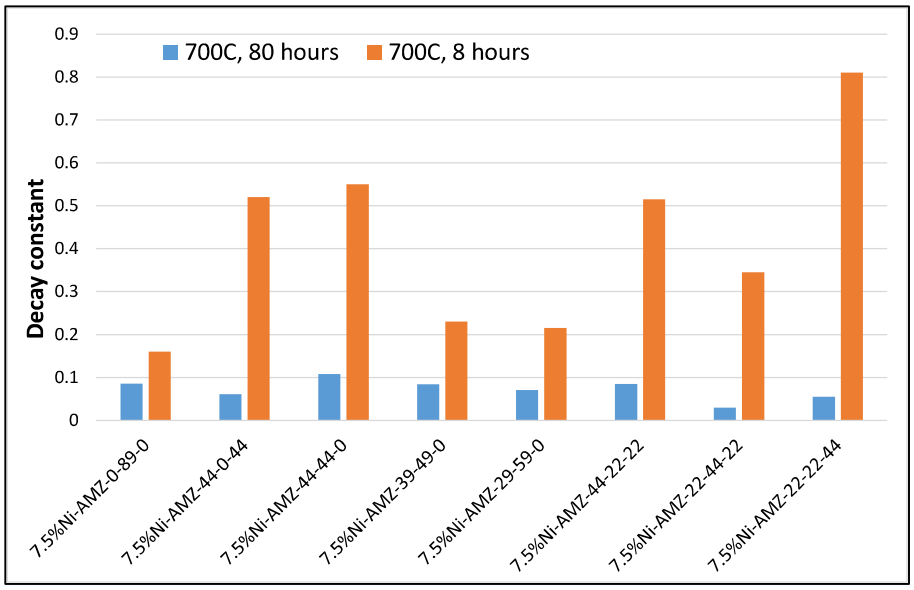

Figure 81: Decay Constants of Ethanol Conversion operated at 8 hours and 80 hours at 700°C.

As seen from this Figure, the trends are largely similar to those at 650°C. The quaternary 7.5%Ni-AMZ-22-44-22 catalyst shows significantly slower deactivation than the remaining catalysts. Both the 7.5%Ni-AMZ-22-44-22 and 7.5%Ni-AMZ-22-22-44 quaternary catalysts show slower deactivation than the binary Al-Mg and Al-Zr catalysts and the binary 7.5%Ni-AMZ-0-89-0 catalyst. As seen from the rate of coke laydown with time on stream (Figure 82) below, the latter catalysts lay down coke at a much faster rate during the initial 8 hours on stream.

The percentage of coke deposited on the catalyst at 8 hours and 80 hours on stream is shown in Figure 82 below. As seen from this Figure, the slope of coke deposition is significantly larger for the first 8 hours on stream than in subsequent time on stream up to 80 hours. Thus, coke is deposited significantly faster during the initial 8 hours on stream on the fresh catalyst. The ternary Al-Zr catalyst (7.5%Ni-AMZ-44-0-44) shows significantly different behavior. It shows significantly higher coke formation than the remaining catalysts during the first 8 hours on stream and much slower coking during the remaining 80 hours on stream.

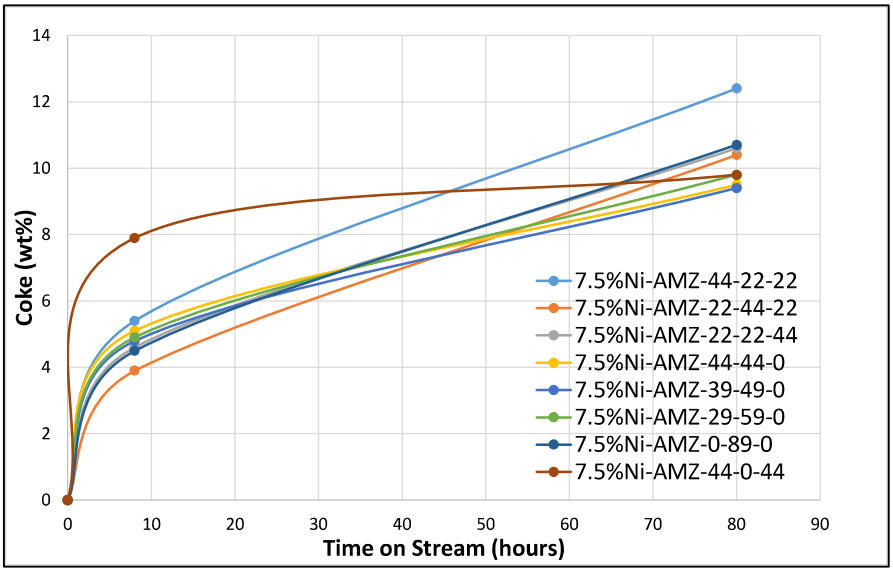

Figure 82: Coke deposits for various catalysts operated at 8 hours and 80 hours at 750°C.

This is consistent with the decay slopes shown in Figure 81 above wherein 7.5%Ni-AMZ-44-0-44 deactivates significantly faster during the short-duration runs and significantly slower in long-duration 80 hours runs. As also seen from this Figure, the overall coke content deposited on catalyst 7.5%Ni-AMZ-44-0-44 at 80h on stream is lower than that of binary Mg (7.5%Ni-AMZ-0-89-0) and quaternary Al-rich (7.5%Ni-AMZ-44-22-22) catalysts and much closer to the ternary Al-Mg catalysts with skewed composition.

Ogo et.al. [1] have reviewed data of ESR on non-noble transition metal catalysts. Therein Shao et.al. [38] report a mixed oxide catalyst $LaNi_{0.85}Zn_{0.15}O_{3-8}$ operated at 973°K (700°C), S/C 3.0, WHSV 18.4 h^{-1} with 100% ethanol conversion and 83% selectivity to H_2. The rate of coking of this catalyst as reported by them is 19.9 mg C/g/h for 8 hours operation versus 2.0 mg C/g/h for 100 hours operation (995% higher at the lower duration of operation). Data of rate of coking observed in the current study is provided in Table 5 below. The rate of coking mg C/g cat/h for the 8 and 80 h runs and the relative coking rate for 8h on stream relative to 80h on stream on percentage basis is provided in the last column of this table. The data is sorted on percentage relative coking rates.

Table 5: Coke content and relative coking rates for various catalysts

Catalyst	mg C/g/h	mg C/g/h	Relative coking rates of 8 hours relative to 80 hours
Time on stream>>	8h	80h	(%)
7.5Ni-AMZ-22-44-22	4.88	1.3	375
7.5Ni-AMZ-0-89-0	5.63	1.34	420
7.5Ni-AMZ-22-22-44	5.75	1.33	432
7.5Ni-AMZ-44-22-22	6.75	1.55	435
7.5Ni-AMZ-29-59-0	6.13	1.23	498
7.5Ni-AMZ-39-49-0	6	1.18	508
7.5Ni-AMZ-44-44-0	6.38	1.19	536
7.5Ni-AMZ-44-0-44	9.88	1.23	803

As seen from the results compiled in this Table, a similar trend in coke formation as reported by Shao et.al. [38] is observed in the present study (significantly higher coking rate for short duration operation). The quaternary catalysts of the present study show relatively slower coking in the initial 8 hours on stream (375-432%) relative to 80 hours operation than the ternary Al-Mg catalysts (498-536%). The binary 7.5%Ni-AMZ-0-89-0 catalyst shows behavior similar to that of the quaternary catalysts (420%). The ternary Al-Zr catalyst shows the highest coking rate (803%) during the first 8 hours relative to 80 hours on stream. Between the quaternary catalysts, the 7.5Ni-AMZ-22-44-22 shows a significantly slower coking rate during the initial 8h on stream than the remaining two catalysts. Thus, increasing Mg in the catalyst quaternary catalyst formulation retards coking. Likewise, amongst the ternary Al-Mg catalysts, the coking rate decreases with the increasing Mg content of the catalyst. The quaternary catalyst appears to benefit from both the lower acidity imparted by Mg and lattice oxygen mobility imparted by the combination of ceria and zirconia.

The data on the coking rate for Ni catalysts which are compiled by Ogo et.al. [1] ranges from 0.15 to 394 mg/g cat/h for various Ni-based catalysts operated at a variety of conditions for ESR. Data from this table shows that the rare earth with zirconia or iron or Zn or $MgAl_2O_4$ shows low coking rates (0.15 to 6.1 mg/gcat/h). Coking rate on Ni/α-Al_2O_3 is 4.7 and 394 mg/g cat/h (in separate studies) whereas it is 20 mg/g cat/h for a Ni-Al-Mg spinel 32.4 mg/gcat/h for a Ni-Mg-Al hydrotalcite promoted with Ce (10Ce/$Ni_1Mg_2Al_1$ hydrotalcite), 1.4 and 23 mg/g cat/h for 8Ni/8Ce-$MgAl_2O_4$, 149 mg/g cat/h for 10Ni/$MgAl_2O_4$. In comparison to values reported in the

literature for similar catalysts, the catalysts of the current study show relatively low coking rates. Comparing the results of the current work with that of the literature compiled by Ogo et.al. [1], it is clear that the results of the current study are consistent with those reported in the literature. It is also evident from the literature that the catalyst composition, method of preparation and reaction conditions influence coking rates significantly. The presence of magnesia and rare earths Ce and La appears to be responsible for lower coking rate in the catalysts of the current study. Magnesia decreases acidity whereas the combination of ceria and zirconia enhances lattice oxygen mobility. Zhang et.al [39] have studied Ni supported on La_2O_3 and reported that La_2O_3 reacts with CO_2 to form $La_2O_2CO_3$ which in turn reacts with coke deposited to convert the deposits to CO and make the active metal available for reaction.

The average conversion of ethanol over the run length is presented in Figure 83 below for the catalysts which were operated for 80 hour on stream at 650°C and 700°C.

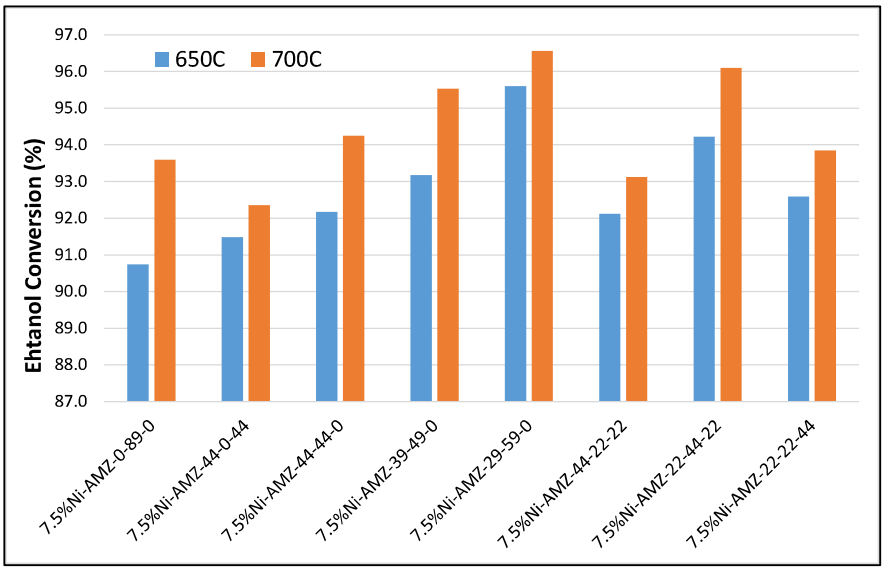

Figure 83: Average conversion of ethanol for various catalysts operated for 80 hours on stream.

As seen from this figure the trend for average conversion is 7.5%Ni-29-59-0 > 7.5%Ni-22-44-22 > 7.5%Ni-39-49-0 > 7.5%Ni-44-44-0 > 7.5%Ni-22-22-44 > 7.5%Ni-44-0-44 > 7.5%Ni-44-22-22 > 7.5%Ni-0-89-0. Thus, the ternary Al-Mg catalyst with the highest ratio of Mg/Al shows the highest conversion. Ternary Al-Zr catalyst (7.5%Ni-44-0-44) shows a low conversion. The binary Mg catalyst which showed comparable conversion to the ternary Al-Mg catalysts in short duration (8 hours) runs shows amongst the lowest conversion in the long duration runs indicating relatively

faster deactivation with increased time on stream. The Al or Zr-rich quaternary catalysts show the lowest average conversion due to about 4% lower initial conversion.

The average yield of H_2 for catalysts operated for 80 hours at 650° and 700°C is shown in Figure 84 below.

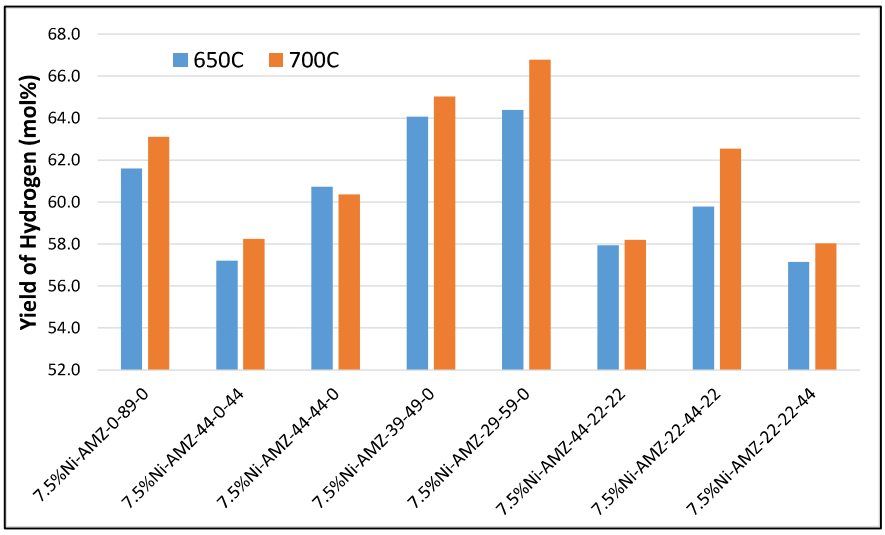

Figure 84: Average yield of H_2 for catalysts operated for 80 hours at 650°C and 700°C.

As seen from this Figure the ternary Al-Mg catalysts with composition skewed in favor of Mg show the highest H_2 yield followed by the binary Mg catalyst. The trend is 7.5%Ni-AMZ-29-59-0 > 7.5%Ni-AMZ-39-49-0 > 7.5%Ni-AMZ-0-89-0 = 7.5%Ni-AMZ-22-44-22 ≥ 7.5%Ni-AMZ-44-44-0 > 7.5%Ni-AMZ-44-22-22 = 7.5%Ni-AMZ-22-22-44 = 7.5%Ni-AMZ-44-0-44. Thus, the yield of H_2 increases with increasing Mg in the catalyst for the ternary Al-Mg catalysts. This is consistent with the results of the short runs with 8 hours of time on stream. However, the binary Mg catalyst shows lower average H_2 yields than the ternary Al-Mg catalysts which is different from the trend of short duration (8 hours) runs, where it showed comparable yield. The difference between 7.5%Ni-AMZ-39-49-0 and 7.5%Ni-AMZ-29-59-0 can be clearly distinguished from the long-duration runs. The latter gives higher yield. The yield of H_2 increases with increasing reaction temperature for all catalysts. Ternary Al-Zr catalyst shows low H_2 yield. Similarly, the quaternary catalysts rich in Al or Zr show lower H_2 yield compared to the Mg-rich quaternary catalyst.

The yield of CO for the long duration 80 hours run at 650°C and 700°C is shown in Figure 85 below.

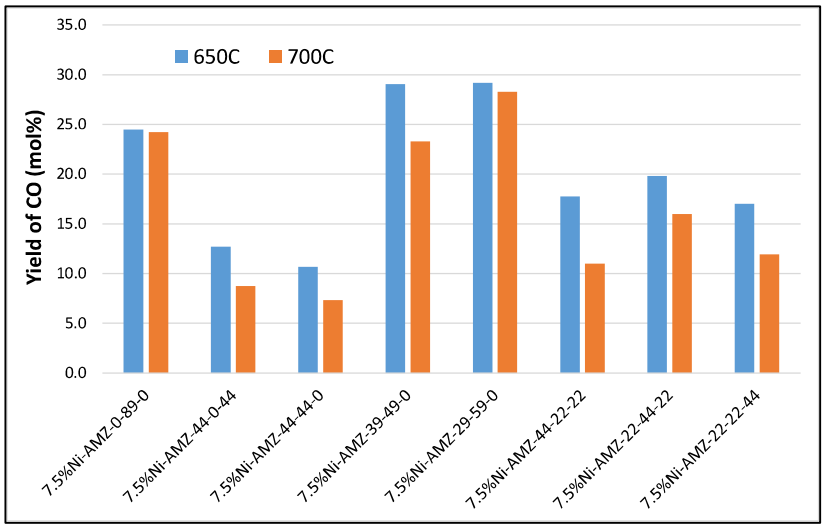

Figure 85: Average yield of CO for catalysts operated for 80 hours at 650°C and 700°C.

As seen from this Figure yield of CO also increases with an increase in the Mg content of the catalysts within the ternary catalysts. The skewed Al-Mg catalysts show a higher yield than balanced Al-Mg catalysts. However, the balanced Al-Mg ternary catalyst shows a lower yield of CO than the binary MgO catalyst. Ternary Al-Zr catalysts show low CO yield compared to the ternary Al-Mg catalysts. Amongst the quaternary catalysts, the Mg-rich catalyst shows the highest yield of CO. Trend is Mg-rich>Al-rich≥Zr rich. The quaternary catalysts show higher yields of CO than the balanced ternary Al-Mg or Al-Zr catalysts but lower than the binary MgO or ternary Al-Mg with a composition skewed in favor of Mg. The yield of CO decreases upon increasing temperature due to its conversion to other products. The trends are consistent with those of the short duration runs.

The trend of the yield of CO_2 of catalysts operated for 80 hours at 650°C and 700°C is shown in Figure 86 below.

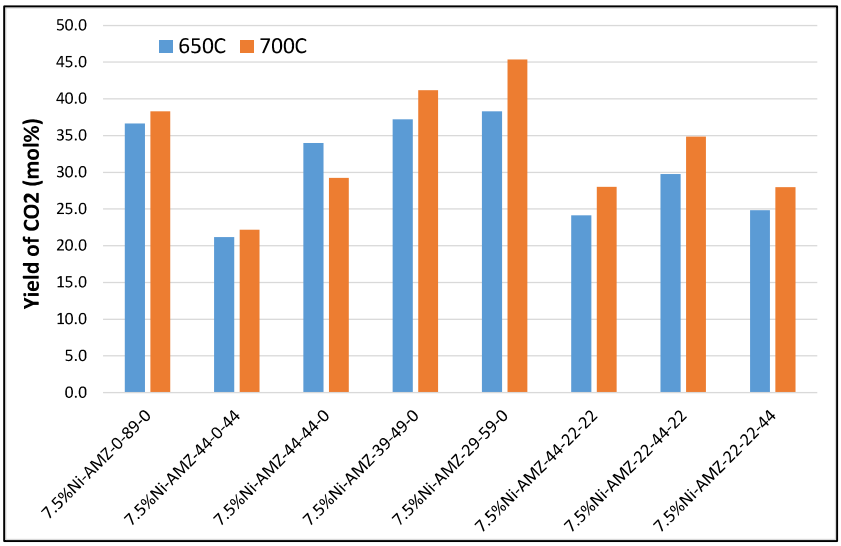

Figure 86: Average yield of CO_2 for catalysts operated for 80 hours at 650°C and 700°C.

As seen from this Figure the yield of CO_2 increases with an increase in Mg content for ternary Al-Mg catalysts. The ternary catalysts with a composition skewed in favor of Mg show higher yield than the ternary Al-Mg catalysts with a balanced composition. Ternary Al-Zr catalyst shows low CO_2 yield which reflects on its low activity for the side reactions. The binary MgO catalyst shows yields in between the balanced and skewed Al-Mg catalysts. Amongst the quaternary catalyst, the trend is Mg-rich > Al-rich = Zr-rich. The yield of CO_2 increases with an increase in reaction temperature. The trend is consistent with those of the short duration runs.

The trend of the H_2/CO molar ratio of catalysts operated for 80 hours is shown in Figure 87 below.

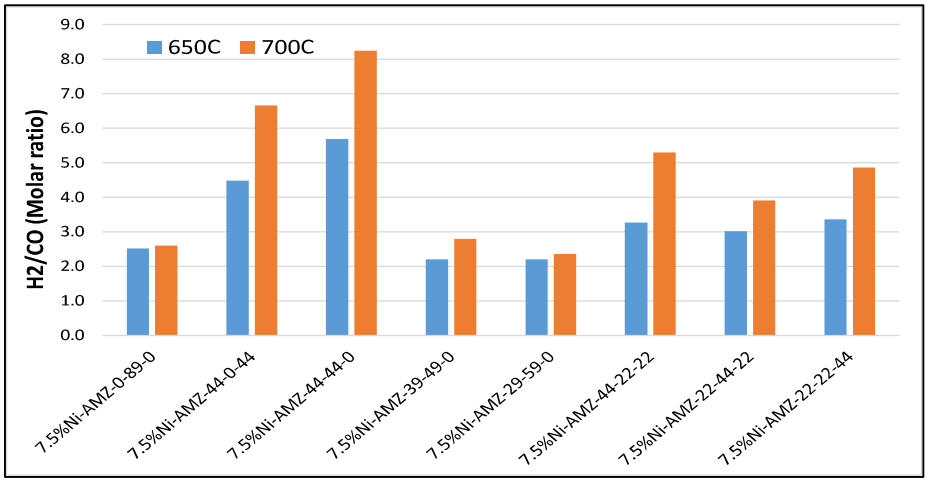

Figure 87: Trend of the H_2/CO molar ratio for catalysts operated for 80 hours at 650°C and 700°C.

As seen from this Figure the balanced Al-Mg catalysts show the highest (significantly higher than the rest) ratio. The ternary Al-Zr catalyst also shows high H_2/CO, only next to the Al-Mg catalyst with a balanced composition. The skewed Al-Mg catalysts show a ratio close to that of the binary MgO catalyst. Amongst the quaternary catalysts, the trend is Al-rich>Zr-rich>Mg-rich. The trends are consistent with those of the short-duration runs. Thus, the presence of Al in the ternary Al-Mg catalysts and Zr in quaternary catalysts favors the H_2/CO ratio.

The trend of the H_2/CO_2 molar ratio of catalysts operated for 80 hours is shown in Figure 88 below.

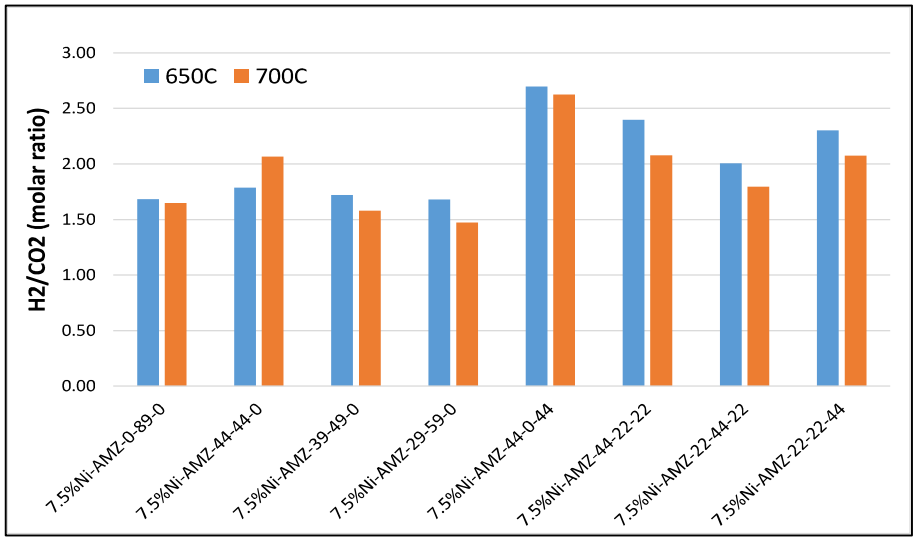

Figure 88: Trend of the H_2/CO_2 molar ratio for catalysts operated for 80 hours at 650°C and 700°C.

As seen from this Figure ternary Al-Zr and quaternary catalysts rich in Al or Zr show a higher ratio than binary Mg or ternary Al-Mg catalysts. This is consistent with trends observed for the short-duration runs. The reason for this is explained in an earlier section, wherein it is shown that while ternary Al-Zr catalysts promote the WGS reaction, the Al-Mg catalysts promote the Boudouard reaction with increasing reaction temperature.

4.8: Characteristic of Coke by HRTEM

The spent catalysts from the long duration run comprising 80 h time on stream at each of 650°C and 700°C at space velocity $8h^{-1}$, Steam/Ethanol 3 molar, Nitrogen/Ethanol 1.0 molar, atmospheric pressure, catalyst particle size 0.5-1.0 mm were characterized by HR-TEM. The following eight catalysts were characterized:

7.5%Ni-AMZ-0-89-0 (binary Mg), 7.5%Ni-AMZ-44-44-0 (ternary Al-Mg with balanced composition), 7.5%Ni-AMZ-39-49-0 (ternary Al-Mg with skewed composition), 7.5%Ni-AMZ-29-59-0 (ternary Al-Mg with skewed composition), 7.5%Ni-AMZ-44-0-44 (ternary Al-Zr with balanced composition), 7.5%Ni-AMZ-44-22-22 (quaternary Al-rich), 7.5%Ni-AMZ-22-44-22 (quaternary Mg-rich) and 7.5%Ni-AMZ-22-22-44 (quaternary Zr rich). The HRTEM micrograph of these catalysts is presented in Figures 89 to 96. They are compared with micrographs of reduced catalysts before use in ESR.

As seen from these micrographs diverse morphologies of carbon are observed which is attributed to differences in metal support interaction which in turn are due to differences in the composition of the support.

The HR-TEM of binary Mg catalyst AMZ-0-89-0 is shown in Figure 89 (a) and 89(b) below.

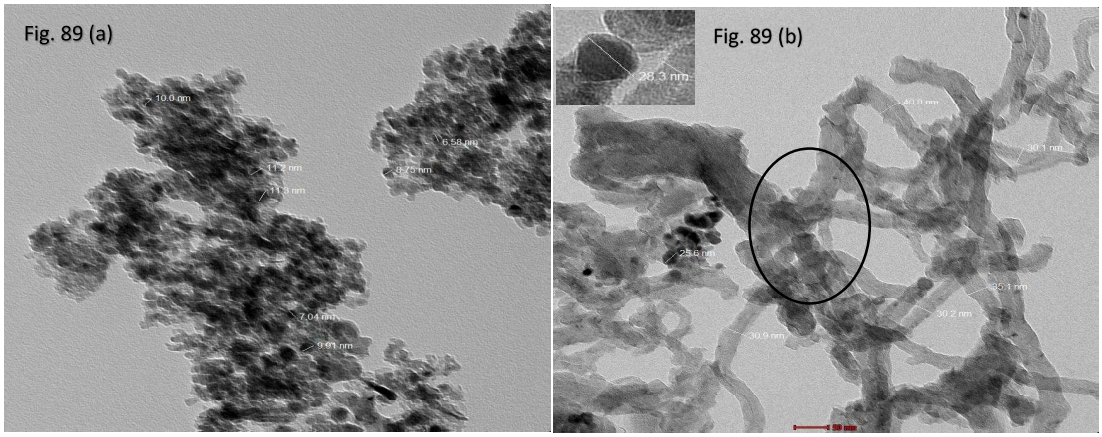

Figure 89: TEM of 7.5%Ni-AMZ-0-89-0 a) Reduced catalyst and b) After use for ESR

As seen from the above Figure the reduced and stabilized catalyst shows globular morphology with Ni particles dispersed across the matrix. The light-colored globules are the Magnesia matrix and the dark-colored particles are Ni(0). The latter are faceted. The median particle size of Ni(0) is 9.9 nm. Upon use for steam reforming of ethanol 'octopus' type (multiple filaments radiating from a common Ni particle - encircled portion of Figure 83b), filamentous coke is observed to form. Formation of this type of carbon is reported by Monthioux et.al. [40] on bimetallic $Ni_{0.8}Cu_{0.2}MgAl$ catalyst and also by Helveg et.al. [41]. The diameter of the carbon filaments observed in the current study is typically 30-35 nm and they appear to be multi-walled (inset

Figure 89b). Formation of 'octopus' carbon filaments is attributed to the growth of filaments from different facets of the same metal crystal [40].

The dark-colored pear shape particle at the tip of a carbon filament (inset Figure 89 (b) upper left) is Ni particle which is dislodged from the support matrix. Thus, this catalyst predominantly shows a "tip-growth" mechanism of filamentous carbon formation. Thus, the Ni is not strongly adhering to the magnesia support. Whisker coke by “tip growth” mechanism is reported to form by the dissolution of carbon into Ni to form a suspected carbide, which dislodges the Ni particle from the support and grows in the form of a whisker of carbon with the Ni particle located at its tip. Since the Ni at the tip is accessible to reactants catalyst activity is maintained [36]. Ni particle size in the used catalyst is larger 18.6 nm (median) than that in the reduced and stabilized catalyst which is 9.9 nm. Thus, there is growth in particle size suggesting active metal sintering.

The HRTEM of ternary Al-Mg catalyst with balanced composition 7.5%Ni-AMZ-44-44-0 is shown in Figure 90 (a) reduced and stabilized catalyst; and Figure 90 (b) catalyst after use for ESR

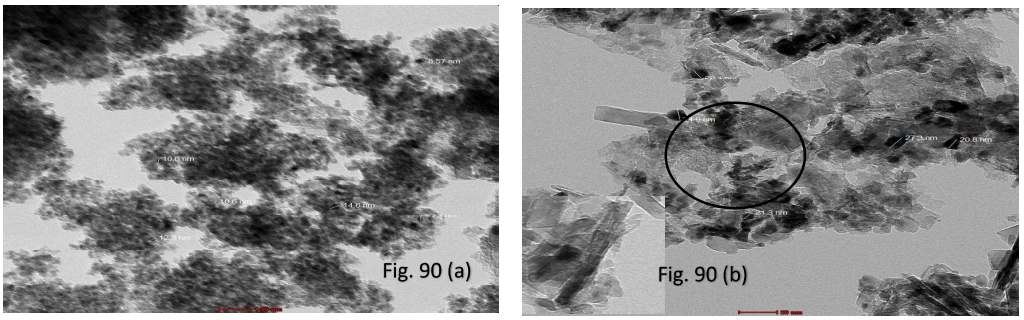

Figure 90: HRTEM of 7.5%Ni-AMZ-44-44-0 a) Reduced catalyst and b) After use for ESR.

As seen from the Figure the incorporation of Al along with Mg does not change the morphology of the matrix of the reduced catalyst. The particle size of Ni(0) in the reduced catalyst is 9.2 nm (median size) which is comparable to that of the binary Mg catalyst. Whereas it increases to 20.6 nm (median size) after use for ESR. Thus, significant sintering of Ni(0) is observed after use for ESR. Further, significant changes are observed in the morphology of coke. The flexible long wavy filamentous nature of coke in the case of binary Mg catalyst 7.5%Ni-AMZ-0-89-0 changes to short straight rod-like cylindrical morphology. Further, Ni particles are absent at the tip of the carbon

filaments indicating "base growth" of the carbon filament (encircled portion of Figure 90 (b)) which indicates that Ni is strongly adhering to the support and hence not dislodged. Two carbon filaments are observed to grow in opposite directions from the Nickel particle located on the Al-Mg support. This is different from that of the binary 7.5%Ni-AMZ-0-89-0 Mg catalyst which predominantly shows "tip growth" of carbon filaments indicating poor adherence of Ni to the support. The inset lower left of Figure 90 (b) above indicates the formation of a "complete knot bamboo" type carbon filament. A magnified image is shown in Figure 91 (b) below. The coke in the inset of Figure 91 (b) shows a "bamboo-like" construction with clear knots/nodes. Figure 91 (b) below shows a detailed micrograph of bamboo filament present in this sample.

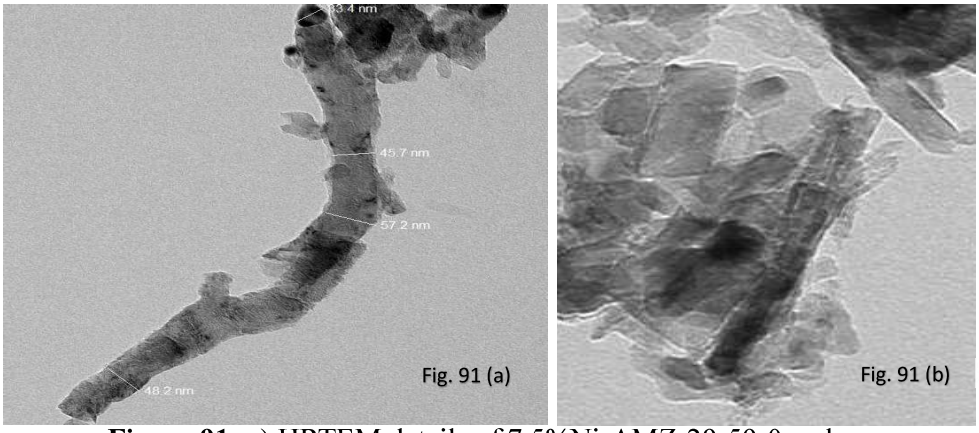

Figure 91: a) HRTEM details of 7.5%Ni-AMZ-29-59-0 and
b) details of 7.5%Ni-AMZ-44-44-0

The picture on the left 91(a) is of ternary Al-Mg catalyst 7.5%Ni-AMZ-29-59-0 (skewed composition) and the one on the right 91(b) is of 7.5%Ni-AMZ-44-44-0 (balanced composition). Both show "bamboo type" filaments with clear complete nodes which are seen as spaced lines across the diameter of the filament. Tip growth is observed in 7.5%Ni-AMZ-29-59-0, which is richer in magnesia content. This is similar to 7.5%Ni-AMZ-0-89-0.

This type of coke formation is reported by Chen et.al. [42] and also by Monthioux et.al. [40]. Tong et.al. [43] have reviewed literature about the formation of bamboo-type carbon nanotubes. Saito et.al. [44] attribute the formation of bamboo-like carbon tubes to the intermittent advance of the active metal particle of the catalyst within the carbon tube. Lin et.al. [45] have described bamboo carbon tubes with complete and incomplete knots. The difference is attributed to the relative rate of contraction of Ni particles and the rate of growth of the inner layer of carbon near the

Ni particle. Faster growth of the carbon layer leads to a complete knot, whereas faster contraction of the Ni particle results in an incomplete knot. The results of the current study conform to the former case.

The HR-TEM of ternary Al-Mg catalyst with skewed composition 7.5%Ni-AMZ-39-49-0 is shown in Figure 92 (a) and Figure 92 (b) below. Figure 92 (a) is that of reduced and stabilized catalyst; and Figure 92 (b) that of the catalyst after use for ESR.

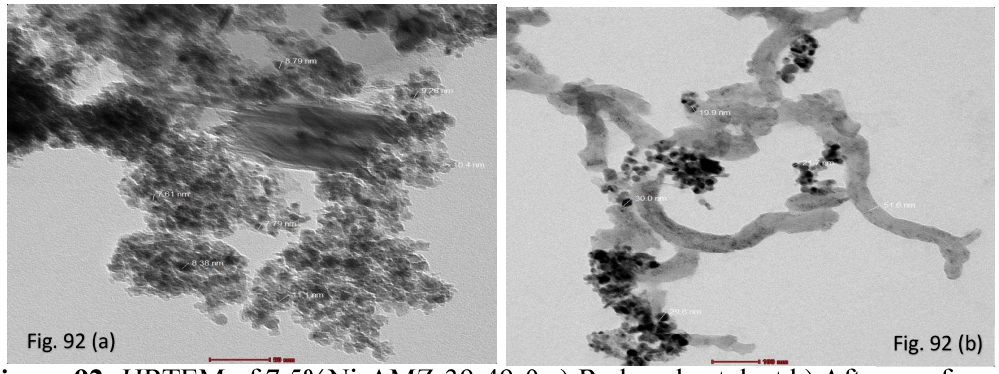

Figure 92: HRTEM of 7.5%Ni-AMZ-39-49-0 a) Reduced catalyst b) After use for ESR

As seen from Figure 86 the reduced catalyst shows morphology similar to that of the ternary Al-Mg catalyst with balanced composition (globular with Ni particles dispersed in it). The spent catalyst shows filamentous carbon with 51 nm diameter and Ni particles 20.4 nm (median size) which are larger compared to fresh unused reduced and stabilized catalysts (where it is 8-12 nm). Thus, significant sintering of Ni(0) is observed in this catalyst upon use for ESR. Metal particles are seen at the end of some of the filaments which indicates a tip growth mechanism similar to binary AMZ-0-89-0. The filaments without metal particles may be those that have broken when the sample was ground mildly for TEM analysis.

Detailed micrographs of the 7.5%Ni-AMZ-39-49-0 spent catalyst are shown in Figure 93 below.

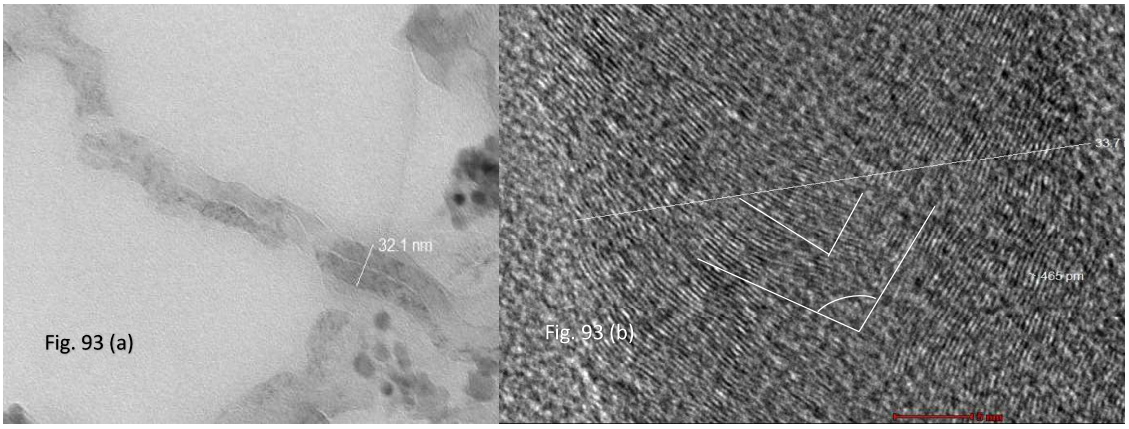

Figure 93: Magnified HRTEM image of 7.5%Ni-AMZ-39-49-0 showing Herringbone structure in carbon filament.

As seen from Figure 93 (a) on the left a lighter "vein" is seen running along the central axis of the carbon filament which indicates it is hollow. Baker et.al. [46] and Helveg et.al [41] have shown by electron microscopy that these filaments are hollow. Thus, this filament appears to be a hollow carbon nanotube. Picture b) on the right shows lattice fringes of the carbon filament of the same sample. Considering the angle which is close to 90°, and the discontinuity in the lattice fringes in the central axis portion of the filament, this appears to be a herringbone bamboo nanofiber. A similar structure is reported by Monthioux et.al. [40]. The lattice 'd' spacing of this sample is 465 pm, which is closer to that reported for d100 of thermally stabilized polyacrylonitrile fibers ~520-536 pm [47].

The HR-TEM of ternary Al-Mg catalyst 7.5%Ni-AMZ-29-59-0 with skewed composition is shown in Figure 94 below. This catalyst has a higher Mg content than 7.5%Ni-AMZ-44-44-0 or 7.5%Ni-AMZ-29-39-0.

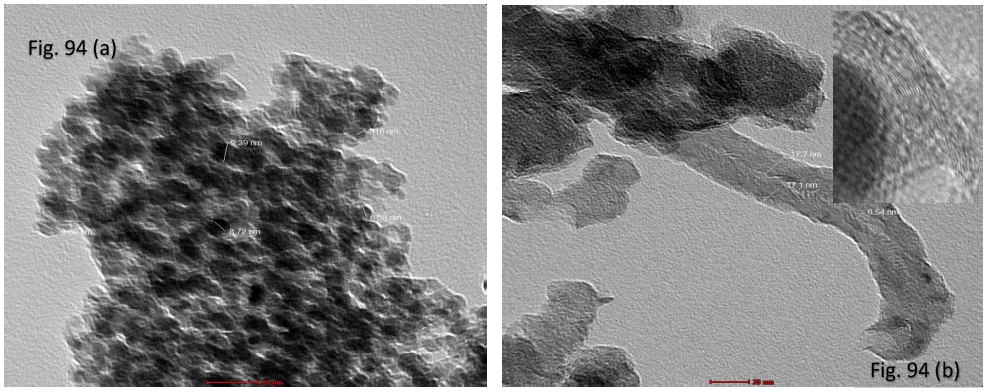

Figure 94: HRTEM of 7.5%Ni-AMZ-29-59-0 a) Reduced catalyst b) After use for ESR

As seen from this Figure the reduced catalyst shows a matrix consisting of globular particles with faceted particles of Ni 8-12 nm in diameter dispersed across this matrix. The used catalyst shows Ni(0) particles 17.1 nm (median size) which are significantly larger than the fresh unused reduced and stabilized catalysts (where it is 8-12 nm). Thus, sintering of Ni(0) is observed in this catalyst upon use for ESR. The spent catalyst shows strands of filamentous carbon 30-60 nm in diameter (Figure 94(b)). The open ends of these filaments suggest that they are hollow, as also the ridge running across the centre of the filament. They also appear to be the tip-growth type with pear-shaped Ni particles seen at their tip (refer Appendix 12). The inset (upper right of Figure 94 (b)) also shows the presence of encapsulating or pyrolytic carbon with the carbon covering the surface of the metal particle. Fayaz et.al [47] have reported formation of this type of coke on lanthana doped cobalt/alumina catalysts. They describe it as onion shell-like graphitic coke which covers the metal particles.

The HRTEM of ternary Al-Zr catalyst with balanced composition 7.5%Ni-AMZ-44-0-44 is shown in Figure 95 (a) and Figure 95 (b) below.

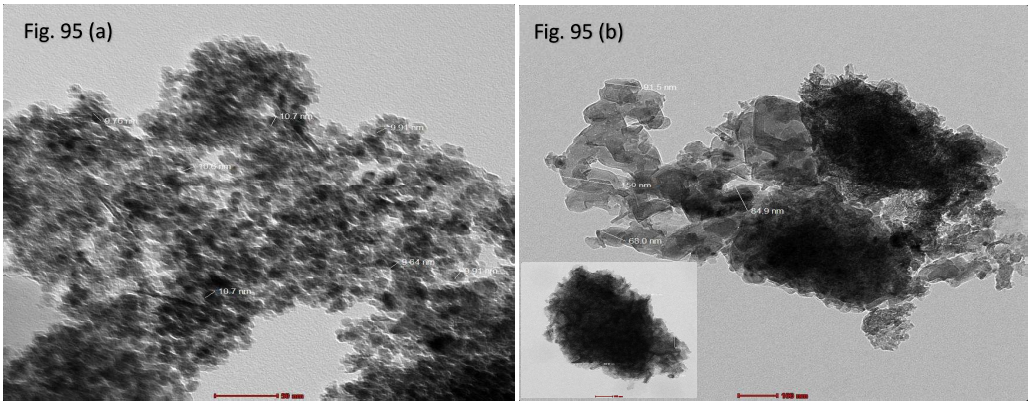

Figure 95: HRTEM of catalyst 7.5%Ni-AMZ-44-0-44 a) Reduced catalyst b) After use for ESR.

The reduced catalyst Figure 95 (a) shows a matrix with two distinct morphologies both with well-dispersed NiO particles. One is globular whereas the other is dark-colored lath-shaped particles about 110 nm in length which could be γ-Al_2O_3. Yuan et.al. [49] have reported similar morphology for γ-Al_2O_3 prepared by calcination of pseudo-boehmite at 600°C. The matrix which is darker in color is attributed to zirconia. The spent catalyst (Figure 95 (b)) shows the presence of two kinds of carbon. Light-colored filaments at the upper right corner and dark/dense lath/rod-shaped carbon which has a length of 90-102 nm which is close to the length of the light-colored lath

shapes observed in the fresh catalyst. The morphology of carbon is very different from that observed in binary Mg or ternary Al-Mg catalysts. The median particle size of Ni(0) is 10.7 nm in reduced catalysts and 13.6 nm in catalysts used for ESR. Thus, the extent of sintering is significantly lesser than in the case of ternary Al-Mg catalysts (7.5%Ni-AMZ-44-44-0, 7.5%Ni-AMZ-39-49-0, 7.5%Ni-AMZ-29-59-0).

The HRTEM of the quaternary Al-rich catalyst 7.5%Ni-AMZ-44-22-22 is shown in Figure 96 (a) and Figure 96 (b) below.

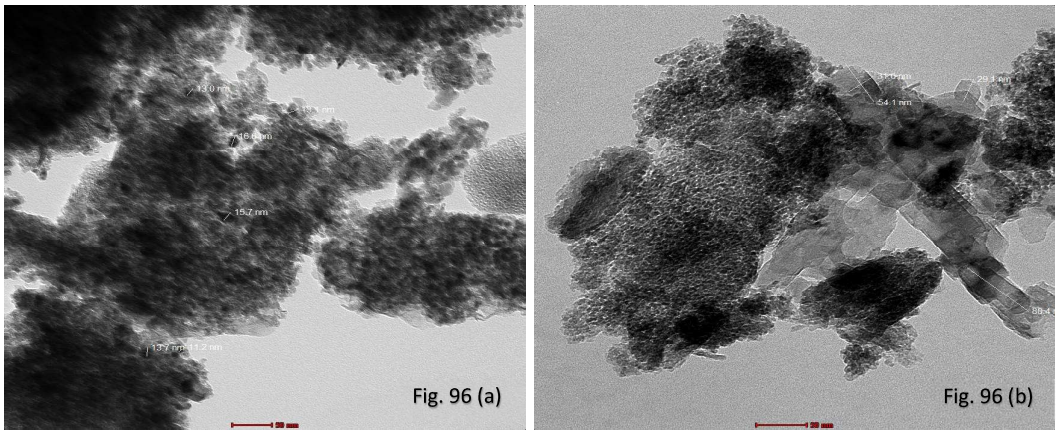

Figure 96: HR-TEM of 7.5%Ni-AMZ-44-22-22 a) Reduced catalyst
b) After use for ESR

As seen from Figure 96 (a) above shows a largely irregular globular morphology with some lamellar dark-colored particles (left side of Figure 96 (a). Such morphology is observed in catalysts containing Zirconia and alumina. The micrograph of the spent catalyst, Figure 96 (b), shows two distinct types of carbon: filamentous rod-like growing away from the catalyst surface (lower right corner) and very thin filamentous carbon covering the Ni particles and matrix (left side of the figure). The latter type of coke is also reported by Alberton et.al. [50] in steam reforming of ethanol over Ni/Al_2O_3 catalysts. Since Ni particles are not seen at the end of the filament's growth mechanism appears to be base growth.

The HR-TEM of quaternary Mg-rich catalyst 7.5%Ni-22-44-22 is shown in Figure 97 (a) and Figure 97 (b) below.

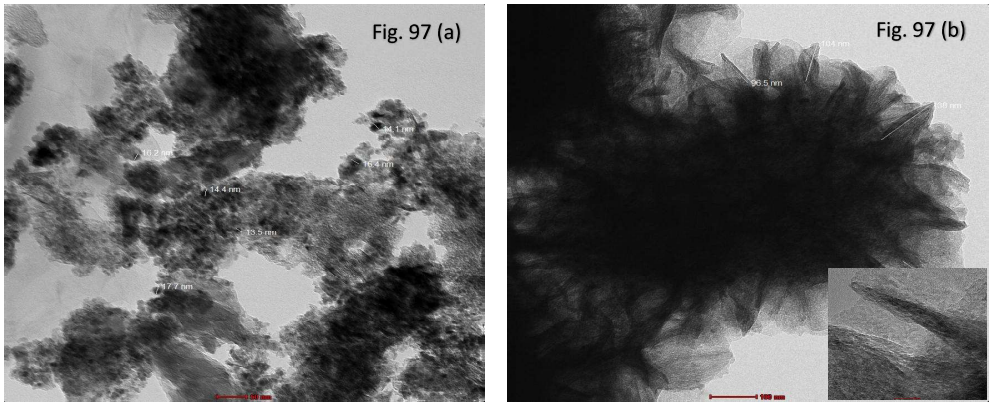

Figure 97: HR-TEM of 7.5%Ni-AMZ-22-44-22 a) Reduced catalyst b) After use for ESR

As seen from this Figure the reduced catalyst shows a light-colored granular matrix along with dark-colored patches. Ni particles with facets (dark-colored particles) are seen distributed across the matrix. There is a small increase in the size of Ni particles compared to fresh reduced and stabilized catalysts. 13.3 nm versus 10.3 nm. This is significantly smaller than that of binary Mg or ternary Al-Mg catalysts. The spent catalyst shows a form of carbon which may be described as "whiskers or tentacles". It is broad at the base which rests on the surface of the catalyst and tapering at the tip which grows outwards. A magnified image is provided inset. The morphology of this carbon is very different from that observed in the remaining catalysts (except AMZ-22-22-44). Basca et.al. [51] have reported carbon nanotubes of similar morphology by HRTEM. Since Ni particles are not seen at the tip the mechanism appears to be base growth.

The HR-TEM of quaternary Zr-rich catalyst 7.5%Ni-22-22-44 is shown in Figure 98 (a) and Figure 98 (b) below.

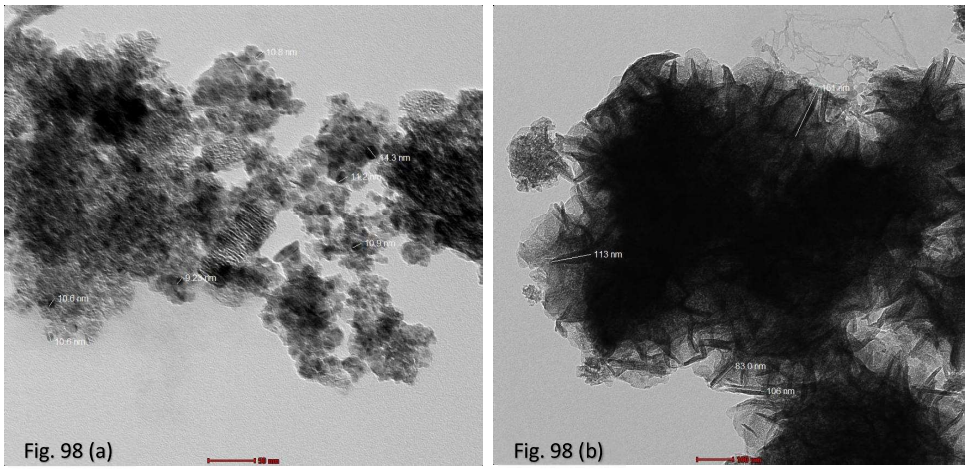

Figure 98: HR-TEM of 7.5%Ni-AMZ-22-22-44 a) Reduced catalyst; b) After use for ESR

As seen from this Figure the reduced catalyst shows morphology similar to the remaining two quaternary catalysts. It shows both dark lamellar and light globular particles. The carbon deposited on the spent catalyst shows morphology similar to the quaternary Mg-rich 7.5%Ni-AMZ-22-44-22 catalyst. The carbon whiskers/tentacles have a broad base and taper as they grow outwards. Their length varies from 50-160 nm. A small patch of filamentous carbon that encapsulates the surface of the catalyst is also seen (left top corner). This is similar in morphology to AMZ-44-22-22 (Al-rich quaternary catalyst). Since Ni particles are not seen at the tip the mechanism appears to be base growth similar to 7.5%Ni-AMZ-22-44-22. Ni particles are not visible in the spent catalyst due to the presence of coke which lends dark color.

Thus, as seen from the above Figures the morphology of carbon and also the growth mechanism are strongly influenced by the composition of the support. Further, the agglomeration of Ni is significantly less in quaternary catalysts and ternary Al-Zr catalyst when compared to binary or ternary catalysts containing Mg. Thus, composition of the support strongly influences the sintering behavior of Ni and morphology of coke deposits.

The percentage of carbon deposited on the spent catalysts, its morphology, and the decay constants at 700°C are compiled in Table 6 below

Table 6: Percentage of carbon deposited on the spent catalysts, its morphology, and the decay constants at 700°C.

Sr #	Catalyst	Carbon morphology	Carbon (wt%)	Decay constant of ethanol conversion
1	AMZ-0-89-0	Filamentous Octopus type (Tip growth)	10.7	0.0857
2	AMZ-44-44-0	Rod-like, cylindrical Bamboo type (base growth)	9.5	0.1075
3	AMZ-39-49-0	Filamentous, herringbone nanotube (tip growth)	9.4	0.0839
4	AMZ-29-59-0	Filamentous hollow nanotube and pyrolytic encapsulating carbon (tip growth)	9.8	0.0702
5	AMZ-44-0-44	Filamentous and rod-like carbon (base growth)	9.8	0.0606
6	AMZ-44-22-22	Filamentous encapsulating and rod-like (base growth)	12.4	0.0845
7	AMZ-22-44-22	Whisker carbon broad base tapered tip (base growth)	10.4	0.0295

8	AMZ-22-22-44	Whisker carbon broad base tapered tip (base growth)	10.6	0.0552

As seen from Table 6, coke content varies from 9.4-12.4 wt%. Excluding 7.5%Ni-AMZ-0-89-0 and 7.5%Ni-AMZ-44-22-22 the remaining catalysts show coke within a still narrower range 9.4-9.8 wt%. Decay slopes are relatively smaller for 7.5%Ni-AMZ-44-0-44, 7.5%Ni-22-44-22 and 7.5%Ni-22-22-44.

Further, as seen from this Table amongst the ternary Al-Mg catalysts, the catalyst with balanced composition (7.5%Ni-AMZ-44-44-0), which contains the lowest Mg content, shows coke morphology that is very different from that of the remaining Al-Mg or binary Mg catalysts. This catalyst is relatively rich in Al. It also presents base growth whereas the binary Mg and ternary Al-Mg catalysts with skewed composition show tip growth. This catalyst also shows the highest decay rate of ethanol conversion with time amongst binary Mg and ternary Al-Mg catalysts in long duration. Decay slope decreases with increasing Mg in these catalysts. The binary Mg catalyst which does not contain Al shows a decay slope next to 7.5%Ni-AMZ-44-44-0.

The ternary Al-Zr catalyst 7.5%Ni-AMZ-44-0-44 shows the smallest decay slope amongst ternary catalysts in long duration (80 hours) runs. Its Al content is similar to that of ternary Al-Mg catalyst 7.5%Ni-AMZ-44-44-0. This catalyst shows mixed morphology, filamentous carbon as well as rod-like carbon. It shows base growth similar to the ternary Al-Mg catalyst with balanced composition, 7.5%Ni-AMZ-44-44-0. Coke morphology is also similar to this latter catalyst.

Amongst the quaternary catalysts, the Al-rich catalyst 7.5%Ni-AMZ-44-22-22 shows a different morphology of coke. The coke is filamentous but not extending outwards. It is localized over the surface of the catalyst. Some rod-like coke is also observed. Thus, rod-like coke appears to form in catalysts that are rich in Al, viz. 7.5%Ni-AMZ-44-44-0, 7.5%Ni-AMZ-44-0-44 and 7.5%Ni-AMZ-44-22-22. There may be heterogeneous regions in these catalysts that are rich in Al on which the rod-like carbon grows.

The quaternary Mg-rich (7.5%Ni-AMZ-22-44-22) and Zr-rich (7.5%Ni-AMZ-22-22-44) show whiskers/tentacles of coke that grow outward from the catalyst substrate. These tentacles are broad at the base and tapering at the tip. This morphology is very different from that of the remaining catalysts. These catalysts show amongst the lowest decay slopes in long duration 80 hour runs). 7.5%Ni-AMZ-22-44-22 shows the

smallest slope followed by 7.5%Ni-AMZ-22-22-44. The results indicate that this morphology of carbon preserves catalyst activity to the largest extent in long-duration runs.

The decay slopes of the short-duration runs at 700°C are shown in Figure 81 above. The trend of increasing deactivation along with values of slope in braces is AMZ-0-89-0 (0.16) <AMZ-29-59-0 (0.215) <AMZ-39-49-0 0.23) <AMZ-22-44-22 (0.345) <AMZ-44-0-44 (0.52) <AMZ-44-44-0 (0.55) <AMZ-22-22-44 (0.81). This trend shows that catalysts that are rich in Al or Zr present faster deactivation than those which are rich in Mg. Comparing this trend with the morphology of coke formed during the long duration runs it is seen that the binary Mg and ternary Al-Mg catalysts which show filamentous coke also show lower deactivation compared to the Al or Zr-rich catalysts which show rod-like or whisker/tentacle morphology. However, in long-duration runs the catalysts which show whisker/tentacle morphology of coke show slower deactivation.

The particle size of Ni determined by HRTEM for reduced catalysts and spent ESR catalysts is compared in Table 7 below. The values of peak reduction temperature in TPR are shown in brackets against the names of the catalysts.

Table 7: Particle size of Ni determined by HRTEM for reduced catalysts and spent ESR catalysts.

Sr No	Catalyst	Reduced & Stabilized Median size Ni(0) (nm)	Spent catalyst Median size Ni(0) (nm)
1	7.5%Ni-AMZ-0-0-89 (448°C)	10.3	NA
2	7.5%Ni-AMZ-0-89-0 (464°C)	9.9	18.6
3	7.5%Ni-AMZ-44-0-44 (535°C)	10.7	13.6
4	7.5%Ni-AMZ-44-44-0 (580°C)	9.2	20.6
5	7.5%Ni-AMZ-39-49-0 (568°C)	10.3	20.4
6	7.5%Ni-AMZ-29-59-0 (563°C)	12.4	17.1
7	7.5%Ni-AMZ-0-44-44 (762°C)	14	NA
8	7.5%Ni-AMZ-22-44-22 (731°C)	13.3	10.3

As seen from this Table, catalysts that contain Zr (7.5%Ni-AMZ-44-0-44 and 7.5%Ni-AMZ-22-44-22) do not show a significant change in particle size of Ni whereas catalysts that do not contain Zr show a significant increase. Inclusion of Al with Mg in

ternary Al-Mg catalysts (7.5%Ni-AMZ-44-44-0, 7.5%Ni-AMZ-39-49-0, 7.5%Ni-AMZ-29-59-0) does not retard sintering during use for ESR. This indicates that Ni sinters less on catalysts whose supports contain zirconia. Comparing these trends with those of TPR it is seen that there is no clear trend of sintering of Ni with peak temperature of reduction of NiO. Incidentally, the Tammann and Huttig temperatures for Ni(0) are 590°C and 245°C, both of which are well below the range of operating temperature for the ESR of these samples, which is 700°C.

4.9: Catalyst Regeneration

The Mg-rich quaternary Al-Zr catalyst 7.5%Ni-AMZ-22-44-22 which shows the slowest decay in ethanol conversion with time on stream in long duration runs at 700°C (Figure 81 earlier) was subjected to regeneration. It was regenerated by controlled coke combustion in air. The temperature was programmed in stages of 3°C/min to 250°C (1 hour hold), 3°C/min to 350°C (2 hours hold), 3°C/min to 400°C (1 hour hold), 3°C/min to 450°C (1 hour hold), 3°C/min to 500°C (4 hours hold). A mixture of air in N_2 with an O_2 concentration of 2 vol% was used initially. Later the concentration of O_2 was progressively increased to 21% (pure air) for the proof burns at 500°C.

The metrics such as ethanol conversion, H_2 yield, H_2/CO and H_2/CO_2 are calculated. The trend of conversion of ethanol of the fresh catalyst is compared with that of the regenerated catalyst in Figure 99 below.

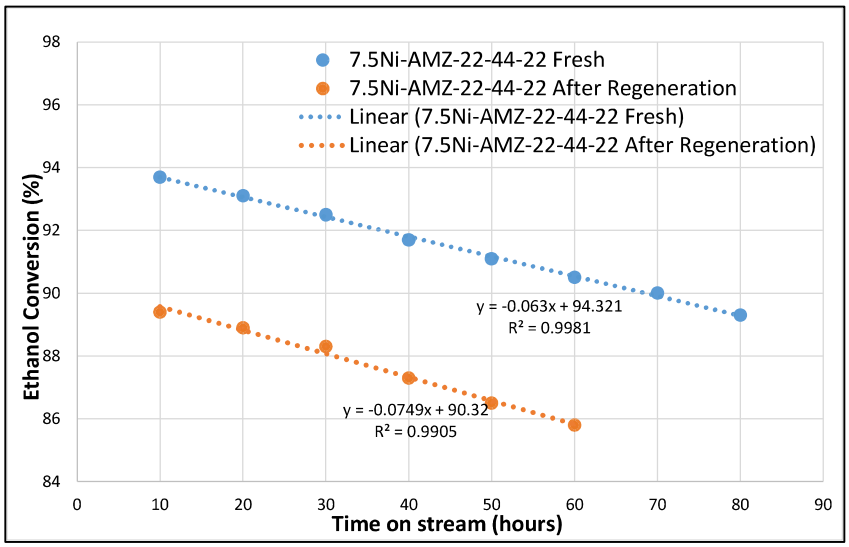

Figure 99: Trend of conversion of ethanol of the fresh catalyst and of the catalyst regenerated at 500°C

As seen from this Figure, the regenerated catalyst gives approximately 4.2% lower conversion of ethanol than the fresh catalyst. The slope of decay in conversion is also higher for the regenerated catalyst.

The yield of H_2 of the fresh and regenerated catalyst is compared in Figure 100 below.

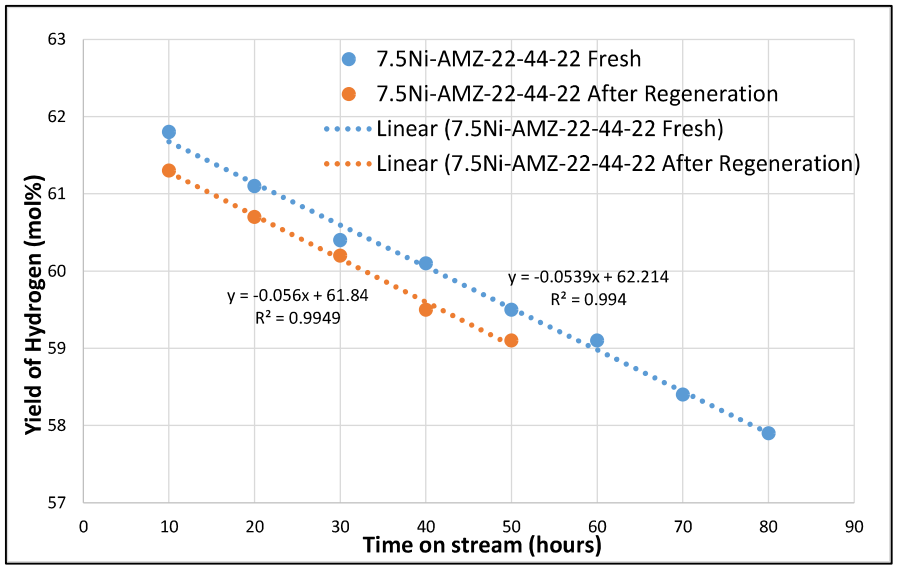

Figure 100: Yield of H_2 of the fresh catalyst and of the regenerated catalyst

The slope of decay in yield of H_2 with time is also compared in the Figure. As seen, the fresh catalyst gives about a 3% higher yield initially, but the yield decreases more rapidly with time on stream than that of the regenerated catalyst.

The H_2/CO and H_2/CO_2 of the regenerated catalyst are 4.4 and 2.9 molar, which is very close to that of the fresh catalyst which is 4.5 and 2.7 molar respectively. Hence the regenerated catalyst shows the same mechanism as the fresh catalyst.

Thus, the catalyst is not regenerated back to its original activity probably due to incomplete combustion of carbonaceous deposits. The sintering of the active Ni phase is ruled out based on HR-TEM data which shows reasonably small increase in particle size of Ni of this catalyst. Trimm et.al [36] report that amorphous/filamentous coke is more easily combustible than graphitic/encapsulating coke. Hence, the catalyst was regenerated using the same protocol but increasing the final temperature to 650°C. The trend of drop in conversion with time is compared for the fresh and regenerated catalysts in Figure 101 below.

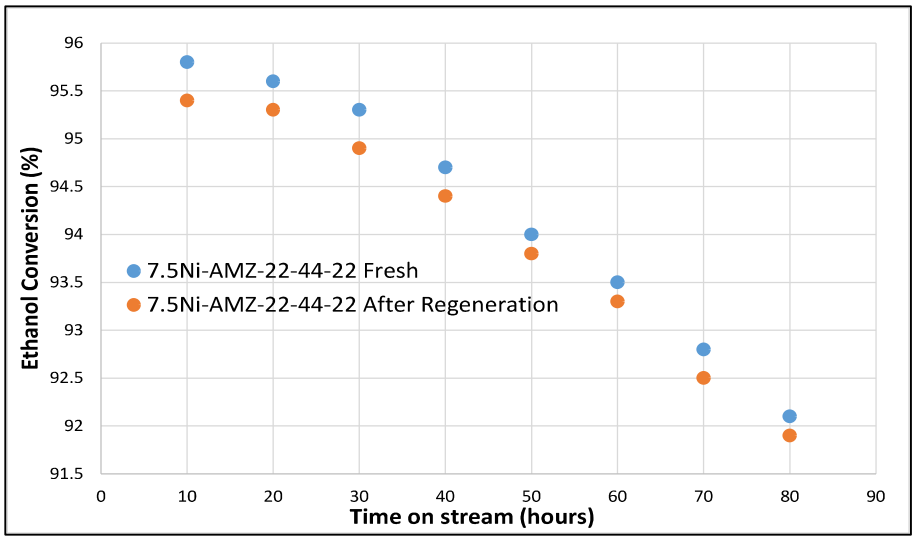

Figure 101: Ethanol Conversion of Fresh and Regenerated catalyst calcined at 650°C.

As seen from Figure 101 above, catalyst 7.5%Ni-AMZ-22-44-22 regains its activity due to complete combustion of coke at the higher regeneration temperature. As seen from Table 7 this catalyst does not show a significant increase in Ni(0) particle size by HRTEM after use for long duration run in ESR. Incidentally, this catalyst shows a reduction of NiO at high temperatures (731°C) in TPR studies which indicates strong metal-support interaction. This could be the reason for insignificant sintering of Ni during use for ESR. Y. Liu et.al [52] have reported that cobalt supported on ceria is completely regenerated by calcination in air at 450°C. Sergio Iglesias-Vazquez et.al [53] have studied nickel aluminate-based catalysts which are reduced at temperature 700°C-850°C and then tested for ESR. They report that the catalysts which are reduced at lower temperature 700°C-750°C can be fully regenerated by calcination in air at 850°C after use for ESR. According to them, a higher temperature is required for both oxidation of coke and reconstruction of the spinel phase.

Trimm et. al. [36] has cited the following coke-forming reactions in steam reforming:

$CH_4 = C + H_2$ Reaction 1

$2CO = CO + CO_2$ Reaction 2

$CO + H_2 = C + H_2O$ Reaction 3

$mC_nH_{2n+2} = nC + (n+1)H_2$ Reaction 4

Of these reactions, 2 and 3 are reported to be favored at lower temperatures, whereas reactions 1 and 4 are favored by higher reaction temperatures. Formation of two types of carbon viz. Cα and Cβ are cited. Of these, the former is reported to polymerize to form the latter and it is easier to gasify than the latter. Thus, some encapsulating coke is present on the used catalyst, (as observed from HRTEM, Figure 88 (b), which requires combustion at higher temperatures for complete regeneration. H_2 yield, H_2/CO ratio is also similar to fresh catalyst indicating that there is no change in the mechanism.

Whisker coke is stated to form by the dissolution of carbon into Ni to form a suspected carbide which leads to the formation of a whisker of carbon with the Ni particle located at its tip. Since the Ni at the tip is accessible catalyst activity is maintained. In contrast, encapsulating or pyrolytic coke which is believed to be type Cβ is relatively difficult to gasify and leads to loss in catalyst activity.

J.R. Rostrup-Nielsen [54] propose ensemble size control as a means of controlling coke formation by minimizing the probability of polymerization of Cα to Cβ.

A second strategy is to use basic catalysts to promote coke gasification. KOH (taught in patents of ICI), Magnesia (taught in patents of HTAS) and Urania (taught in patents of British Gas) are used in commercial catalyst formulations, each with its pros and cons. Catalysts containing Magnesia show lower coke content after use for ESR in the current study, which is consistent with this approach.

Avoiding carbide formation by adding p-block elements as dopants/alloys in the catalyst is another strategy.

Basic oxides metal oxides (RE oxides like La or Ce) are also reported to slow down overall coke deposition.

4.10: Conclusions

Steam reforming of ethanol utilizes a renewable reactant and hence helps to partially offset global warming. Monocomponent and bicomponent catalysts have been studied extensively and it is inferred that multi-functionality is important for this reaction. This requires multicomponent catalysts. To this end, the current study focuses

on linking the properties and performance of binary, ternary and quaternary nickel-based catalysts with ESR.

Myriad reactions are thermodynamically possible in ethanol steam reforming. These mainly lead to the formation of syngas (CO and H_2), CO_2, methane, ethylene, carbon and small quantities of acetaldehyde and acetone.

The set of 17 catalysts prepared with supports whose composition is systematically varied are used for the steam reforming of ethanol. The results of the current study show that the composition of the support has a profound influence on activity, product selectivity, stability, and morphology of coke. The presence of Mg in the catalyst formulation enhances the conversion of ethanol in all three classes of catalyst viz. binary, ternary, and quaternary. Catalysts with a composition skewed in favor of Mg show higher conversion than catalysts with a balanced composition. Higher nickel content also influences the conversion of ethanol.

Ethanol conversion does not correlate with the BET surface area of the catalyst. Dispersion of Ni is influenced by metal support interactions and degree of reducibility. Catalysts containing Mg show higher activity which is attributed to the formation of Ni-Mg solid solution. The formation of a solid solution is supported by the results of TPR reducibility and XRD.

Conversion of ethanol shows a completely linear inverse relationship with the particle size of Ni(0) determined by HRTEM when Ni is supported on supports of similar composition, indicating that ESR is a structure-sensitive reaction. When a comparison of dispersion is made with activity for catalysts with different compositions of support, the inherent/intrinsic chemical nature, which in turn influences reaction energetics predominates over metal dispersion.

The yield of H_2 increases with increasing reaction temperature and it is higher for catalysts containing Mg. Both steam reforming and water gas shift (WGS) reactions contribute to its formation. The yield of CO decreases with increasing reaction temperature due to WGS and Boudouard reactions. Similar to the yield of H_2, catalysts containing Mg show higher yields of CO. The change with increasing temperature is less for catalysts containing Mg. The trend with composition is similar to that of H_2. The yield of CO_2 increases with temperature indicating that it is forming at the expense

of CO. Change with temperature is relatively more for catalysts containing Mg. The yields of methane and ethylene increase with reaction temperature.

The correlation of ratios of H_2/CO, H_2/CO_2 and H_2/CH_4 are used to explain differences in trends of product yield with catalyst composition. Distinct trends are observed concerning catalyst composition. H_2/CO changes significantly with temperature for catalysts not containing Mg than for those which contain Mg. On the contrary H_2/CO_2 remains relatively unchanged for catalysts not containing Mg. H_2/CH_4 decreases sharply with temperature for all the catalysts irrespective of composition. Catalysts not containing Mg show a relatively higher change. These trends clearly show that the reforming of ethanol proceeds by a water-lean stoichiometry on all the catalysts. WGS reaction predominates on catalysts that do not contain Mg whereas the Boudouard reaction predominates in the case of catalysts that contain Mg. Trends of H_2/CH_4 suggest that the formation of CH_4 by the methanation of CO (which requires H_2 as reactant) should also be accompanied by other reactions such as the steam reforming of ethanol under water-rich conditions which produce the additional H_2 warranted in this case.

The formation of ethylene is observed. This is expected because, upon calcination at 650°C, the alumina is expected to exist predominantly in the γ form, which is acidic and is used commercially to dehydrate ethanol to ethylene. Further, zirconia is also known to be amphoteric and active for the dehydration reaction. A reasonable correlation of ethylene yield with the acidity of the catalyst is observed.

Methane appears to form by the methanation of CO which occurs simultaneously with the reforming of ethanol under water-rich conditions. Yields of methane are comparable for all the catalysts at lower temperatures ($\leq$ 600°C) and slightly higher for binary and ternary catalysts containing Mg.

Small quantities of acetaldehyde and acetone are observed to form. Their yield decreases with increasing reaction temperature. These compounds are intermediates and the observations are consistent with reports in the literature.

The product yields and the reactions involved differ significantly based on whether the binary and ternary catalyst contains Mg or not. This difference is diluted in

the case of quaternary catalysts which contain all three elements Al, Mg and Zr in varying proportions.

Binary Mg and ternary Al-Mg catalysts give the highest H_2 yield in both short and long-duration runs, however, they deactivate at a faster rate than ternary Al-Zr or quaternary catalysts.

Two distinct regimes of catalyst deactivation are observed. Short-term catalyst deactivation shows different trends and higher rates of coke formation compared to long-term deactivation. Coke deposition is significantly faster during the initial hours of operation (first 8 hours on stream). All the catalysts which contain Mg show slower short-term deactivation than those that do not contain Mg. These also show relatively less coke formation. The primary mode of deactivation appears to be a coke laydown. The reasonable trend between decay slopes of ethanol conversion and coke content of the spent catalyst and the catalyst regaining activity to that of the fresh catalyst after controlled oxidation of coke reinforces this observation. The Boudouard reaction and polymerization of ethylene appear to be the most probable reactions that deposit coke. A reasonable correlation between coke content and acidity of the catalyst for most of the catalysts except ternary Al-Mg, supports the polymerization of ethylene as a source of coke laydown in these catalysts. Decay slopes of ethanol conversion also show a reasonable trend with acidity.

Further, deactivation decreases with increasing reaction temperature. Trends of H_2/CO_2 and H_2/CH_4 indicate that steam gasification of coke could be the likely cause for this behavior. Trends of decay of ethanol conversion with composition are markedly different for low temperature (550°C) and high temperature (750°C) which indicate that different reactions take place at these temperatures.

OSC does not appear to influence deactivation in short-duration runs, whereas it does appear to influence deactivation in long-duration runs.

Deactivation in long-duration runs is significantly slower, almost a fifth of short-duration runs due to a sharp decrease in the rate of coke laydown. Slower deactivation at higher reaction temperatures is consistent in both short and long-duration runs. The trend of deactivation changes significantly with catalyst composition. Binary Mg and ternary Al-Mg catalysts which showed slow short-term deactivation, deactivate much faster than ternary Al-Zr and quaternary AMZ-22-44-22

or AMZ 22-22-44 in long-duration runs. Ternary Al-Zr and quaternary catalysts rich in Mg or Zr show slower deactivation than binary Mg or ternary Al-Mg catalysts. The slower deactivation in zirconia-containing catalysts is primarily due to the better resistance to sintering of Ni and the contribution from OSC, which is high in these catalysts due to the synergistic effects of Zr and Ce.

A distinct difference in coke morphology is observed with the catalyst composition. Different types of coke (filamentous, filamentous encapsulating, octopus, herringbone bamboo, rod-like, whisker/tentacle with broad base and tapering tip, and pyrolytic) are observed in the catalysts. Rod-like carbon appears to be characteristic of catalysts rich in Al. Quaternary Mg and Zr-rich catalysts show whisker/tentacle-type carbon. Ternary Al-Zr AMZ-44-0-44 shows rod-like dense carbon. Catalysts presenting whisker/tentacle coke show the slowest deactivation, followed by filamentous coke. More than one type of coke is also observed on any given catalyst which is attributed to the multi-component nature of the support.

Thus, the composition of the catalyst affects catalyst characteristics such as microstructure, acidity, reducibility, dispersion, and reaction energetics which in turn affect activity and product selectivity/yields. The composition also influences specific reactions which form these products. The type of carbon deposited, and rate of activity decline is also influenced by catalyst composition. Support composition also affects the kind of reactions taking place. Such data is useful in understanding the link between catalyst composition and performance which helps develop catalysts with improved performance.

References:

1) Shuhei Ogo, Yasushi Sekine; Fuel Processing Technology, 199 (2020); 106238.
2) J.L. Contreras, J. Salmones, J.A. Colín-Luna, L. Nuño, B. Quintana, I. Córdova, B. Zeifert, C. Tapia, G.A. Fuentes; Catalysts for H_2 production using the ethanol steam reforming (a review); International Journal of Hydrogen Energy; 39 (2014); 18835-18853.
3) Meng Ni, Dennis Y.C. Leung, Michael K.H. Leung; A review on reforming bio-ethanol for hydrogen production; International Journal of Hydrogen Energy 32 (2007); 3238-3247.

4) Ashutosh Kumar, R. Prasad and Y.C. Sharma; Steam reforming of ethanol: Production of renewable hydrogen; International Journal of Environmental Research & Development; 4(3), (2014); 203-212.
5) Lisiane V. Mattos, Gary Jacobs, Burtron H. Davis, and Fábio B. Noronha; Production of Hydrogen from Ethanol: Review of Reaction Mechanism and Catalyst Deactivation; Chemical Review; 12 (7), (2012); 4094-4123.
6) Marinela D. Zhurka, Angeliki A. Lemonidou, James A. Anderson and Panagiotis N. Kechagiopoulos; Kinetic analysis of the steam reforming of ethanol over Ni/SiO_2 for the elucidation of metal-dominated reaction pathways; Reaction Chemistry and Engineering; 3 (2018); 883-897.
7) Seung Ju Han, Yongju Bang, Jaekyeong Yoo, Jeong Gil Seo, In Kyu Song; Hydrogen production by steam reforming of ethanol over mesoporous Ni-Al_2O_3-ZrO_2 xerogel catalysts: Effect of nickel content; International Journal of Hydrogen Energy; 38 (2013); 8285-8292.
8) Gleicielle T. Wurzler, Raimundo C. Rabelo-Neto, Lisiane V. Mattos, Marco A. Fraga, Fábio B. Noronha; Steam reforming of ethanol for hydrogen production over MgO-supported Ni-based catalysts; Applied Catalysis A: Gen; 518 (2016); 115-128.
9) K. Tomishige, Y. Chen, X. Li, K. Yokoyama, Y. Sone, O. Yamazaki, K. Fujimoto; Studies in surface science and catalysis; 114 (1998); 375-378.
10) Prakash Biswas and Deepak Kunzru; Steam reforming of ethanol for the production of hydrogen over Ni/CeO_2-ZrO_2 catalyst: Effect of support and metal loading; International Journal of Hydrogen Energy; 32 (2007); 969-980.
11) Agustín E. Galetti, Mariana N. Barroso, Manuel F. Gomez, Luis A. Arrua, Antonio Monzón & M. Cristina Abello; Promotion of $Ni/MgAl_2O_4$ catalysts with rare earths for the ethanol steam reforming reaction; Catalysis Letter; 142 (2012); 1461-1469.
12) Hyun-Seog Roh, Yong Wang, David L. King, Alexandru Platon & Ya-Huei Chin; Low temperature and H_2 selective catalysts for ethanol steam reforming; Catalysis Letter; 108 (2006); 15-19.
13) Ji Hwan Song, Seung Ju Han & In Kyu Song; Hydrogen production by steam reforming of ethanol over mesoporous Ni-Al_2O_3-ZrO_2 catalysts; Catalysis Surveys from Asia; vol. 21 (2017); 114-129.

14) Christopher M.A. Parlett , Ayse Aydin, Lee J. Durndell, Lucia Frattini, Mark A. Isaacs, Adam F. Lee, Xiaotong Liu, Luca Olivi, Rima Trofimovaite, Karen Wilson, Chunfei Wu; Tailored mesoporous silica supports for Ni catalyzed hydrogen production from ethanol steam reforming; Catalysis Communications; 91 (2017); 76-79.

15) C. Phichitkul (Catalyst activity and deactivation mechanism of supported NiO in CH_4 oxidation; Ph.D. Thesis; 1981, California Institute of Technology and Engineering.

16) Tetsunori Nakayama, Masahiko Arai, Yoshiyuki Nishiyama; Dispersion of Nickel particles supported on alumina and silica in Oxygen and Hydrogen; Journal of Catalysis; 87(1), (1984); 108-115.

17) Yaoyuan Zhang, Yun Zhao, Tatiana Otroshchenko, Shanlei Han, Henrik Lund, Uwe Rodemerck, David Linke, Haijun Jiao, Guiyuan Jiang, Evgenii V. Kondratenko; The effect of phase composition and crystallite size on activity and selectivity of ZrO_2 in non-oxidative propane dehydrogenation; Journal of Catalysis; 371 (2019); 313-324.

18) R.Z.C. van Meerten, A.H.G.M. Beaumont, P.F.M.T. van Nisselrooij, J.W.E. Coenen; Structure sensitivity and crystallite size change of nickel during methanation of CO/H_2 on nickel-silica catalysts; Surface Science Letters; 135(1), (1983); 565-579.

19) Charlotte Vogt, Jelle Kranenborg, Matteo Monai, and Bert M. Weckhuysen; Structure sensitivity in steam and dry methane reforming over Nickel: activity and carbon formation; Catalysis; 10(2020);1428-1438.

20) Adriana Romero, Matías Jobbágy, Miguel Laborde, Graciela Baronetti, Norma Amadeo; Ni(II)-Mg(II)-Al(III) catalysts for hydrogen production from ethanol steam reforming: Influence of the activation treatments; Catalysis Today; 149 (1-3), (2010); 407-412.

21) Zuogang Guo, Shurong Wang, Long Guo, and Xinbao Li; Catalytic steam reforming of ethanol for hydrogen production over Ni/CeO_2-ZrO_2 catalysts; BioResources; 6(4), (2011); 4092-4102.

22) Prakash Biswas & Deepak Kunzru; Steam reforming of ethanol on Ni-CeO_2-ZrO_2 catalysts: Effect of doping with copper, cobalt and calcium; Catalysis Letter; 118 (2007); 36-49.

23) A.J. Vizcaíno, P. Arena, G. Baronetti, A. Carrero, J.A. Calles, M.A. Laborde, N. Amadeo; Ethanol steam reforming on Ni/Al_2O_3 catalysts: Effect of Mg addition; International Journal of Hydrogen energy; 33 (2008); 3489-3492.

24) Alessandro Di Michele, Anna Dell'Angelo, Antonio Tripodi, Elnaz Bahadori, Felipe Sànchez, Davide Motta, Nikolaos Dimitratos, Ilenia Rossetti, Gianguido Ramis; Steam reforming of ethanol over $Ni/MgAl_2O_4$ catalysts; International Journal of Hydrogen energy; 44(2), (2019); 952-964.

25) M.C. Sánchez-Sánchez, R.M. Navarro, J.L.G. Fierro; Ethanol steam reforming over Ni/M_xO_y-Al_2O_3 (M=Ce,La,Zr and Mg) catalysts: Influence of support on the hydrogen production; International Journal of Hydrogen Energy; 32 (2007); 1462-1472.

26) H. Wang, Y. Liu, L. Wang, Y.N. Qin ; Study on the carbon deposition in steam reforming of ethanol over Co/CeO_2 catalyst; Chemical Engineering Journal; 145(1), (2008); 25-31.

27) Jordi Llorca, Narcís Homs, Joaquim Sales, Pilar Ramírez de la Piscina; Efficient production of hydrogen over supported cobalt catalysts from ethanol steam reforming; Journal of Catalysis; 209(2), (2002); 306-317.

28) Paula Osorio-Vargas, Cristian H. Campos, Rufino M. Navarro, Jose L.G. Fierro, Patricio Reyes; Improved ethanol steam reforming on Rh/Al_2O_3 catalysts doped with CeO_2 or/and La_2O_3: influence in reaction pathways including coke formation; Applied Catalysis A: General; 505 (2015); 159-172.

29) Gerd Rabenstein and Viktor Hacker; Hydrogen for fuel cells from ethanol by steam- reforming, partial-oxidation and combined auto-thermal reforming: A thermodynamic analysis; Journal of Power Sources; 185(2), (2008); 1293-1304.

30) Sania M. de Lima, Adriana M. Silva, Uschi M. Graham, Gary Jacobs, Burtron H. Davis, Lisiane V. Mattos, Fábio B. Noronha; Ethanol decomposition and steam reforming of ethanol over $CeZrO_2$ and $Pt/CeZrO_2$ catalyst: Reaction mechanism and deactivation; Applied Catalysis A; 352(1-2), (2009); 95-113.

31) Zongyuan Liu, Tomáš Duchoň, Huanru Wang, Erik W. Peterson, Yinghui Zhou, Si Luo, Jing Zhou, Vladimir Matolín, Dario J. Stacchiola, José A. Rodriguez, and Sanjaya D. Senanayake; Mechanistic Insights of Ethanol Steam Reforming over Ni–CeO_x(111): The Importance of Hydroxyl Groups for Suppressing Coke Formation; The Journal of Physical Chemistry C ; 119 (32), (2015); 18248-18256.

32) Julia Vecchietti, Patricia Pérez-Bailac, Pablo G. Lustemberg, Esteban L. Fornero, Laura Pascual, Marta V. Bosco, Arturo Martínez-Arias, M. Verónica Ganduglia-Pirovano, Adrian L. Bonivardi; Shape-Controlled Pathways in the Hydrogen Production from Ethanol Steam Reforming over Ceria Nanoparticles; Catalysis ; 12 (16), (2022); 10482-10498.

33) Zhengyi Pan, Qian Zhang, Wenquan Wang, Lulin Wang, Guang-Hui Wang; Size-Tunable Carbon-Doped Ni Nanoparticles for Switchable Reductive Amination of Biomass-Derived Carbonyl Compounds to Primary Amines and Secondary imines; Sustainable Chemistry & Engineering; 10 (11), (2022); 3777-3786.

34) Emilia Saraceno, Concetta Ruocco and Vincenzo Palma; A review of coal and biomass hydrogasification: Process layouts, hydrogasifiers and catalysts; Catalysts; 13(2), (2023); 417.

35) F. Frusteri, S. Freni, V. Chiodo, S. Donato, G. Bonura, S. Cavallaro; Steam and auto-thermal reforming of bio-ethanol over MgO and CeO_2 Ni supported catalysts; International Journal of Hydrogen energy; 31(15), (2006); 2193-2199.

36) D.L. Trimm; Catalysts for the control of coking during steam reforming; Catalysis Today; 49(1-3), (1999), 3-10.

37) Guisnet M and Magnoux P; Coking and deactivation of zeolites: Influence of pore structure; Applied Catalysis; 54(1), (1989); 1-27.

38) Jingjing Shao, Guangming Zeng, Yongdan Li; Effect of Zn substitution to a $LaNiO_{3-\delta}$ perovskite structured catalyst in ethanol steam reforming; International Journal of Hydrogen Energy; 42(27), (2017); 17362-17375.

39) Zhang; ZL; Verykios; XE; MacDonald; SM; Affrossman; S; Comparative study of Carbon dioxide reforming of methane to syngas over Ni/La_2O_3 and conventional Ni based catalysts; Journal of Physical Chemistry; 100(2), (1996); 744-754.

40) M. Monthioux, L. Noé, L. Dussault, J.-C. Dupin, N. Latorre, T. Ubieto, E. Romeo,C. Royo, A. Monzónc and C. Guimonb; Texturising and structurising mechanisms of carbon nanofilaments during growth; Journal of Materials Chemistry; 17 (2007); 4611-4618.

41) S. Helveg, J. Sehested, J.R. Rostrup-Nielsen; Whisker carbon in perspective; Catalysis Today; 179 (2011), 42-46.

42) Jiuling Chen, Yongdan Li, Yanmei Ma 1, Yongning Qin, Liu Chang; Formation of bamboo-shaped carbon filaments and dependence of their morphology on catalyst composition and reaction conditions; Carbon; 39(10), (2001); 1467-1475.

43) Sirui Tong ,Bin Miao, Lan Zhang and Siew Hwa Chan; Decarbonising natural gas: a review of catalytic decomposition and carbon formation mechanisms; Energies; 15 (2002); 2573.

44) Yahachi Saito and Tadanobu Yoshikawa; Bamboo-shaped carbon tube filled partially with nickel; Journal of Crystal Growth; 134 (1-2), (1993); 154-156.

45) Ming Lin , Joyce Pei Ying Tan, Chris Boothroyd, Kian Ping Loh, Eng Soon Tok, Yong-Lim Foo; Dynamical observation of bamboo-like carbon nanotube growth; Nano Letters; 7(8), (2007); 2234-2238.

46) R. Baker, M. Barber, P. S. Harris, F. Feates, R. J. Waite; Nucleation and growth of carbon deposits from the nickel catalyzed decomposition of acetylene; Journal of Catalysis; 26(1), (1972); 51-62.

47) Ismail Karacan and Gulhan Erdogan; The role of thermal stabilization on the structure and mechanical properties of polyacrylonitrile precursor fibers Fibers and Polymers; 13(7), (2012); 855-863.

48) Fahim Fayaz, Long Giang Bach, Mahadi B. Bahari, Trinh Duy Nguyen, Khanh B. Vu, Ramesh Kanthasamy, Chanatip Samart, Chinh Nguyen-Huy, Dai-Viet N. Vo; Stability evaluation of ethanol dry reforming on Lanthania-doped cobalt-based catalysts for hydrogen-rich syngas generation; International Journal of Energy Research; 43 (2019); 405-416.

49) Xiaohong Yuan; Formation and properties of 1-D alumina nanostructures prepared via a template-free thermal reaction; Procedia Engineering; 102 (2014), 602-609.

50) Andre L. Alberton, Mariana M.V.M. Souza b, Martin Schmal; Carbon formation and its influence on ethanol steam reforming over Ni/Al_2O_3 catalysts; Catalysis Today; 123 (2007); 257-263.

51) R R Bacsa, E Flahaut, Ch Laurent, A Peigney, S Aloni, P Puech and W S Bacsa; Narrow diameter double-wall carbon nanotubes: synthesis, electron microscopy and inelastic light scattering; New Journal of Physics; 5 (2003); 1.

52) Yanyong LiuYanyong Liu, Kazuhisa Murata and Megumu Inaba; Steam reforming of bioethanol to produce hydrocarbons over Co/CeO_2 catalysts derived from $Ce_{1-x}Co_xO_{2-y}$ precursors; Catalysts; 6(2), (2016); 26.

53) Sergio Iglesias-Vázquez, José Valecillos, Aingeru Remiro, D,Javier Bilbao andAna Guadalupe Gayubo; Stability of a $NiAl_2O_4$ derived catalyst in the ethanol steam reforming in reaction-regeneration cycles: Effect of reduction temperature; Catalysts; 12(5), (2012); 550.

54) J.R. Rostrup-Nielsen in C.H.Bartholomew, J.B. Butt (Eds.), Studies in Surface Science and Catalysis; 68 (1991); 85.

THIS PAGE IS LEFT BLANK INTENTIONALLY